UNCLASSIFIED

AD NUMBER

AD845757

NEW LIMITATION CHANGE

TO

Approved for public release, distribution unlimited

FROM

Distribution authorized to U.S. Gov't. agencies and their contractors; Administrative/Operational Use; NOV 1968. Other requests shall be referred to Aero Propulsion Lab., Wright-Patterson AFB, OH 45433.

AUTHORITY

AFAPL ltr, 12 Apr 1972

THIS PAGE IS UNCLASSIFIED

AFAPL-TR-68-132

AD845757

PULSED PLASMA TECHNOLOGY IN MICROTHRUSTERS

William J. Guman
Fairchild Hiller Corp./Republic Aviation Division

TECHNICAL REPORT AFAPL-TR-68-132

November, 1968

DDC
RECEIVED
JAN 13 1969
B

Air Force Aero Propulsion Laboratory
Air Force Systems Command
Wright-Patterson Air Force Base, Ohio 45433

C5

NOTICE

When Government drawings, specifications, or other data are used for any purpose other than in connection with a definitely related Government procurement operation, the United States Government thereby incurs no responsibility nor any obligation whatsoever; and the fact that the Government may have formulated, furnished, or in any way supplied the said drawings, specifications, or other data, is not to be regarded by implication or otherwise as in any manner licensing the holder or any other person or corporation, or conveying any rights or permission to manufacture, use, or sell any patented invention that may in any way be related thereto.

This document is subject to special export controls and each transmittal to foreign governements or foreign nationals may be made only with prior approval of the Air Force Aero Propulsion Laboratory (APIE-2), Wright Patterson Air Force Base, Ohio.

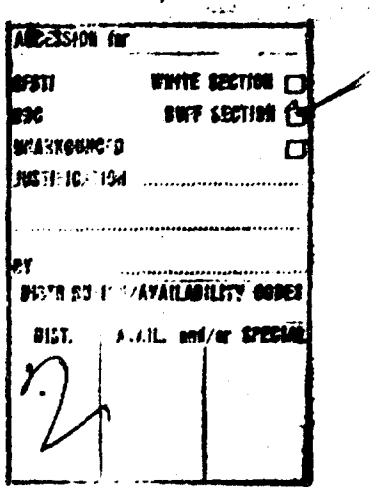

Copies of this report should not be returned unless return is required by security considerations, contractual obligations, or notice on a specific document.

AFAPL-TR-68-132

PULSED PLASMA TECHNOLOGY IN MICROTHRUSTERS

William J. Guman
Fairchild Hiller Corp./Republic Aviation Division

This document is subject to special export controls and each transmittal to foreign governments or foreign nationals may be made only with prior approval of the Air Force, Aero Propulsion Laboratory (APIE-2), WPAFB, Ohio.

FOREWORD

This final report was prepared by Fairchild Hiller Corporation, Republic Aviation Division under Air Force Contract F33615-67-C-1395, "Pulsed Plasma Technology in Microthrusters," PCD-TR-68-14.

The research reported upon was supported by the Air Force Aero Propulsion Laboratory. The program was monitored in the Electric Propulsion Technology Section of the Air Force Aero Propulsion Laboratory originally by Mr. D. Fritz, later by Lt. D. F. O'Brien, and most recently by Mr. W.C. Burson, respectively.

Work on this contract started in February 1967 and was completed June 1968 and the pertinent studies of this period are reported herein. This report was submitted by the author October, 1968.

Dr. W. J. Guman, the principal investigator, wishes to acknowledge the significant contributions of Mr. I. Granet in thruster life testing and thermal analysis, Mr. R. Paige in discharge initiating studies, Mr. R. Rupp in exploratory thruster system studies, Mr. A. Temps in power conditioner analysis and testing, and Messrs: J. Pearson and J. Varga in thrust stand design, respectively. The capacitor development work carried out at the Sprague Electric Company was under the direction of Mr. C. Chase of the Sprague Electric Company, with Mr. F. Pinkall the program engineer.

Publication of this report does not constitute Air Force approval of the reports findings or conclusions. It is published only for the exchange and stimulation of ideas.

Philip E. Stover, Chief
Propulsion & Power Branch
Aerospace Power Division

ABSTRACT

This Final Report describes the pertinent results of the studies carried out in advancing solid propellant pulsed plasma microthruster system technology in the thrust range from below 1 micropound up to roughly 200 micropounds and encompassing the (system) specific impulse range up to 2400 seconds. Thruster nozzles have been operated up to 3800 hours at the 50 micropound thrust level. Radiation cooled energy storage capacitors driving thrusters at 7.7 joules/lb have been developed with a life of 7.1×10^6 discharges (476 lb-sec of total impulse). Discharge initiating circuitry has been operated for 1.54×10^8 discharges and 80% efficient power conditioners have been developed and tested beyond 4.5×10^7 discharges. Complete thruster systems have been operated up to 630 hours at the 140 micropound thrust level (317 lb-sec of total impulse). A thrust stand capable of accurately and rapidly measuring thrust of a microthruster was delivered to the Air Force Aero Propulsion Laboratory.

Since an ion pumped vacuum chamber having sorption roughing was not available, it was not possible to reliably determine maximum thruster system life capability.

The results of this program have made it possible to design, test and deliver flight qualified thrusters and power conditioners to another laboratory under a separate program within roughly 30 weeks for installation in a synchronous orbit satellite.

Guidelines for including a solid propellant pulsed plasma microthruster system in application studies are included.

CONTENTS

Section			Page
I	INTRODUCTION		1
	1.1 General		1
	1.2 System Description		2
	1.3 Major Accomplishments		4
II	MICROTHRUSTER SUBSYSTEM TECHNOLOGY		5
	2.1 Thruster Studies		5
	2.1.1	Brief Thruster Description	5
	2.1.2	Analytic Considerations	10
		2.1.2a MHD Thrusting	14
		2.1.2b Gasdynamic Pressure Thrust ("Expansion Thrusting")	15
		2.1.2c Gasdynamic Expansion Nozzle Considerations	18
		2.1.2d Thrust Vector Control by Exhaust Beam Deflection	22
	2.1.3	Generalized Thruster Data Realized	24
		2.1.3a Energy Per Unit Mass and Energy Per Unit Area	25
		2.1.3b Specific Impulse and Energy Per Unit Area	30
		2.1.3c Specific Impulse, Specific Thrust, and Nozzle Length	35
		2.1.3d Specific Thrust and Capacitor Resistance	35
		2.1.3e Thrust Efficiency and Discharge Energy	38
		2.1.3f Thrust Efficiency and Energy Per Unit Area	38
		2.1.3g Impulse Bit and Discharge Energy	40
		2.1.3h Thrust Level as a Function of Life	43

CONTENTS (Cont'd)

Section			Page
2.2	Capacitor Studies and Development		43
	2.2.1 Introduction		43
		2.2.1a Capacitor d.c. Life as a Function of Charge Cycle	47
		2.2.1b Preliminary Analysis on Thermal Testing of Capacitors	50
		2.2.1c Capacitor Quality by Thermal Tests	61
2.3	Power Conditioning Subsystem		65
	2.3.1 General		65
	2.3.2 Analysis		66
		2.3.2a Numerical Examples	76
	2.3.3 Experimental Studies		78
		2.3.3a Life Tests	81
		2.3.3b Efficiency Measurements	84
		2.3.3c Weight	85
2.4	Discharge Initiation Subsystem		86
	2.4.1 General		86
	2.4.2 Ignition Circuits		89
		2.4.2a Krytron Ignition System	89
		2.4.2b Spark Gap Ignition System	93
		2.4.2c Transformer Ignition System	93
	2.4.3 Surface Igniter Plug		102
2.5	Other Pertinent Studies		109
	2.5.1 Propellant Studies		109
	2.5.2 Preliminary RFI Studies		114
	2.5.3 Exhaust Beam Observations		117
III	MICROTHRUSTER SYSTEM TESTS		121
3.1	Extended System Life Tests		121

CONTENTS (Cont'd)

Section		Page
IV	THRUST BALANCE	135
	4.1 General Description	135
	4.2 Typical Results	140
V	APPLICATION STUDIES	143
	5.1 General Applicability	143
	5.2 Thruster System Weight Reduction Scheme	150
VI	CAPACITOR DEVELOPMENT	157
	6.1 Problem Statement	157
	6.2 Testing and Test Facilities	157
	6.3 Initial Design	158
	6.4 Second Generation Metallized Capacitors	160
	6.5 L, R, and Q Considerations	161
	6.6 6.0μf Capacitor of Metallized Mylar	161
	6.7 Change of Scope	162
	6.8 First Generation Mylar Foil Capacitors (10 Joule)	162
	6.9 Second Generation of Mylar Foil Capacitors (20 Joule)	163
	6.10 Third Generation of Mylar Foil Capacitors (20 Joules)	165
	6.11 Fourth Generation of Mylar Foil Capacitors (20 Joule)	166
	6.12 First Generation of 40 Joule Mylar Foil Capacitors	167
	6.13 Five (5) Joule Capacitors of Mylar Foil Construction	167
	6.14 Conclusions	168
VII	REFERENCES	183
VIII	PROJECT PUBLICATIONS	185

ILLUSTRATIONS

FIGURE		PAGE
1	System Component Schematic	2
2	Thruster and Propellant Subsystem Schematic	5
3	Assembly of Thruster 97-E-1	6
4	Operational Thruster System	7
5	Operational Thruster System	8
6	Parallel Rail Electrode Configuration	11
7	Geometric Variables	13
8	Typical Thruster on Thrust Stand in Vacuum Chamber	31
9	Typical Thrust Recording and Calibration Set-Up Exterior to Vacuum Chamber	31
10	Energy/Mass vs. Energy/Area	32
11	Specific Impulse as a Function of Discharge Energy per Unit Propellant Area	34
12	Specific Impulse as a Function of Nozzle Length	37
13	Specific Thrust as a Function of Nozzle Length	37
14	Thrust Efficiency as a Function of Discharge Energy	39
15	Thrust Efficiency as a Function of Energy per Unit Area	41
16	Impulse Bit vs. Discharge Energy	42
17	Capacitor Charging Alternatives	49
18	Slab Geometry Notation	53
19	Cylindrical Geometry Notation	56
20	Schematic Q Variation	63
21	Schematic Q Variation	64
22	Equivalent Circuit Schematic	67
23	Equivalent Circuit Schematic Continued	69
24	40 Watt Breadboard Power Conditioner	79
25	20 Watt Packaged Power Conditioner	80
26	Power Conditioner Discharge Simulator	82
27	Discharge Initiation Subsystem Block Diagram	86
28	Single Frequency Laboratory Driver	87
29	Variable Frequency Laboratory Driver	88
30	Krytron Ignition System	90

ILLUSTRATIONS (Cont'd)

FIGURE		PAGE
31	Prototype Krytron Ignition System	91
32	Block Diagram Spark Gap Ignition System	94
33	Spark Gap Ignition System	95
34	Spark Gap Ignition System Schematic	96
35	Spark Gap Ignition System Life Test	97
36	Transformer Discharge Initiating Network	99
37	Discharge Circuit Thermal Test at 5Hz	100
38	Typical Output Pulse	101
39	Surface Igniter Plug After 5×10^6 Discharges	104
40	Discharge Initiating Circuit and Surface Igniter Plug	105
41	Equivalent Circuit	106
42	Plug Energy vs. Plug Resistance	108
43	CTFE 2300, Magnified 122x	113
44	Discharge Voltage and Exhaust Pnototube Measurements	119
45	Typical Vacuum Exhaust Plume of a Parallel Rail Thruster	119
46	Exhaust Pattern on Vacuum Chamber End Flange	120
47	Void Pattern in Exhaust Beam Projected onto End Flange	120
48	Dual Nozzle Thruster System	125
49	Thruster System Electronics	125
50	View Looking into Thruster after 3800 Hours of Operation	128
51	Cathode After 3800 Hours of Operation	128
52	7x Magnification of Cathode After 3800 Hours of Operation	129
53	Cathode Erosion Below Deposit	129
54	Propellant Remnants After Each Refueling	130
55	Thruster of Log 104-E-5	131
56	Propellant of Log 104-E-5 After 535 Hours at 140μ lb	131
57	Flight Qualified Pulsed Plasma Microthruster	133
58	Flight Qualified Pulsed Plasma Microthruster	134
59	Principle of Seismic Pendulum	136
60	Thrust Measuring System Schematic	138

ILLUSTRATIONS (Cont'd)

FIGURE		PAGE
61	Thrust Stand	139
62	Control Console	141
63	Ball Calibrator Output at 20 micropunds	142
64	Thruster Output of 7.6 micropound Thrust Level	142
65	Weight Ratio as a Function of Number of Capacitors	152
66	Comparison of Schemes	153
67	Weight Ratio as a Function of Number of Clusters	155
68	Temperature - Time History	177
69	Temperature - Time History	179
70	Temperature - Time History	180
71	Temperature - Time History	181
72	Temperature - Time History	182

TABLES

NUMBER		PAGE
1	Effect of Idealized Expansion Cone Upon Performance	22
2a	Thruster Tests with Varying Parameters (all tests at least 8 hours of continuous operation)	27
2b	Thruster Tests with Varying Parameters (Cont'd)	29
3	Specific Thrust - Capacitor Resistance Studies	36
4	Thrust and Impuse as a Function of Consecutive Discharges	44
5	Power Conditioner Life Test Studies	83
6	Power Conditioner Weight	85
7	Discharge Initiation Subsystem Comparison	92
8	Fluorocarbon and Plastic Propellants	110
9	Diagnostic Comparison of Propellants	113
10	Extended Thruster Tests	122
11	Extended Thruster Tests	123
12	Extended Thruster Tests	124
13	Applicability Tabulation	145
14	Possible Designs of a 100 μlb Thrust Level Thruster Delivering 1000-lb-sec Total	149
15	Record of Capacitor Tests	171
16	Record of Capacitor Tests	173
17	Record of Capacitor Tests	175

SECTION I

INTRODUCTION

1.1 GENERAL

This report presents the most relevant results of the research carried out toward improved technology for pulsed plasma microthrusters in the range of thrust varying from one micropound up to about 150 micropounds. Quite generally, all studies being reported upon encompassed pulsed plasma thruster systems generating below 500μ lb of thrust; i.e., a level referred to as the micropound regime in order to distinguish them from larger millipound thrust level devices that have been reported elsewhere. The studies were carried out during a period of 16 months at the Republic Aviation Division of the Fairchild Hiller Corporation for the Aero Propulsion Laboratory of the United States Air Force.

Prior to the present program the state-of-the-art of pulsed plasma microthruster system technology had advanced to the level where a completely self contained 80 micropound thrust level gaseous propellant pulsed plasma microthruster was integrated as a system including telemetry in a satellite for possible launch.[1] The essential undesirable features of this latter system were the use of a mechanical valve for metering gaseous propellant and the use of relatively heavy capacitors. The advent of valveless solid propellant pulsed plasma thrusters marked a new era for pulsed plasma thrusters and became the stimulus for the present program. By eliminating the propellant metering valve, the thruster acquired an inherent high level of reliability with a passive failure mode; i.e., no disturbing torques or forces can be impressed onto a satellite in the event of thruster failure. In addition, the performance level of the solid propellant system in the thrust range below roughly 500μ lb matched or even exceeded that reported of other operational electric microthruster systems. Since an ion pumping vacuum facility with sorption roughing was not available maximum life capability of the thruster system was never established even though one thruster was operated for 3800 hours.

SECTION I

INTRODUCTION

1.1 GENERAL

This report presents the most relevant results of the research carried out toward improved technology for pulsed plasma microthrusters in the range of thrust varying from one micropound up to about 150 micropounds. Quite generally, all studies being reported upon encompassed pulsed plasma thruster systems generating below 500μ lb of thrust; i.e., a level referred to as the micropound regime in order to distinguish them from larger millipound thrust level devices that have been reported elsewhere. The studies were carried out during a period of 16 months at the Republic Aviation Division of the Fairchild Hiller Corporation for the Aero Propulsion Laboratory of the United States Air Force.

Prior to the present program the state-of-the-art of pulsed plasma microthruster system technology had advanced to the level where a completely self contained 80 micropound thrust level gaseous propellant pulsed plasma microthruster was integrated as a system including telemetry in a satellite for possible launch.[1] The essential undesirable features of this latter system were the use of a mechanical valve for metering gaseous propellant and the use of relatively heavy capacitors. The advent of valveless solid propellant pulsed plasma thrusters marked a new era for pulsed plasma thrusters and became the stimulus for the present program. By eliminating the propellant metering valve, the thruster acquired an inherent high level of reliability with a passive failure mode; i.e., no disturbing torques or forces can be impressed onto a satellite in the event of thruster failure. In addition, the performance level of the solid propellant system in the thrust range below roughly 500μ lb matched or even exceeded that reported of other operational electric microthruster systems. Since an ion pumping vacuum facility with sorption roughing was not available maximum life capability of the thruster system was never established even though one thruster was operated for 3800 hours.

1.2 SYSTEM DESCRIPTION

The solid propellant pulsed plasma thruster system being reported upon is comprised of four major subsystems:

1. The thruster nozzle, capacitor, propellant subsystem
2. The power conditioning subsystem
3. The discharge initiating subsystem
4. The driver

The inter-relationship of these in the thruster system is shown schematically in Figure 1. The power conditioner accepts a low (typically 16 to 28V d.c.) d.c. voltage and converts it to a high voltage (typically 1 KV to 1.5 KV) for charging the thruster capacitor and it also supplies a moderately high voltage (typically 500 volts) for the discharge initiating circuit, respectively. The discharge initiating circuit upon receiving a command pulse from the driver produces a "microdischarge" (i.e., fraction of a joule) in the thruster nozzle for the purpose of discharging the main thruster circuit. The thruster nozzle, capacitor, propellant subsystem converts stored electric energy and solid propellant into an impulse bit for each microdischarge of the discharge initiating circuit.

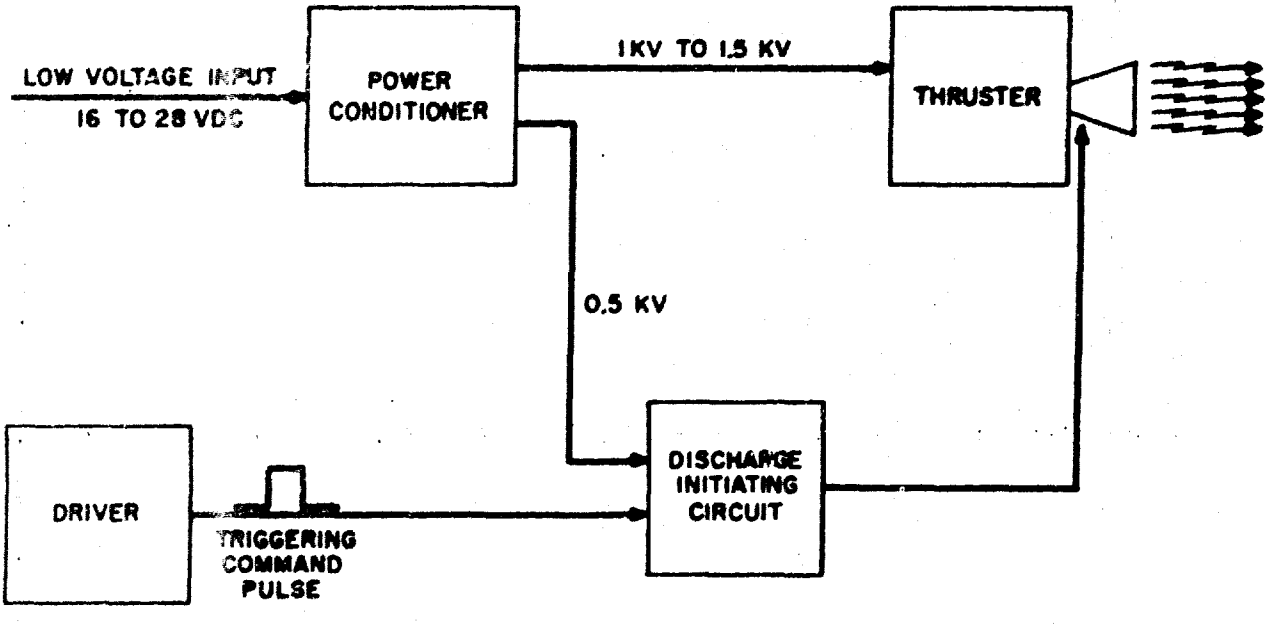

Figure 1. System Component Schematic

A steady thrust level (T) is generated by the operation of the system at a pulse frequency (f) in accordance with the relation $T = fI$ where I denotes the discrete impulse bit generated by each individual discharge.

As a functional system, the application of a low voltage (6 to 28 V d.c.) to the power conditioner charges the main thruster capacitor and "arms" the discharge initiating network. Upon receiving a trigger input, the discharge initiating circuit generates a "microdischarge" within the thruster nozzle which discharges the main thruster capacitor. This latter discharge depolymerizes and energizes the Teflon propellant. This energy addition process converts the depolymerized Teflon into a plasma which is accelerated electromagnetically and gasdynamically through the interelectrode nozzle assembly and then discharged into space. The time to charge the main thruster capacitor is a function of the power conditioner and is typically equal to the reciprocal of the thrust pulse repetition rate (i.e., period) for which the system is designed. During the course of the present study this charge period has been anywhere from 0.25 seconds to one second. The interval of time between application of a trigger pulse until the main thruster discharge occurs is a fraction of a microsecond whereas the duration of the thrusting action is anywhere from 2 microseconds up to 20 microseconds depending upon the energy level of the discharge and electrode nozzle configuration.

Some of the essential features of the system being reported upon are:

- Simple, rugged, compact system with inherent high reliability and long life
- Zero warm-up time, zero stand-by power
- Fail-safe system - no torques or forces can be generated by the inert system
- Solid Propellant Features:
  - Available propellant accurately measurable in zero-g
  - No tankage, feed lines, seals, valves
  - Inherently compatible with zero-g cryogenic temperatures and space environment
  - Non-corrosive, non-toxic, long shelf life
  - Not affected by either rapid or severe temperature changes

- Repeatable, discrete impulse bits compatible with digital logic control
- Steady thrust level variable by a factor of 10
- Good performance compatible with attitude control and low power application
- Operation unaffected by large variation in environmental temperatures

1.3 MAJOR ACCOMPLISHMENTS

Several major milestones in pulsed plasma microthruster system technology have been achieved in carrying out the present program. The most notable component life milestones and component performance milestones are, respectively:

Component Life Milestones:

Electrode Nozzle Life

3800 hours at 50μ lb thrust level
(equivalent to 7600 hours at 25μ lb thrust level)

Capacitor Life Pulsed and Radiation Cooled in a Vacuum at 7.7 joules/lb

7.1×10^6 discharges
(delivered 476 lb-sec of total impulse)

Discharge Initiating Circuit

1.54×10^8 discharges

Power Conditioner

4.54×10^7 discharges
3.54×10^7 discharges

Component Performance Milestones:

89% Power Conditioning Efficiency

15.4 watts/lb (or 7.7 joules/lb) radiation cooled energy storage capacitor with reliably long vacuum discharge life.

The achievements of the present program have made it possible to successfully meet the stringent hardware and thruster system performance requirements of the LES-6 satellite.

SECTION II

MICROTHRUSTER SUBSYSTEM TECHNOLOGY

2.1 THRUSTER STUDIES

2.1.1 Brief Thruster Description

A schematic representation of a typical parallel rail pulsed plasma thruster* with its propellant subsystem is shown in Figures 2 and 3 with representative laboratory hardware shown in Figures 4 and 5, respectively.

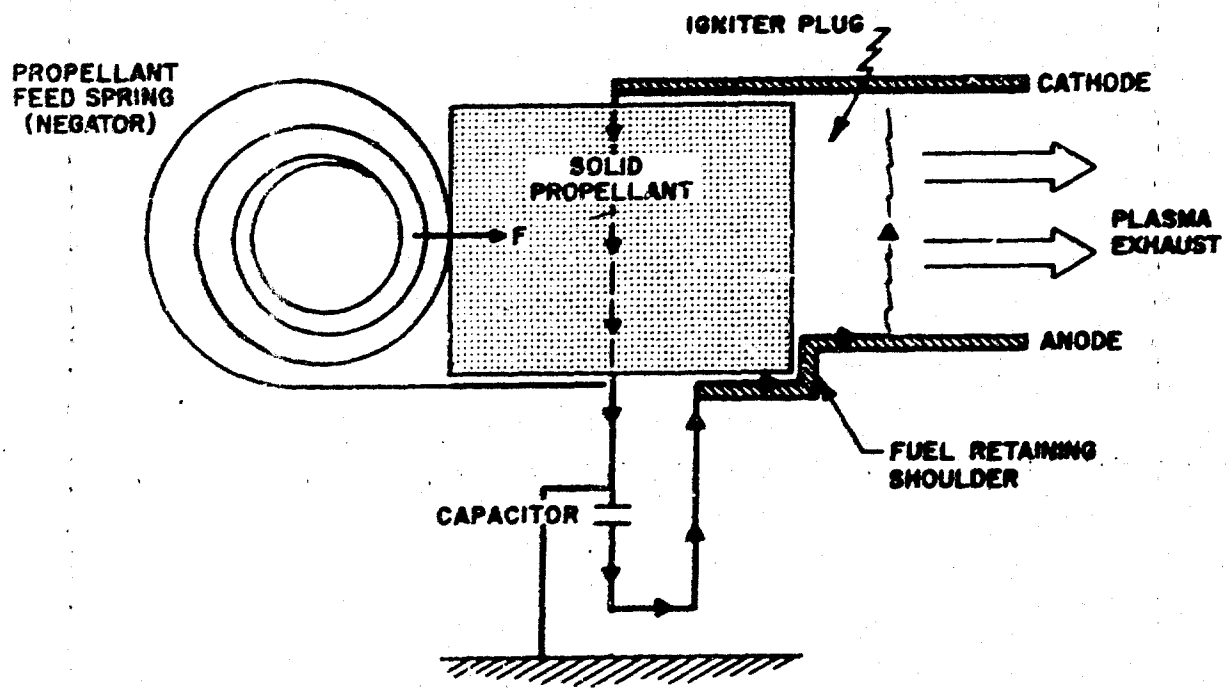

Figure 2. Thruster and Propellant Subsystem Schematic

The terminals of a low inductance energy storage capacitor are connected by a low inductance, low resistance path to the anode and to the cathode

---

* Coaxial electrode nozzle configurations also tested in this program are described by the configuration obtained by revolving the planar section shown in Figure 2 about an axis of symmetry drawn through the anode just below the fuel retaining shoulder.

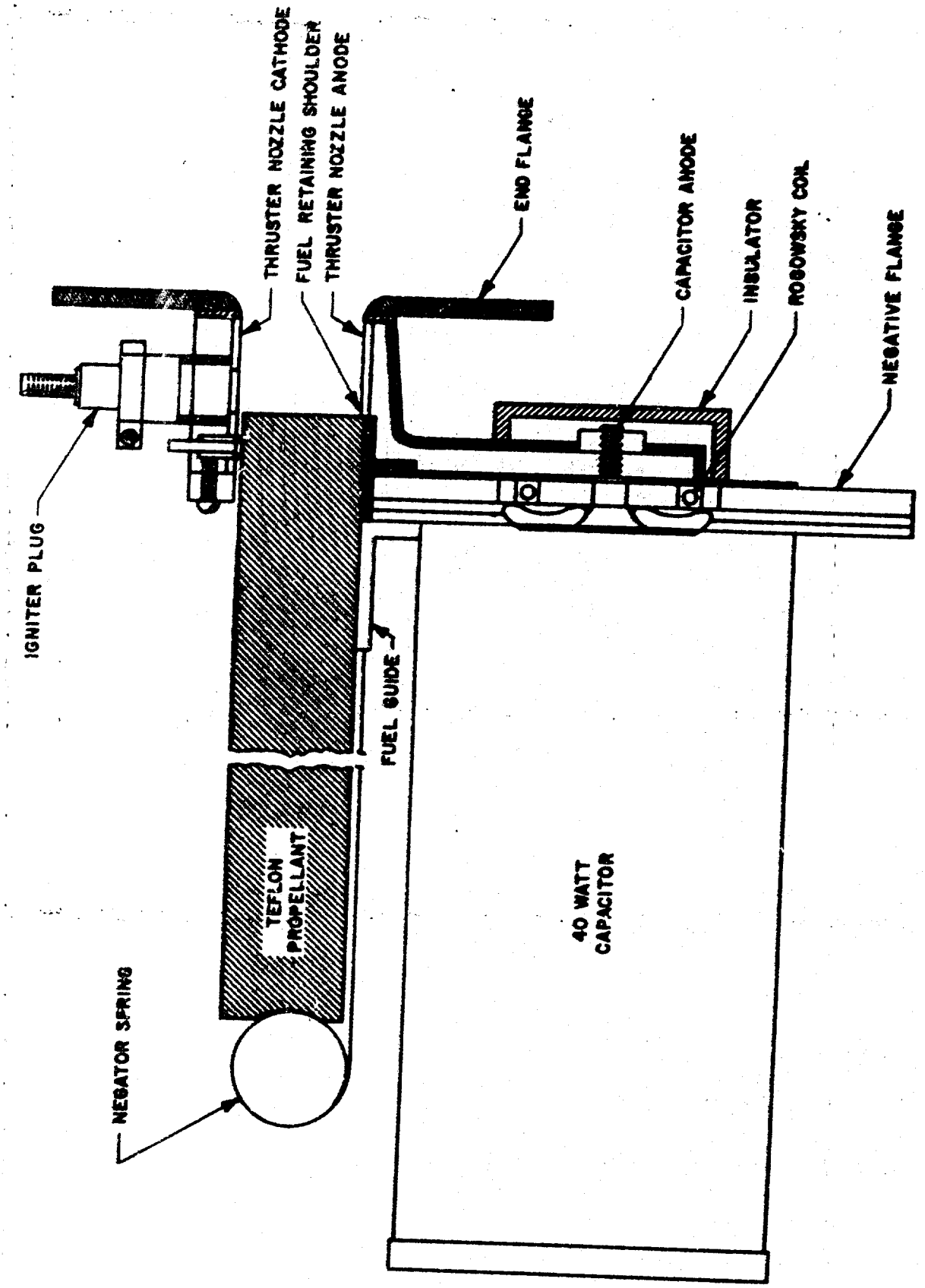

Figure 3. Assembly of Thruster 97E-1

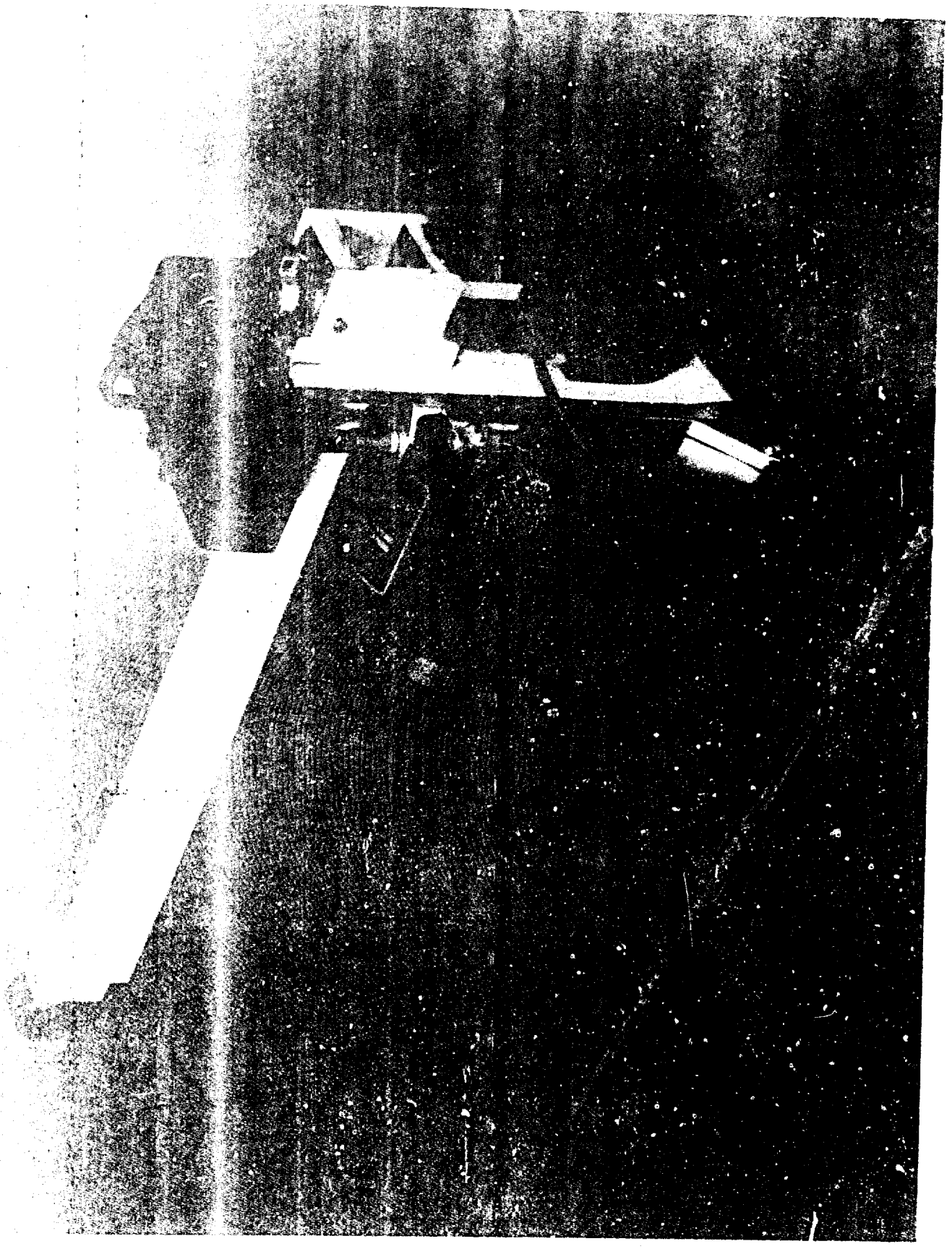

Figure 4. Operational Thruster System

Figure 5. Operational Thruster System

of the thruster nozzle respectively. The anode of the thruster nozzle is provided with a fuel retaining shoulder which properly locates the solid propellant within the thruster nozzle. A constant force steadily provided by a Negator* spring assures that an edge of the propellant is held against the fuel retaining shoulder independent of thruster pulse repetition rate, thruster attitude, thermal environment or absence of gravity.

To generate an impulse bit, the energy storage capacitor is charged to its operating voltage. The applied voltage appears simultaneously across the interelectrode spacing between the anode and cathode of the thruster nozzle. Because of the presence of a vacuum in this interelectrode spacing the applied voltage is retained until the discharge initiating circuitry injects a micro-discharge into the interelectrode spacing. The micro-discharge "closes" the electric circuit and allows the main thruster discharge to deliver energy into the interelectrode spacing without any additional switching gear. This main discharge depolymerizes surface layers of Teflon propellant which in turn becomes energized and ejected through the thruster nozzle.

Since the Teflon also depolymerizes behind the fuel retaining shoulder the Negator spring replenishes the consumed propellant by moving propellant into the region depleted by the previous discharge. This movement is essentially imperceptible, being typically of the order of Angstrom units per discharge. The total amount of Teflon remaining is easily measured by a sliding potentiometer even in zero-g environment.

In one of the tests to be described in Section 3.1 approximately 27 inches of Teflon rod was depolymerized during the test thereby verifying the fuel retaining shoulder concept to be perfectly sound and reliable for long thruster mission times. Since the height of the propellant is made larger than the height of the accelerating electrode nozzle (see Figure 2) it is not possible for the propellant to be ejected through the nozzle by the propellant feed spring even with (negligible) electrode erosion that occurs during extremely long periods of thruster operation.

---

* Hunter Spring, Hatfield, Pennsylvania

Since Teflon is compatible with vacuum environment, the propellant rod is stored directly in vacuum.

2.1.2 Analytic Considerations

Despite the inherent simplicity of the thruster, a detailed analytic description of the thrusting mechanism of the pulsed plasma thruster, briefly described in Section 2.1.1, is a formidable problem. However, some simple idealized calculations can be carried out in the hope of analytically encompassing the salient features of such a thruster. Quite generally, the thrusting action is due to magnetic pressure forces and also due to gas-dynamic pressure forces. If it is assumed that the thrusting action is due to only either one of these mechanisms, one can obtain analytic expressions of thruster performance for such simple idealized cases.

Consider the parallel rail electrode configuration shown in Figure 2 and assume that end effects can be neglected. The electrode nozzle inductance (L) is approximately:

$$L = \mu_o \frac{d}{b} \ell$$

with μ_o the magnetic permeability, d, b, and ℓ the height, width and length of the nozzle, respectively (See Figure 6). The instantaneous magnetic pressure force being exterted on the back wall of the nozzle is:

$$F_1 = P_m A = \frac{B^2}{2\mu} A$$

with P_m the magnetic pressure $(B^2/2\mu)$ and A the area of the back wall. For the geometry under consideration $B = \mu i/b$ and $A = bd$ with i the total current. Hence,

$$F_1 = \frac{\mu i^2}{2} \frac{d}{b}$$

For a pulsed plasma producing thrust by magnetic pressure only, one finds:

$$T = f \int F_1 \, dt = f \frac{\mu}{2} \frac{d}{b} \int_o^t i^2 \, dt$$

$$= f \frac{L'}{2} \int_o^t i^2 \, dt$$

where f and L' denote thruster pulse frequency and nozzle inductance per unit length, respectively. The last expression is also valid for coaxial electrode configurations.

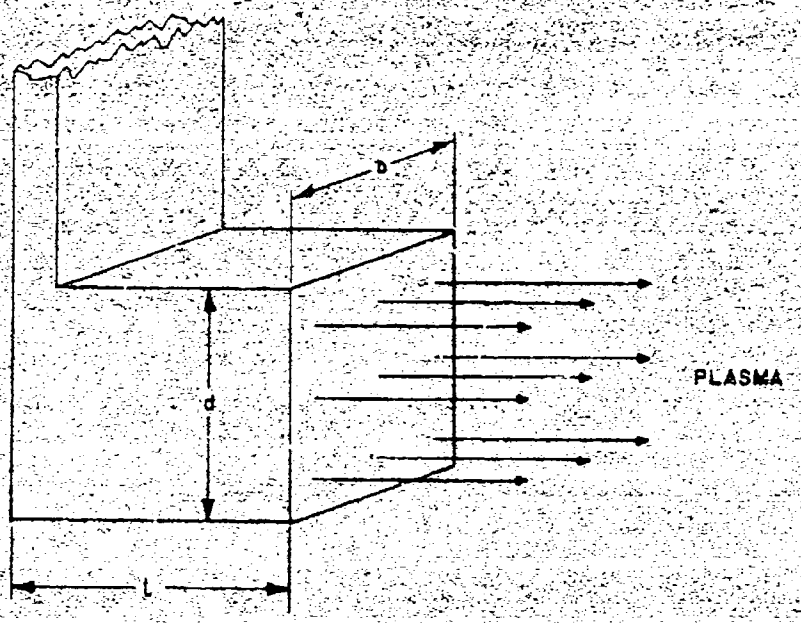

Figure 6. Parallel Rail Electrode Configuration

Consider the discharge circuit to be comprised of a series circuit having fixed values of resistance (R), inductance (L), and capacitance (C). If $R < 2\sqrt{L/C}$, the current will undergo a damped oscillation according to the relation:

$$i = -\frac{V_o}{L} \frac{1}{\sqrt{\frac{1}{LC} - \frac{R^2}{4L^2}}} e^{-\frac{R}{2L}t} \sin \sqrt{\frac{1}{LC} - \frac{R^2}{4L^2}}\, t$$

with V_o the voltage initially stored on the capacitor. This latter equation is of the form:

$$i = \frac{V_o}{L\lambda} e^{-\sigma t} \sin \lambda t$$

Substituting this expression into the generalized thrust equation and performing the appropriate operations produces the relation:

$$T = f\,\frac{L'}{2}\left(\frac{V^2}{L}\right)\frac{1}{4s(\lambda^2 + s^2)}\left[1 - e^{-2st}\left(1 + \frac{s}{\lambda}\sin 2\lambda t + 2\left(\frac{s}{\lambda}\right)^2 \sin^2 \lambda t\right)\right]$$

where:

$$s = R/2L$$

$$\lambda = \sqrt{\frac{1}{LC} - \frac{R^2}{4L^2}}$$

In the limit as $t \to \infty$, one finds the expression for the specific thrust (T/P) to be:

$$\left.\frac{T}{P}\right|_{t\to\infty} \to \frac{L'}{2R}$$

It is interesting to note that according to these idealized simplified considerations specific thrust is essentially independent of capacitor quality Q. The ratio of inductance per unit electrode nozzle length to resistance is the more significant parameter in determining specific thrust. The results suggest that capacitors having the lowest possible internal resistance should be used for optimum thrust. Neglecting weight considerations, this result suggests (at a given energy level) the use of a large number of capacitors connected in parallel instead of a singly wound capacitor. While such an approach reduces not only the resistance, but also the effective inductance, the increase in overall weight resulting from such an approach suggested its use in a limited manner by developing a simple capacitor in which a number of elements were connected in parallel within a given case.

Besides reducing resistance to an absolute minimum for increased specific thrust it is also desirable to have the largest possible inductance per unit nozzle length. Within the accuracy of the present considerations, the inductance per unit nozzle length of a parallel rail and a coaxial nozzle are respectively:

$$L_p = \mu \frac{d}{b}$$

$$L_c = \frac{\mu}{2\pi} \ln \frac{R_o}{r}$$

with d, b, R_o, and r, the spacing between electrodes (see Figure 7) the width of the electrode (see Figure 6), the outer radius and the inner radius of a coaxial nozzle (see Figure 7). Making a comparison of the inductance per unit length for roughly the same thruster nozzle envelope size, one finds:

$$\frac{L_p}{L_c} = \frac{2\pi \, d/b}{\ln \frac{R_o}{r}}$$

with $d/b \simeq 1$, and $0 < \ln R_o/r < 2$ one finds the parallel rail configuration to have a slightly larger inductance per unit nozzle length than the coaxial configuration. Both electrode nozzle configurations have been used in the course of the work being reported upon. While conical electrode nozzle configurations are also considered suitable for thrust generation, such configurations were not examined during the present study.

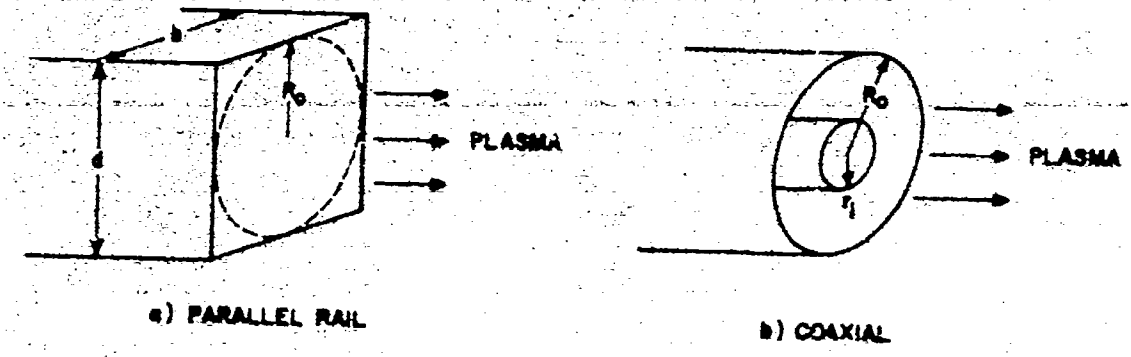

Figure 7. Geometric Variables

Besides the specific thrust, it is also possible to evaluate analytic expressions for specific impulse and thruster efficiency for certain idealized simplified cases, and also expressions for thruster performance assuming the propulsion action to be due to gasdynamics pressure forces only.

2.1.2a - MHD Thrusting

If the propulsive action is due to MHD effects only, the idealized expression for the thrust was shown to be:

$$F = f \frac{L'}{2} \int i^2 dt$$

For a critically damped discharge generated by a series LCR circuit comprised of fixed circuit elements the electric current varies with time as:

$$i = - \frac{V_o}{L} t \exp (- t / \sqrt{LC})$$

with V_o, L, t and C the initial voltage, circuit inductance, time, and capacitance, respectively.

Upon substituting the current expression into the thrust equation and noting that power P equals $f(1/2\, CV^2)$, it can be shown that:

$$\frac{T}{P} \propto \frac{L'}{L/C}$$

For a critically damped discharge the resistance R equals $2\sqrt{L/C}$, hence one can also write:

$$\frac{T}{P} \propto \frac{L'}{R}$$

It is seen that specific thrust of a critically damped discharge also varies directly with inductance per unit nozzle length and inversely with circuit resistance. The conclusions reached for the case of an oscillating current also apply to the case of a critically damped circuit.

Since specific impulse (I_{sp}) is defined by the expression:

$$I_{sp} = T/\dot{W}$$

with T and $\dot{W}$ the thrust and propellant weight flow rate respectively, it is seen that:

$$I_{sp} \propto \frac{L'}{R} \frac{E}{m}$$

with E and m the discharge energy and propellant mass consumed per discharge respectively. This latter expression shows that if propulsive action is due to MHD effects only, it is expected that specific impulse should vary with discharge energy per unit propellant mass.

The thruster efficiency* η is defined as:

$$\eta = \frac{T^2}{2\dot{m}P} = \frac{g}{2}\frac{T}{P} I_{sp}$$

From the relations derived above, it is seen that the efficiency is expected to vary as:

$$\eta \propto \left(\frac{L}{R}\right)^2 \frac{E}{M}$$

One obvious way to increase thrust efficiency, holding all other factors constant, is simply to increase discharge energy. Such an approach can readily be carried out but usually at the expense of system weight. Since efficiency varies with the square of the inductance per unit nozzle length and inversely with the square of the resistance, it appears more desirable to increase efficiency by decreasing circuit resistance and increasing nozzle inductance per unit length even though in practice this latter approach is more difficult to carry out than increasing the discharge energy.

2.1.2b Gasdynamic Pressure Thrust (Expansion Thruster)

If the propulsive action of the thruster is due to gasdynamic

---

* This should not be confused with calorimetric efficiency (see Reference 2).

pressure forces only it becomes possible to postulate an idealized simplified one-dimensional nonsteady analytic model of events occurring in the thruster and to obtain analytic expressions for the propulsion performance. Consider a stationary element of fluid of mass m, of volume V and being given an amount of energy E in a time short compared to the time it takes for fluid to expand into a vacuum. Assume the initial thickness of the element sufficiently thin such that nonsteady pressure waves rapidly traverse the fluid element. A quasi-steady analysis can then be carried out by considering all quantities uniform at any instant but that these quantities may vary from one instant to another. Since the fluid expands into a vacuum the expansion process can be considered isentropic. Within the spirit of the analysis it is also reasonable to assume that at any instant the instantaneous mass averaged flow velocity equal to the sonic velocity* of the expanding fluid element of uniform conditions evaluated at the same instant. For such an "expansion" thruster one can proceed as follows:

The mass flow rate of the gas expanding into the vacuum is thus:

$$dm/dt = V\ d\rho/dt = \rho^* A^* a^*$$

with ρ^*, A^*, and a^* the instantaneous mass density, the area of outflow and the instantaneous speed of sound respectively. Since $a = a_o (\rho/\rho_o)^{(\nu-1)/2}$ the density of the element of mass is found to be:

$$\frac{\rho}{\rho_o} = \left[1 + \frac{\nu-1}{2} \left(\frac{2}{\nu+1} \right)^{\frac{\nu+1}{2(\nu-1)}} \frac{a_o A^*}{V} t \right]^{-\frac{2}{\nu-1}}$$

The propulsive parameters for the idealized unsteady expansion thruster can now be readily evaluated.

The instantaneous stream force F_i (or reaction force) is:

$$F_i = p^* A^* + \rho^* A^* u^{*2}$$

---

* The mass averaged velocity of elements of a centered rarefaction wave of an ideal fluid is equal to $(2/\nu)\, a_o$ with a_o the initial speed of sound and ν the ratio of specific heats.

which for sonic outflow becomes:

$$F_1 = p^* A^* \quad (1 + \nu)$$

The impulse derived by expelling the quantity of mass -m- is given by the expression:

$$I = \int_0^\infty F_1 \, dt = A^* \int_0^\infty (\nu + 1) \, p^*(t) \, dt$$

Noting that the flow is isentropic, one finds:

$$I = \frac{2 p_o V}{a_o} \left(\frac{2}{\nu + 1} \right)^{1/2}$$

where the initial pressure p_o and speed of sound a_o are related to the energy added prior to the expansion process. Since relatively large temperature changes occur as a result of energy addition, the initial temperature can be neglected compared to the final fluid temperature. Hence one can write:

$$a_o \approx \sqrt{(E/m)(\nu - 1)}$$

and within the assumptions of an ideal fluid:

$$p_o V_o = (\nu - 1) \, E/\nu$$

Hence the impulse bit can be expressed as:

$$I = (\nu - 1)^{1/2} \, 2\nu^{-1} \, m \, (E/m)^{1/2} \, (2/\nu + 1)^{1/2}$$

If the propulsive performance is due to only a nonsteady gasdynamic expansion process, then the specific thrust (thrust to power ratio) becomes:

$$\frac{T}{P} = \frac{I}{E} \propto \frac{1}{\sqrt{E/m}}$$

or, the specific thrust is found to vary inversely with the square root of the energy per unit mass.

The average specific impulse (I_{sp}) of the entire discharge is:

$$I_{sp} = \frac{T}{\dot{W}} = \frac{I}{W}$$

or

$$I_{sp} \propto \sqrt{E/m}$$

It is interesting to note that specific impulse is found to vary as the square root of E/m if the thruster behaves as only a nonsteady gasdynamic expansion thruster and directly as E/m if it derives thrust by magnetic pressure only.

It can readily be shown that subject to the assumptions invoked, the nonsteady gasdynamic expansion thruster will have a thrust efficiency equal to:

$$\eta = \frac{T^2}{2 \dot{m} P} = \frac{\gamma - 1}{\gamma^2} \left(\frac{4}{\gamma + 1} \right)$$

or a function of the specific heat of the fluid. Sonic flow limits the efficiency.

The above idealized considerations suggest certain parameters that ought to govern thruster performance. An experimental diagnostic program was carried out during which a wide variation in parameters were introduced in order to check the usefulness of the idealized considerations in the thruster design.

2.1.2c Gasdynamic Expansion Nozzle Considerations

As indicated above, it is believed that the thruster delivers thrust because of gasdynamic pressure forces and MHD forces. The question can be raised whether or not the addition of an expansion nozzle will affect the thrust level by converting thermal energy to kinetic energy. If the thruster delivered thrust only due to MHD forces the addition of an expansion cone would not affect the thrust level (other than perhaps even reducing the thrust level slightly due to wall viscous losses). Thus it is of interest to determine by simple calculations the possible effect of an expansion nozzle on thrust magnitude.

In the simple calculations presented below it is assumed that viscous effects are absent, that the plasma exhaust is always in thermal equilibrium, that the solid particles of the plasma are sufficiently small so that the plasma behaves as an ideal gas and that the thermogasdynamical properties of the pulsed plasma in any plane normal to the thrusting direction vary as a square wave. This last assumption is probably the least valid of the assumptions made. However, it permits the simplest calculation to be carried out concerning the effect of an exhaust cone on thrust level.

The effect on thrust of an "ideal" expansion nozzle compared to no expansion is found as follows:

The thrust level T of the pulsed device is given by:

$$T = fI$$

with f the pulse frequency and I the impulse per pulse. For a square wave the impulse will equal the product of the instantaneous force F_i and the duration of the pulse τ, i.e.,

$$T = fI = f \int F_i \, d\tau$$

For the case under consideration the pulse frequency f and duration τ are constants, respectively. Hence one needs to examine the instantaneous force F_i only. This latter quantity is given by:

$$F_i = \int_A (P - P_\infty) \, dA + \int_A \rho u^2 \, dA$$

where P and P_∞ denote the pressure in the exhaust plane and the ambient pressure respectively. The quantities ρ and u denote the mass density and velocity in the exhaust plane, respectively. The integration is carried out across the exit plane A of the exhaust. Under the assumption of a square wave type of exhaust, the last expression reduces to:

$$F_i = (P - P_\infty) A + \dot{m} u_e$$

where $\dot{m} = \rho u A$ is the mass flow rate. If the exhaust is expanded to match the pressure of a perfect vacuum, one finds:

$$F_i = P_e A_e + \dot{m} u_e = P_e A_e (1 + \nu M_e^2)$$

where ν, A_e and M_e denote the ratio of specific heat, exit area and discharge Mach number respectively. If no expansion nozzle is used, the exit Mach number will equal unity and one finds:

$$F_i^* = (\nu + 1) P^* A^*$$

which can readily be reduced to:

$$F_i^* = \frac{P_o A^* (\nu + 1)}{(\frac{\nu+1}{2})^{\nu/\nu-1}}$$

where A^*, P_o are the final exit area (throat area) and initial stagnation pressure respectively. If an ideal expansion nozzle is used, $P_e = 0$ and,

$$F_{i\,max} = \dot{m}^* u_{max}$$

where the maximum exhaust velocity is found from thermal considerations to be:

$$u_{max} = \sqrt{\frac{2 \nu R T_o}{\nu - 1}}$$

where R and T_o denote gas constant and initial stagnation temperature respectively. Thus, one finds:

$$F_{i\,max} = \frac{\nu P_o A^*}{(\frac{\nu+1}{2})^{\nu/\nu-1}} \sqrt{\frac{\nu + 1}{\nu - 1}}$$

The ratio of the maximum instantaneous force to the value one obtains with no expansion cone is then:

$$\frac{F_{i\,max}}{F_i^*} = \sqrt{\frac{\nu^2}{\nu^2 - 1}}$$

or a function of the ratio of specific heats only. For rocket exhausts a value of 1.23 is typical. Hence:

$$\frac{F_{i\,max}}{F_i^*} \simeq 1.73 \quad (\text{if } \nu = 1.23)$$

This result shows that a 73% increase in thrust can be expected by the addition of an "ideal" nozzle. Such an increase warrants some further consideration regarding the thrust increase that could be expected if a nozzle is added which is not ideal (i.e., which does not have an infinite exit area to throat area ratio).

If the nozzle does not fully expand the exhaust, one will discharge into ambient vacuum from some finite area nozzle. The instantaneous force is thus:

$$F_i = P_e A_e (1 + \nu M_e^2)$$

$$= P_o A^* \frac{P_e}{P_o} \frac{A_e}{A^*} (1 + \nu M_e^2)$$

The ratio of this force to the force obtained with no nozzle becomes:

$$\frac{F_i}{F_i^*} = \frac{1}{\nu + 1} \left(\frac{\nu + 1}{2}\right)^{\nu/\nu - 1} \frac{P_e}{P_o} \frac{A_e}{A^*} (1 + \nu M_e^2)$$

This expression is most readily evaluated by referring to compressible flow tables in which case it is easier to use the alternate expression:

$$\frac{F_i}{F_i^*} = \frac{\frac{P_e}{P_o} \frac{A_e}{A^*} (1 + \nu M_e^2)}{\frac{P^*}{P_o} (\nu + 1)} = \frac{\text{vacuum thrust coefficient}}{(P^*/P_o) \quad (\nu + 1)}$$

Selecting values of M_e one finds values of A_e/A^* and P_e/P_o from the tables. Table 1 presents some values of F_i/F_i^* for values of:

ν = 1.4, 1.23, and 1.18, respectively.

The results presented in Table 1 show that the effect of variable ν on F/F_i^* at a given area ratio A_e/A^* does not have too significant effect in the value of F/F_i^*. Similarly, it is seen that for a given value of ν increasing the area ratio from 10 to 24 will not significantly affect the thrust. However, it is seen that for area ratios of about 10 to 20 one can expect roughly 30% increase in thrust compared to the case of no nozzle. This latter result is significant enough to justify looking at the effect upon thrust of an expansion cone on the pulsed plasma microthruster.

TABLE 1. Effect of Idealized Expansion Cone Upon Performance

$\frac{A_e}{A^*}$	$\frac{F}{F_i^*}_{\nu=1.4}$	$\frac{F}{F_i^*}_{\nu=1.23}$	$\frac{F}{F_i^*}_{\nu=1.18}$
1	1	1	1
2	1.16	1.18	1.18
3	1.20	1.24	1.26
5	1.25	1.31	1.34
9	1.29	1.38	1.41
10	1.30	1.39	1.41
14	1.32	1.42	1.45
20	1.33	1.44	1.48
24	1.34	1.46	1.50
50	1.36	1.50	1.56

2.1.2d Thrust Vector Control by Plasma Exhaust Beam Deflection

The possibility of exerting forces on plasmas by means of large magnetic fields is the basis of much of our present day plasma technology. The varied applications of this principle include confinement pressure on thermonuclear plasmas as well as acceleration forces in plasma guns. The configurations of magnetic field and plasma which may be utilized in thrust vector control of electric engine exhause are numerous; and each configuration must be analyzed to allow

optimization. Here, however, an attempt will be made only to place overall bounds on energy requirements and to estimate the magnitude of the effect which can be expected of a pulsed plasma thruster.

The minimum energy requirement in establishing a magnetic field is the actual energy density in the field integrated over the volume in which the field exists. Of course in practice circuit losses must be also supplied. If these are neglected, the energy supplied is:

$$\frac{B^2}{8\pi} V \text{ in ergs}$$

where B is the magnetic induction in gauss and V is the volume in cubic centimeters. If the volume of the plasma is spherical, and if it is further supposed that the magnetic field is negligibly small over volumes larger than the plasma, then the volume V may be assumed to be $4/3\ \pi r^3$ where r is the radius of the sphere of plasma. Then the energy in the field is:

$$\frac{B^2}{8\pi} (4/3\ \pi r^3) = \frac{B^2}{6} r^3$$

Now in some ideal configuration the force exerted by the field on this plasma is the "magnetic pressure", $B^2/8\pi$, times the projected area of the sphere πr^2 or:

$$\frac{B^2}{8\pi} (\pi r^2) = \frac{B^2}{8} r^2$$

Let it be further assumed that the energy available for vector control ε is some fraction of the energy presently available for production of thrust. Then:

$$\varepsilon = \frac{B^2}{6} r^3 \qquad (1)$$

and the force exerted is:

$$F = \frac{B^2}{8} r^2 \qquad (2)$$

In terms of Equation (1):

$$F = \frac{3}{4} \frac{\varepsilon}{r} \qquad (3)$$

The impulse which can be exerted by the field is Ft, where t is the duration of time in which the field exerts a force on the sphere of plasma. This is roughly the time of passage of the plasma through the field. If the velocity of the plasma is v, then:

$$t = \frac{2r}{v} \tag{4}$$

and,

$$Ft = \frac{3}{2} \frac{\epsilon}{v} \tag{5}$$

To be useful, the impulse Ft produced in Equation (5) must be a substantial fraction of the normal reaction thrust produced during operation of the engine. For a typical engine (Log 98E-5), the total energy utilized in a discharge is 21 joules. The velocity of the plasma 5.9×10^5 cm/sec. The impulse produced per discharge is 30.2 dyne-sec. If ϵ is permitted to be 2.1 joules or 2.1×10^7 ergs, then:

$$Ft = \frac{3}{2} \frac{(3.1 \times 10^7)}{5.9 \times 10^5} = 53 \text{ dyne-sec.}$$

Thus, the calculated Ft, the sideward impulse produced by the magnetic field, is of the same order as the backward thrust produced by the discharge. The calculated Ft is of course an over-estimate since all losses were neglected and it was assumed that the magnetic field could be limited to the volume of the plasma. However, if even ten percent of this sideward impulse can be produced, this method will be feasible.

2.1.3 Generalized Thruster Data Realized

The experimental data to be presented was obtained with thrusters tested in relatively large vacuum chambers compared to the thruster and its exhaust plume. All thrust data was obtained on a thrust balance. A typical laboratory setup of a test is shown in Figures 8 and 9, respectively. Details of this thrust balance are presented in Section III. Calibrations of the thrust stand were always taken prior to the thrust measurement with the thruster mounted on the thrust balance in a vacuum environment. The calibration and thrust reading can be obtained within a few minutes during the course of any given test. Any performance data

involving specific impulse was obtained with a thruster operating continuously for at least four hours. All specific impulse figures represent the value describing the complete test independent whether the test duration was four hours or several months.

A large number of thruster tests have been carried out during the course of the present program. These tests encompassed a relatively large number of variables, many of these suggested by the idealized analytic considerations presented in the previous sections. Some of the more relevant variables being:

a) Discharge energy
b) Pulse rate
c) Propellant frontal area
d) Electrode geometry (parallel rail or coaxial)
e) Electrode nozzle length
f) Exhaust cone geometry
g) Electrode material
h) Capacitor design of several manufacturers
i) Varying capacitor inductance and resistance

Some of the pertinent parameters of a number of tests are presented in Tables 2a and 2b, respectively.

This section presents those parameters which describe thruster performance more generally.

2.1.3a Energy Per Unit Mass and Energy Per Unit Area

The idealized analytic considerations of the previous section suggest the parameter discharge energy per unit propellant mass (E/M) useful for correlating experimental data. Some very elementary considerations suggested that this parameter might be directly related to the discharge energy per unit propellant frontal area (E/A). This latter parameter is a more useful parameter to use than the former in thruster design. Figure 10 presents the variation of E/M with E/A determined from experiments involving a large variation in thruster parameters. Indeed, there appears to exist a reasonably good correlation between

TABLE: 2a THRUSTER TESTS WITH VAR
(All tests at least 8 hours of continuo

E_d = Energy per discharge in joules — ϵ/A = Energy/Area, joule
I_d = Impulse per discharge, μ lb-sec. — W = Propellant consume
A_f = Fuel frontal area, in^2 — ϵ/M = Energy/mass, joule

Log No.	Config.	E_d	I_d	I_{sp}	η	A_f	Capac. Mfg.	W
38	Coax	1.65	5.89	211	1.64	2.531	Corson	2.8
39	Coax	6.6	28.3	386	3.62	2.531	Corson	7.3
40	Coax	13.2	54.5	527	4.76	2.531	Corson	10.3
45	Coax	13.45	50.4	584	4.77	1.178	Corson	8.6
47	Coax	20.8	71.06	785	5.84	0.664	Corson	9.0
52	Coax	1.65	1.87	412	1.01	0.393	Corson	0.4
53	Coax	1.65	5.73	200	1.52	1.227	Corson	2.8
54	Coax	1.50	4.0	185	1.07	1.227	Corson	2.1
56	Coax	17.3	85.4	1200	13.0	0.393	Corson	7.1
57	Coax	6.6	17.0	1090	6.1	0.147	Corson	1.5
58	Coax	20.15	81.7	1225	10.8	0.393	Corson	7.3
59	Coax	6.6	15.4	1010	5.16	0.101	Corson	1.4
60	Coax	23.93	128.0	1740	20.4	0.393	Bendix	7.3
61	Coax	12.0	27.1	1300	6.0	-	Bendix	2.0
62	Coax	23.95	76.4	2400	16.7	0.0824	Bendix	3.1
63	Coax CF	23.93	62.3	1430	8.1	0.00952	Bendix	4.3
65	Coax CF	30.47	77.4	1385	11.4	0.469	Maxwell	5.3
71	11 rail	21.16	81.2	1760	14.7	0.281	Maxwell	4.6
73	11 rail	21.0	97.5	1530	15.5	0.282	Bendix	6.3
74-76	11 rail	21.0	66.0	1350	9.25	0.281	Bendix	4.3
80	11 rail	6.75	9.85	900	2.86	0.141	Corson	1.5
81	11 rail	21.0	51.0	950	5.02	0.281	Bendix	5.3
84	11 rail	20.6	45.0	1280	6.09	0.156	Maxwell	3.3

A

TER TESTS WITH VARYING PARAMETERS
east 8 hours of continuous operation)

= Energy/Area, joules/in^2

= Propellant consumed/discharge, lb

= Energy/mass, joules/lb

I_{sp} = Specific impulse, sec.

η = Thrust efficiency, $T^2/2mP$, in %

Capac. = Capacitance, μ fd

	Capac. Mfg.	$W = \frac{I_d}{I_{sp}}$	Capac.	No. Cap.	ϵ/M	Elect. Material	ϵ/A
1	Corson	2.84×10^{-8}	3.3	1	0.582×10^5	Steel-Al	0.65
1	Corson	7.33×10^{-8}	3.3	4	0.91×10^8		2.6
1	Corson	10.3×10^{-8}	3.3	8	1.28×10^8		5.22
3	Corson	8.64×10^{-8}	7.5	8	1.56×10^8	Steel-Tantalum	11.4
4	Corson	9.06×10^{-8}	7.5	12	2.3×10^8	Steel-Tantalum	31.4
2	Corson	0.45×10^{-8}	3.3	1	3.67×10^8	Brass-Al	4.2
7	Corson	2.86×10^{-8}	3.3	1	5.8×10^7	Molyb-Al	1.35
7	Corson	2.16×10^{-8}	1.5	2	6.95×10^7	Molyb-Al	1.22
3	Corson	7.1×10^{-8}	3.3	12	4.2×10^8	Brass-Al	44.0
	Corson	1.56×10^{-8}	3.3	4	4.22×10^8	Brass-Al	44.8
	Corson	7.33×10^{-8}	1.5	12	2.74×10^8	Brass-Al	51.3
	Corson	1.52×10^{-8}	3.3	4	4.35×10^8	Molyb-Al	65.3
	Bendix	7.35×10^{-8}	18.7	1	3.26×10^8	Molyb-Al	61.0
	Bendix	2.08×10^{-8}	18.7	1	5.78×10^8	SS-Al	-
4	Bendix	3.18×10^{-8}	18.7	1	2.55×10^8	Molyb-Al	292.0
52	Bendix	4.35×10^{-8}	18.7	1	5.52×10^8	Tantalum-Al	2400.0
	Maxwell	5.58×10^{-8}	18.2	1	3.68×10^8	Moly-Al	43.7
	Maxwell	4.6×10^{-8}	18.9	1	4.6×10^8	Al-Al	75.0
	Bendix	6.36×10^{-8}	18.7	1	3.2×10^8	Al-Al	74.5
	Bendix	4.88×10^{-8}	18.7	1	4.3×10^8	Al-Al	75.0
	Corson	1.09×10^{-8}	1.5	4	6.2×10^8	17-ph	48.0
	Bendix	5.37×10^{-8}	18.7	1	3.9×10^8	17-7 ph	74.8
	Maxwell	3.51×10^{-8}	18.05	1	5.86×10^8	Al	132.0

B

TABLE 26. THRUSTER TESTS WITH VARYING PA
(All tests at least 8 hours of continuous opera

E_d = Energy per discharge in joules

I_d = Impulse per discharge, μ lb-sec.

A_f = Fuel frontal area, in^2

ϵ/A = Energy/Area, joules/in^2

W = Propellant consumed/discharge,

ϵ/M = Energy/mass, joules/lb

Log No.	Config.	E_d	I_d	I_{sp}	η	A_f	Capac. Mfg	W
88E-5	11 rail	21.0	71.0	640	4.7	1.00	Maxwell	11.
86D15	11 rail	4.78	9.5	671	2.9	0.141	Corson	1.
86D13	11 rail	9.68	22.9	930	4.78	0.141	Corson	2.
86D16	11 rail	9.68	23.2	1140	5.96	0.141	Corson	2.
91X2	11 rail	1.84	6.0	210	1.49	1.265	Dearborn	2.
86D14	11 rail	4.78	8.66	608	2.39	0.141	Corson	1.
89D8	11 rail	24.2	58.0	1140	5.98	0.562	Sprague	5.
95X1	11 rail	1.86	5.1	204	1.22	0.618	Dearborn	2.
96X1	11 rail	1.85	5.08	220	1.3	0.45	Dearborn	2.
99X1	11 rail	1.85	4.55	319	1.71	0.40	Dearborn	1.
96X3	11 rail	1.85	7.1	251	2.1	0.45	Dearborn	2.

A

ESTS WITH VARYING PARAMETERS (continued)
hours of continuous operation)

Area, joules/in^2

nt consumed/discharge, lb

mass, joules/lb

I_{sp} = Specific Impulse, sec.

η = Thrust efficiency, $T^2/2mP$, in %

Capac. = Capacitance, μ fd

	Capac. Mfg	$W = \frac{I_d}{I_{sp}}$	Capac.	No. Cap.	¢/M	Elect. Material	¢/A
	Maxwell	11.1×10^{-8}	18.6	1	1.89×10^8	430 SS	21.0
d	Corson	1.42×10^{-8}	1.5	3	3.37×10^8	Al-Al	34.0
l	Corson	2.46×10^{-8}	1.5	6	3.93×10^8	Al-Al	68.5
l	Corson	2.03×10^{-8}	1.5	6	4.75×10^8	Al-Al	68.5
3	Dearborn	2.86×10^{-8}	1.88	1	$.64 \times 10^8$	17-7ph	1.45
	Corson	1.42×10^{-8}	1.5	3	3.37×10^8	Al-Al	33.8
	Sprague	5.08×10^{-8}	23.4	1	4.76×10^8		43.0
	Dearborn	2.5×10^{-8}	1.9	1	$.74 \times 10^8$	17-7 ph	3.0
	Dearborn	2.31×10^{-8}	1.9	1	$.8 \times 10^8$	17-7 ph	4.5
	Dearborn	1.92×10^{-8}	2.05	1	1.3×10^8	17-7 ph	4.6
	Dearborn	2.82×10^{-8}	1.9	1	$.65 \times 10^8$	17-7 ph	4.1

B

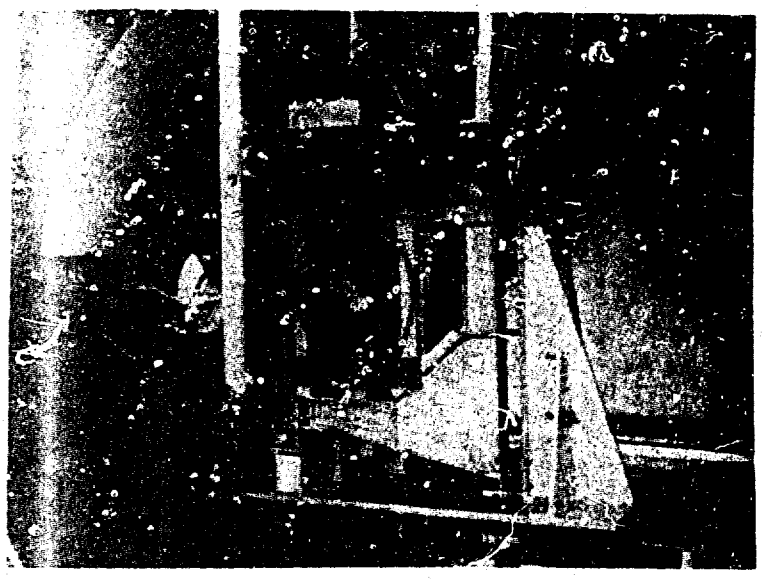

Figure 8. Typical Thruster on Thrust Stand in Vacuum Chamber

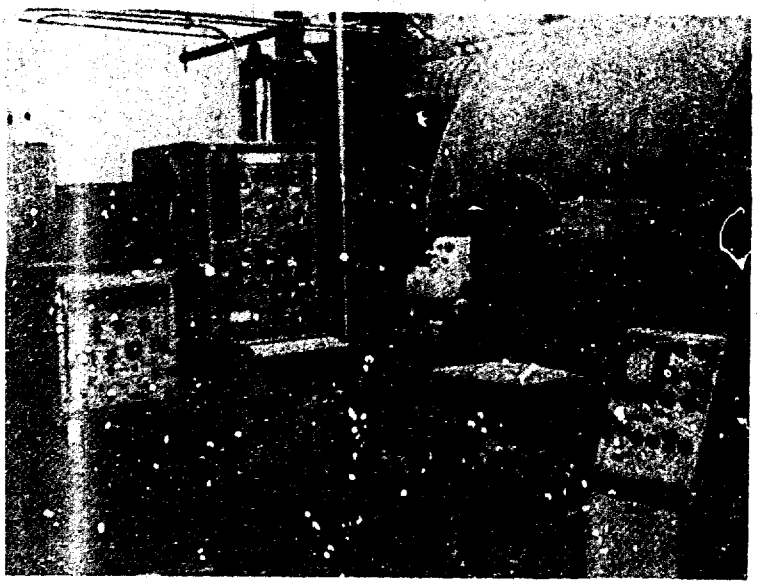

Figure 9. Typical Thrust Recording and Calibration Set-up Exterior to Vacuum Chamber

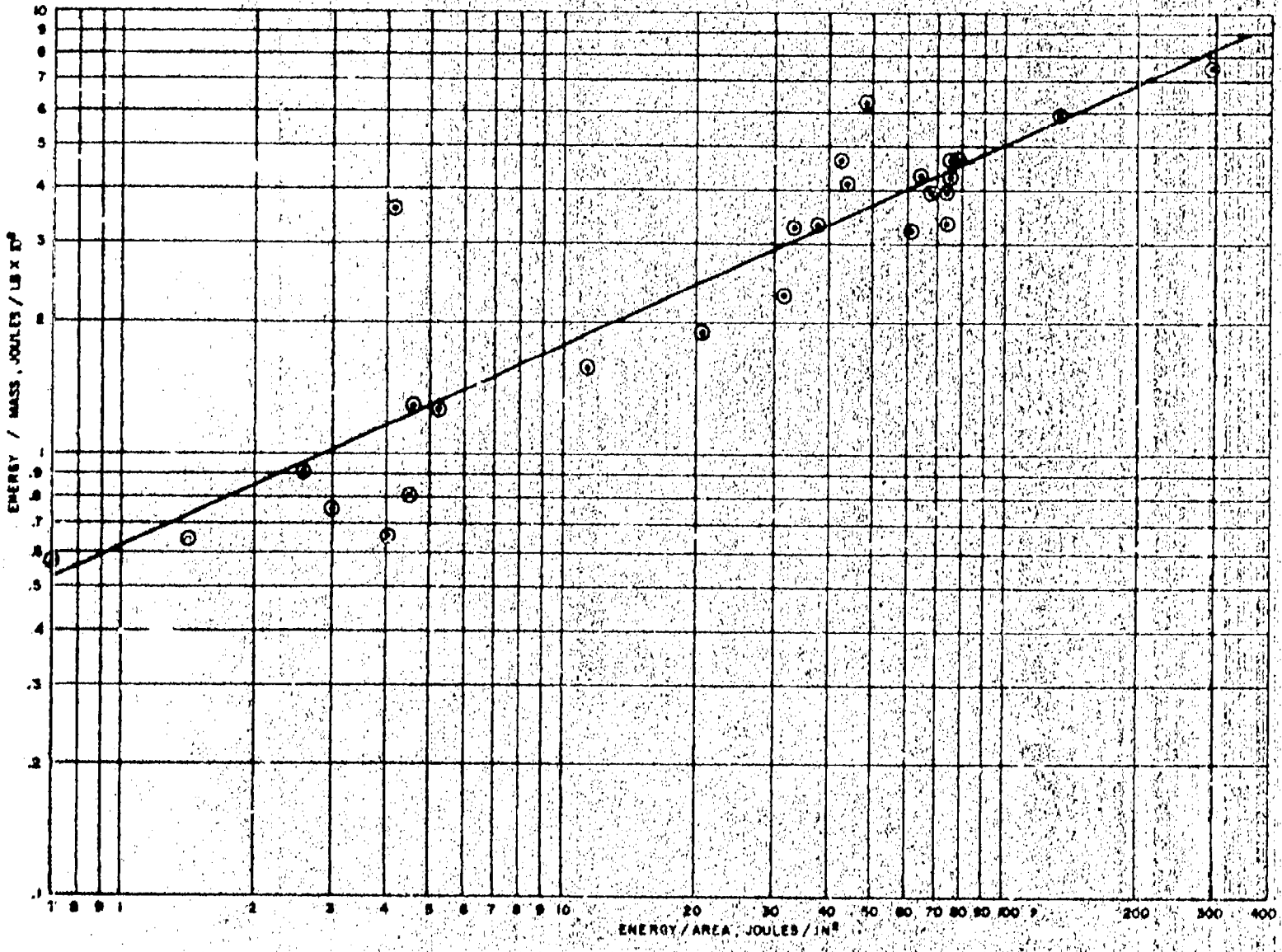

Figure 10. Energy/Mass vs. Energy/Area

these two parameters when the E/M ratio varied over the range 0.58×10^8 joules/lb to 7.55×10^8 joules/lb as the E/A ratio was varied over the range from 0.65 joules/in^2 to 132 joules/in^2. No attempt was made to determine the smallest value of these parameters for which depolymerization would be incomplete (i.e., form a char on the surface of the Teflon).

2.1.3b Specific Impulse and Energy Per Unit Area

Motivated by the idealized analytic considerations, it was desirable to experimentally establish the variation of specific impulse with energy per unit area (i.e., energy per unit area).

Figure 11 presents the specific impulse as a function of the energy per unit area ratio (E/A). The experimental results show that a reasonably good correlation does exist between the specific impulse with the ratio energy-per-unit-propellant area. Very approximately:

$$I \approx 135 \sqrt{E/A}$$

where the energy is expressed in joules and the area in square inches. It is seen that for a specific impulse above 500 seconds, the energy per unit frontal area of the propellant should exceed roughly 15 joules/in^2. A specific impulse in excess of 1000 seconds can be achieved by operating the thrusters at a ratio in excess of roughly 50 joules/in^2.

Sufficient experimental data at a specific impulse in excess of 1000 seconds has been obtained verifying that the solid propellant pulsed plasma microthruster is capable of producing a specific impulse in excess of 1000 seconds. During the course of the present investigation a specific impulse of 2400 seconds was experimentally achieved with Teflon*. A specific impulse in excess of several thousand seconds could be generated should it be so desirable.

---

* Higher values of specific impulse have been observed with other propellants during exploratory experiments carried out during the final phases of the present program.

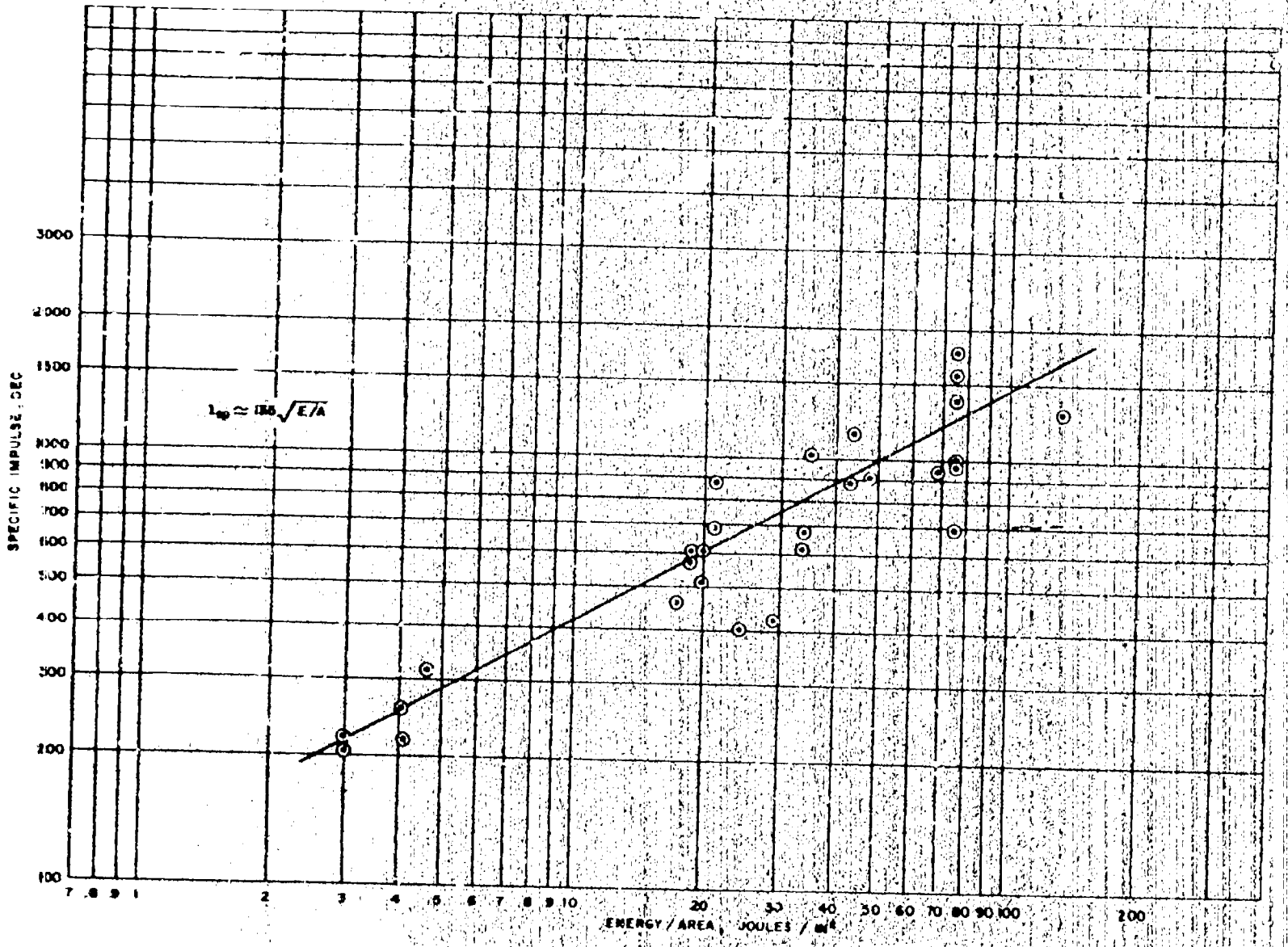

Figure 11. Specific Impulse as a Function of Discharge Energy per Unit Propellant Area

The variation in specific impulse at a given value of the discharge energy per unit propellant area that can be noted in Figure 11 can usually be attributed to geometric changes in the accelerating portion and the expansion area of a thruster nozzle.

2.1.3c Specific Impulse, Specific Thrust and Nozzle Length

The specific impulse of a given thruster operating at a given value of energy per unit area can be varied simply by varying electrode nozzle length (the dimension ℓ in Figure 6). Figure 12 shows the specific impulse to be increased by roughly a factor of 2 as the electrode length was varied from three inches to about 0.25 inches in length. The experimental study was carried out with a given thruster operated at two different energy levels (i.e., two values of E/A). It is also of interest to note at this point that the specific thrust was also found to increase as the nozzle length was decreased (see Figure 13). These latter results show that significant performance improvements can be realized by optimizing the electrode nozzle length. Such an optimization was not carried out during the present study since the program sought to present the broad features and capabilities of the thruster rather than optimizing the thruster for some particular power level of operation.

2.1.3d Specific Thrust and Capacitor Resistance

Besides the variation of specific impulse with energy-per-unit-mass (i.e., energy-per-unit-area), the idealized considerations suggested a dependency between specific thrust and the inverse of discharge circuit resistance. The experiment considered most relevant to the present effort involved the effect of capacitor resistance upon specific thrust for an otherwise identical discharge circuit. Capacitors of roughly the same rating were procured from several manufacturers. These capacitors were inserted in a given thruster circuit and the performance was determined. Table 3 presents the pertinent parameters and the results of this test.

The limited amount of experimental data presented in Table 3 shows that capacitors with roughly the same resistance generated roughly the same

TABLE 3. SPECIFIC THRUST - CAPACITOR RESISTANCE STUDIES

Capacitor Manufacturer	Capacitance (microfarad)	Discharge Energy (joules)	Capacitor Resistance (ohms)	Thrust/Power (μ lb/watt)	Capacitor Inductance (H)	Capacitor Quality $Q = \frac{\omega L}{R}$
A	18.4	20.7	0.045	0.497	11.2×10^{-9}	1.73
B	15.2	17.1	0.027	1.54	59.5×10^{-9}	2.31
B	23.6	26.5	0.00435	2.45	26.8×10^{-9}	7.75
C	20.0	22.5	0.00423	2.35	19.4×10^{-9}	7.42
D	18.65	21.0	0.0041	2.45	24.4×10^{-9}	8.9
B	21.43	24.1	0.00362	2.4	19.95×10^{-9}	8.53

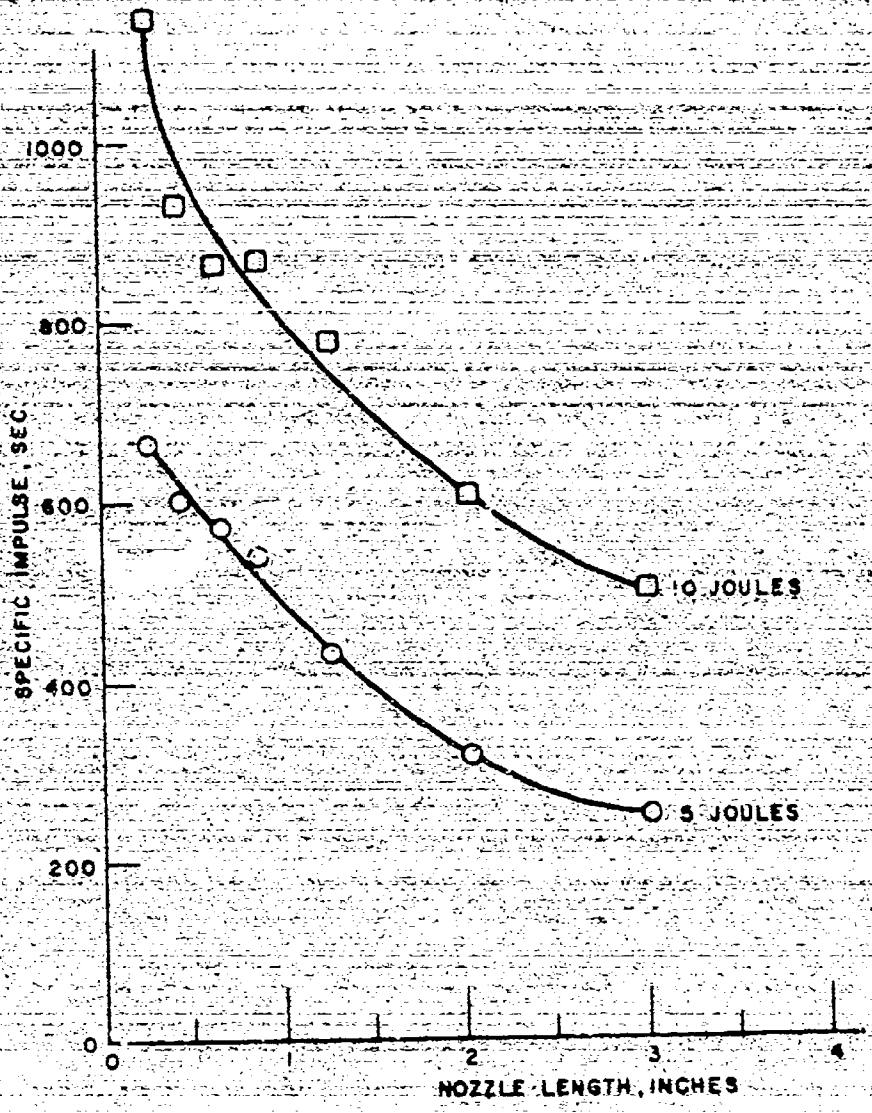

Figure 12. Specific Impulse as a Function of Nozzle Length

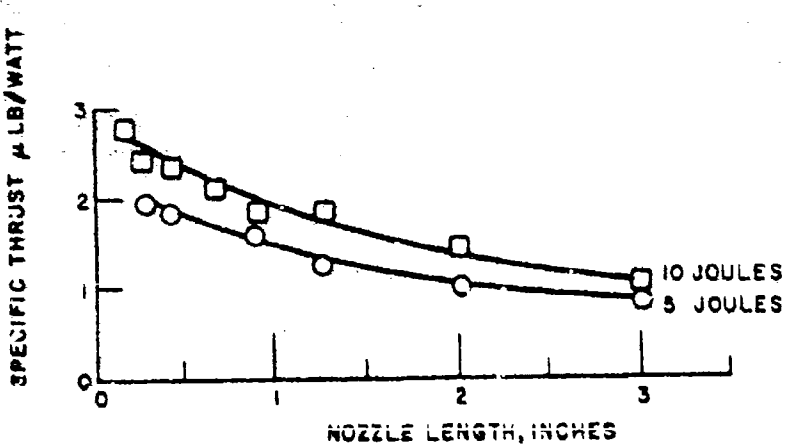

Figure 13. Specific Thrust as a Function of Nozzle Length

specific thrust. The capacitor having the highest internal resistance generated the lowest specific thrust. The variation in specific thrust observed between capacitors having a high internal resistance with those of low resistance was significant. It must be noted, however, that the capacitors which had a large resistance also had a high inductance. Even though the idealized analysis showed no effect of inductance upon specific thrust, some dependency of specific thrust with inductance cannot be ruled out entirely. Of these two variables, resistive energy losses in the capacitor cannot be recovered and thus should be minimized to achieve the largest possible specific thrust with a given thruster.

Besides the correlations that were suggested by idealized analytic considerations, several other useful correlations of experimental data were found to exist. These correlations are presented below.

2.1.3e Thrust Efficiency and Discharge Energy

Figure 14 shows the variation of thrust efficiency with discharge energy for a large number of (nonoptimized) thrusters having parallel rail as well as coaxial electrode nozzle geometries. In general, it is seen that thrust efficiency increases as the discharge energy is increased. Thrust efficiencies of up to 20 percent have been experimentally realized. It is believed that a thrust efficiency in excess of 30 percent could be generated by the solid propellant pulsed plasma microthruster should such an efficiency be the sole criterion as the design objective of the thruster.

2.1.3f Thrust Efficiency and Energy Per Unit Area

As indicated in Section 2.1.3b, for thruster design, it is convenient to know performance variation with energy per unit area of propellant. Figure 14 presents the variation of thrust efficiency with this parameter. It is seen that increasing the magnitude of the energy per unit area of the propellant will produce an increase in thruster efficiency. As indicated above, the variation in efficiency observed at a given value of j/A can be attributed to the effect of other parameters (i.e., nozzle length, capacitor resistance, etc.) on efficiency.

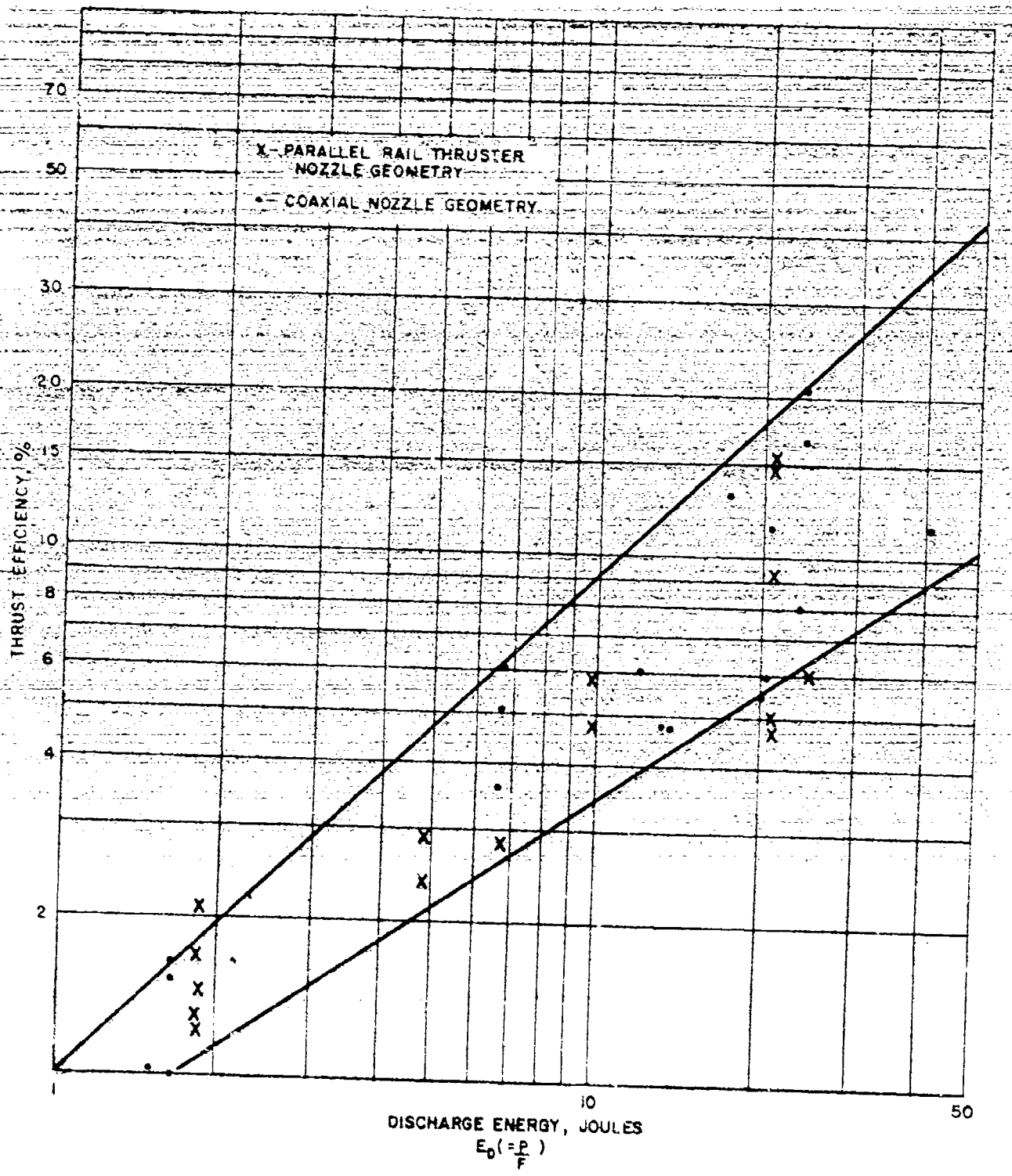

Figure 14. Thrust Efficiency as a Function of Discharge Energy

No experiments have yet been carried out for the sole purpose of producing the largest possible thrust efficiency. From the data presented in Figures 14 and 15, it is seen that such an experiment would involve selecting the largest discharge energy within reason and the smallest propellant frontal area practical. Based upon available experimental data it would appear that a thrust efficiency in excess of 30 percent should be possible with the pulsed plasma microthruster being reported upon.

2.1.3g Impulse Bit and Discharge Energy

In many applications it is more desirable to know the impulse bit (I) rather than the thrust level (T) that is produced. The inter-relationship between these two parameters being:

$$T = f\,I$$

with f the pulse frequency of the thruster. Figure 16 shows impulse bits that are generated per discharge as a function of the initial energy stored in the capacitor*. Most of the experimental data follows a fairly well defined band in which the impulse bit increases with discharge energy. Experimentally, impulse bits of up to 5.2 micropound-second per joule of initial energy have been generated**.

Since the power P is related to the discharge energy E by:

$$P = f\,E$$

it is evident that arbitrary large discrete impulse bits can be generated for an arbitrarily low input power. The period between such discrete pulses can readily be evaluated for any given input power by the same relation.

---

* Not all of this initial energy gets transferred into the discharge. As shown in Section 2.1.3d, significant energy losses may occur within poorly designed capacitors. Similarly, energy losses may occur in the conductive path between the capacitor and the plasma load.

** This value is identical to a specific thrust of 5.2 micropound/watt.

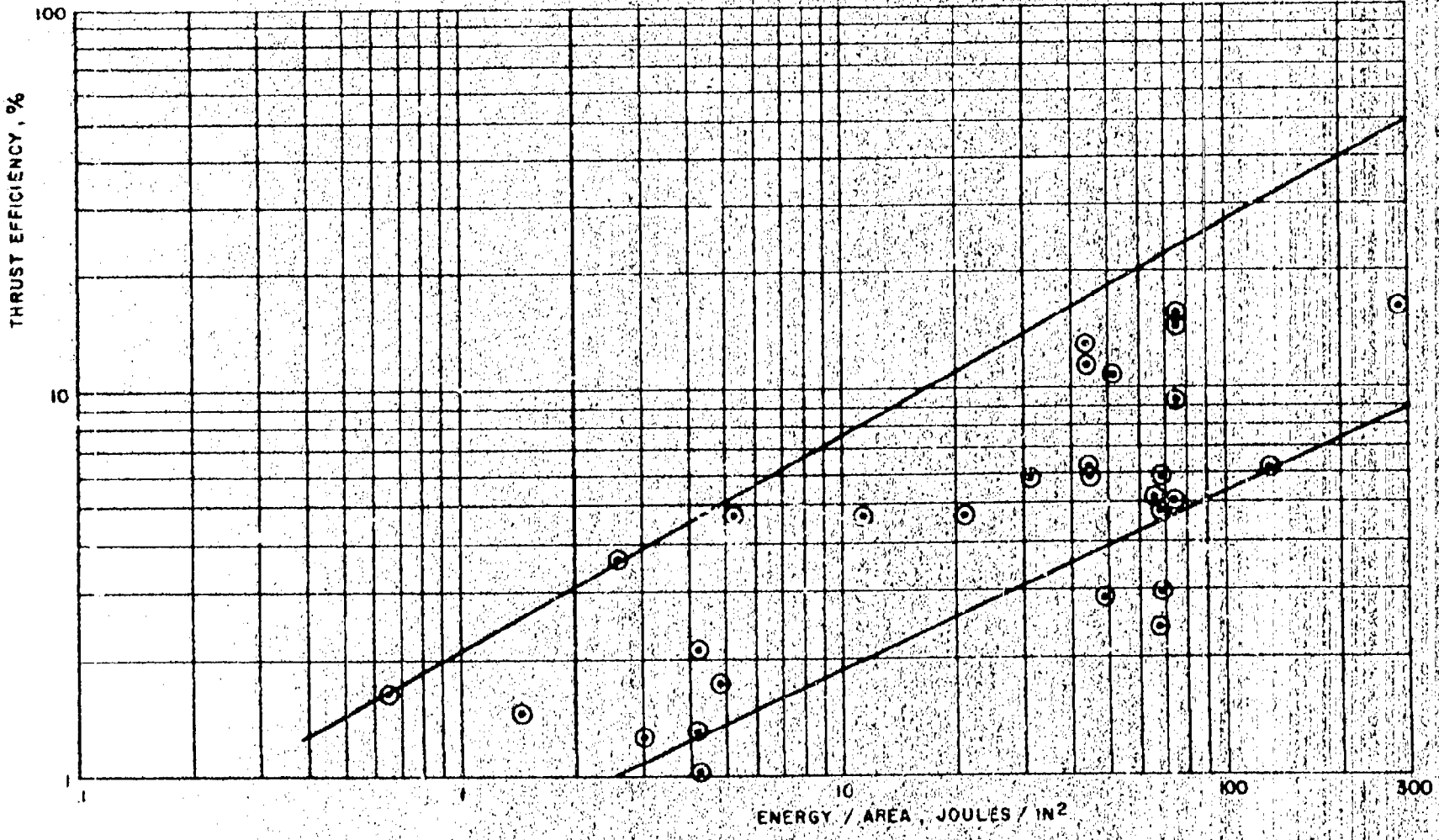

Figure 15. Thrust Efficiency as a Function of Energy per Unit Area

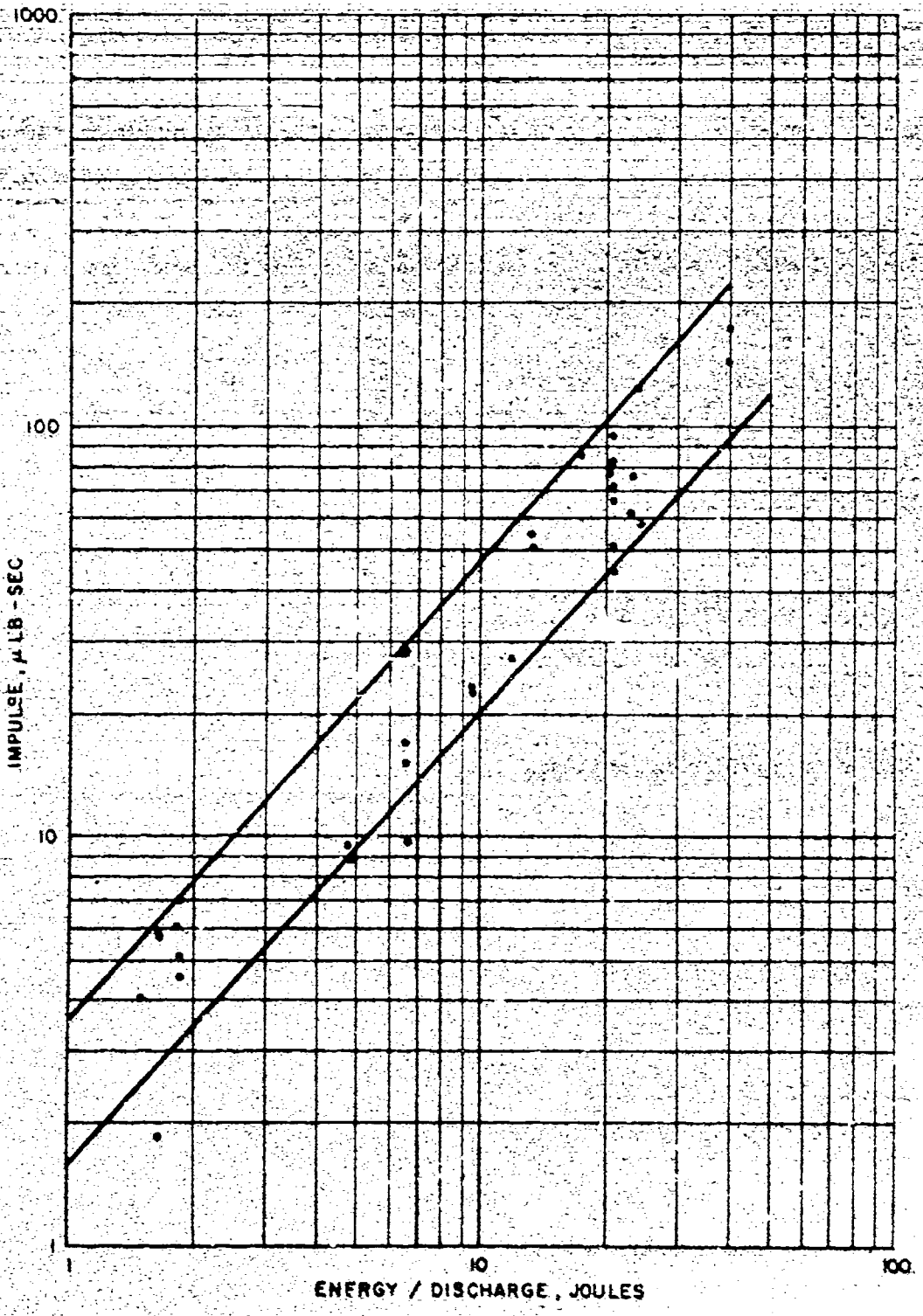

Figure 16. Impulse Bit vs Discharge Energy

At a given power level of operation, one has the choice of operating the thruster either at a low pulse frequency and high discharge energy level, or at a high pulse frequency and a low discharge energy level. From all of the performance data presented in the above sections, it is seen that the first method of thruster operation produces the best all around thruster performance. In addition, to produce a given total impulse (I_t) this first method of operation requires the least number of thruster discharges (n)*. Hence, this method of operation will also have the highest probability of meeting the total impulse requirements of the mission, i.e., to be the most reliable system. The only practical disadvantage of operating a thruster at a low pulse rate is that usually such a system will be heavier than a less reliable system operating at the higher pulse rate. These latter aspects will be treated in more detail in Section IV of this report.

2.1.3h Thrust Level as a Function of Life

A pertinent factor of a thruster is that the delivered thrust level remain essentially invariant during the lifetime of the thruster. It has been found that the thrust level (or impulse bits) of the thruster under study remains fairly constant throughout most of its life. A typical set of thrust data that has been recorded during a continuous test is presented in Table 4.

2.2 CAPACITOR STUDIES AND DEVELOPMENT

2.2.1 Introduction

It is self-evident that the success of a pulsed plasma thruster will depend significantly upon the reliability, weight, size, and power factor (measure of efficiency in releasing the stored energy into a given load) of the energy storage capacitor in its operating environment. At the inception of this program about eighteen capacitor manufacturers were contacted for delivery of energy storage capacitors suitable for a pulsed plasma microthruster operation in a space environment, with the pertinent constraints:

---

* The relation between total impulse, number of discharges to produce that particular value of total impulse and the impulse bit as $I_t = n\,I$.

TABLE 4. THRUST AND IMPULSE * AS A FUNCTION OF CONSECUTIVE DISCHARGES

Number of Discharges	Impulse Per Discharge (μ/pound/second)	Thrust (μ/pound)
0	71.0	142.0
126,156	72.0	144.0
158,688	74.0	148.0
828,581	69.8	139.6
987,488	72.8	145.6
1,165,256	66.9	133.8
1,215,556	69.8	139.6
1,330,254	68.5	137.0
1,433,342	72.0	144.0
1,604,471	70.0	140.0
1,942,861	70.0	140.0
2,065,880	71.0	142.0

* Log 88-E-5

a) Energy density be about 10 joules/lb (power density of about 20 watts/lb or better)

b) Life be about 10^8 discharges in a vacuum, radiation cooled

c) Critically damped discharge to 25% voltage reversal possible

d) Peak currents in excess of 10 Ka (actual magnitude to be essentially determined by stored energy and self-inductance for a critically damped discharge)

e) Maximum continuous temperature 150°F

f) Internal resistance below 5 milli-ohm

g) Self-inductance below 10 nanohenries

h) Energy range desirable: 1 joule to 40 joules in roughly four ranges

i) Operation voltage from 800 volts to 1500 volts.

It was found that only two capacitor manufacturers were prepared to deliver hardware meeting all constraints reasonably well within an acceptably short time. A relatively large number of manufacturers could meet most of the constraints with the exception of the desired energy density. It appears that a figure of anywhere from 2.5 to 3.8 joules/lb encompasses energy storage capacitors readily available from most manufacturers. From prior experience it was known that an arbitrary long life (in excess of 10^9 discharges) in the desired environment could be had if a capacitor were sufficiently derated. Such a derating simply implies using a capacitor rated to operate at some voltage and actually operating it at a very small fraction of this rated voltage.

In order to advance the state-of-the-art of a pulsed plasma thruster system and make it as competitive as possible with other electric thruster systems it was necessary to reduce the weight of the capacitor of a given system to the lowest possible value. For a pulsed plasma system operating repetitively, the rating of a capacitor in joules/lb is in most cases not as useful as its rating in terms of watts/lb*. This latter parameter in conjunction with the specific thrust (thrust

---

* The relation between these two parameters is simply $\frac{P}{W} = f \frac{E}{W}$ when P, W, f, and E denote power, capacitor weight, pulse frequency and stored energy, respectively.

per unit power) very nearly describes a major part of the thruster weight for given values of power and thrust level. It is also quite clear at this point that by heat sinking the capacitor to limit capacitor temperature it would be possible to obtain power densities appreciably larger than the 20 watts/lb figure sought of a radiation cooled capacitor. Furthermore, it is also obvious that limiting peak discharge currents appreciably below those actually occurring during thruster operation would minimize capacitor losses and could thus result in artificially high values of power density for a given capacitor temperature. For these reasons all capacitor tests being reported upon were carried out by operating them radiation-cooled in a vacuum environment concurrently with thruster operation. Therefore, all capacitor life data reported herein represents the lower limit of life. Heat sinking the capacitor in a spacecraft to a temperature below the equilibrium temperature attained by radiation cooling increases capacitor life. Indeed, capacitor life will be increased by a factor of 2 for each 10°C decrease in temperature!

For reasons indicated above the life data and power density of commercially available capacitors were considered of little value for the present effort. Indeed, it was later learned that one of the two manufacturers claiming to be able to meet most of the imposed constraints tested their capacitors in air (i.e., convection and possibly conduction cooled) while discharging into a 1 ohm load (instead of a roughly 3 milli-ohm load). Capacitors of this latter manufacturer while useful, proved very erratic in life when tested as part of a radiation cooled thruster in a vacuum environment.

Since a considerable effort was expended by the Sprague Electric Company in the development of pulsed capacitors suitable for pulsed plasma thrusters in a space environment, the development effort of the Sprague Electric Company toward the goals of the present effort will be presented as a separate section of this report. Supplementary in-house analytic and experimental studies of the capacitor as part of an electric thruster system are presented in the sub-sections below.

2.2.1a Capacitor D.C. Life as a Function of Charge Cycle

An analysis[3] has been carried out which examines the use of a pulse capacitor in conjunction with a power conditioner in a satellite in a manner which results in maximum capacitor life. In the laboratory, pulse capacitors are checked for maximum life by charging and discharging them with regular periodicity until failure. In a satellite it is possible that an interval of time may exist between application of voltage to a capacitor and the subsequent discharge of the capacitor. This interval of time for which the capacitor is fully charged multiplied by the total number of discharges expected of the capacitor in the life of the mission may become an appreciable quantity. Furthermore, the charge cycle waveform of the power conditioner can be designed in any one of a different number of ways to meet the pulse repetition rate required of the thruster. Thus, there exist fundamental questions concerning the charge/discharge cycle for optimum capacitor life.

It is known that a d.c. capacitor has an inherent d.c. life. This life is the number of hours the capacitor can statistically remain on charge at a given voltage level before failure. It is safe to assume that a pulse capacitor will also have an analogous d.c. life. Besides this d.c. life, a pulse capacitor will also have a pulse life, i.e., the number of consecutive discharges the capacitor is likely to survive. When a capacitor is used in conjunction with a power conditioner in a satellite and used intermittently it is desirable to know the best charge/discharge pattern which produces the maximum total life of the capacitor. An attempt has been made to answer this question. In particular, the expected relative life time of a pulse capacitor (i.e., total number of discharges until failure) as a function of the charging time and the holding time in the cyclic operation of a thruster has been examined. As an example, suppose a thruster is to be operated at a pulse frequency of one pulse every six seconds. A large variety of charging schemes can be conceived; i.e., one can charge the capacitor over a six second period, or charge it over a 1.5 second period and hold voltage constant (at the discharge voltage) for 4.5 seconds, or one can charge the capacitor for 1.5 seconds just prior to discharge and let the capacitor remain at zero voltage for 4.5 seconds. Of course, any number of other schemes are conceivable. Intuitively, one suspects that maximum capacitor life results when the capacitor

is charged just prior to discharge. In the analysis it is assumed that if a pulse capacitor is tested until failure then the sum of the percentages of the capacitor d.c. life time expended at each voltage state experienced during the charge cycle must equal 100% of the total d.c. life time of the capacitor. Analytically, this hypothesis can be written in the form:

$$\frac{M_j}{K} \int_0^{\tau} V(t)^{\alpha} \, dt = 1$$

where M_j is the number of cycles until failure, K the constant defined by the voltage power law for the d.c. life of the capacitor ($L = KV^{\alpha}$, with L the life in hours, V the applied voltage, α an empirical constant approximately equal to 6 for mylar capacitors), V(t) the charging voltage wave shape and τ the period of thruster operation.

To illustrate the application of the results of the analysis, consider the three charging modes mentioned above. Assume a constant power charging scheme such as produced by the Wilmore power conditioner. The three sample charge cycles are illustrated in Figure 17 and are defined as:

Cycle 1:	$V(t) = V_m \sqrt{t} / \sqrt{1.5}$	$0 \le t \le 1.5$ sec
	$V(t) = V_m$	$1.5 \le t \le 6$ sec
Cycle 2:	$V(t) = V_m \sqrt{t} / \sqrt{6}$	$0 \le t \le 6$ sec
Cycle 3:	$V(t) = V_m \sqrt{t} / \sqrt{6}$	$0 \le t \le 1.5$ sec
	$V(t) = 0$	$1.5 \le t \le 6$ sec

Substituting these into the former relation with $\alpha = 6$ yields the relative number of discharge cycles M_j until failure.

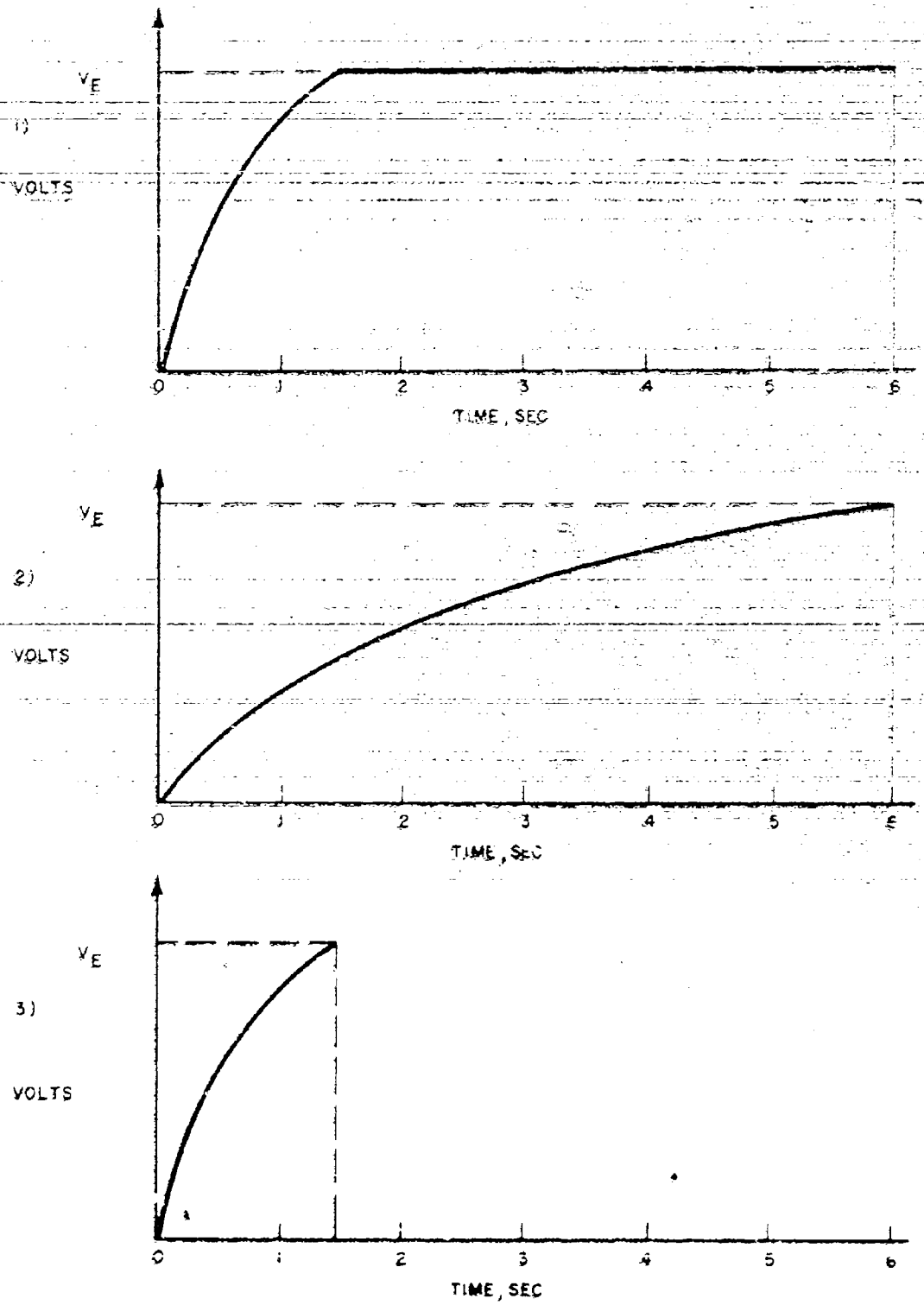

Figure 17. Capacitor Charging Alternatives

$$M_1 = 0.205\ K/V_m^6$$

$$M_2 = 0.667\ K/V_m^6$$

$$M_3 = 2.667\ K/V_m^6$$

These results indicate the expected d.c. life of the capacitor using charging Scheme No. 3 to be 4 times that of Scheme No. 2 and 13 times that of Scheme No. 1. Hence, of the three charging schemes posed, the third scheme would be most preferable. Of course, if the number of cycles M_j should be larger than the number of discharge cycles expected from charge/discharge tests carried out at the voltage level V_m, then the lower number of discharge cycles would govern capacitor life.

The above results were discussed with the Sprague Electric Company. Based upon their experience with pulse capacitors, it was concluded that the ordering of relative life would be as predicted by the above analysis. It was pointed out that experimental verification of the hypothesis would be rather costly to carry out. Therefore, no experimental check of the hypothesis was carried out during the effort being reported upon. The results are nevertheless significant in that they show a preferred manner of thruster-capacitor operation for optimum life.

2.2.1b Preliminary Analysis on Thermal Testing of Capacitors

Based upon Republic's experience as well as conversations held with capacitor manufacturers, it has become evident that there is a lack of information concerning the thermal properties of pulsed capacitors. Specifically, the following questions can be raised in this area:

1) For a given capacitor operated in a given mode what is the peak steady state temperature?

2) For this same capacitor using known materials of known thicknesses what is the equivalent thermal conductivity?

3) Does the thermal contact resistance at the interface of each layer play a significant role in the thermal behavior of a capacitor? Can this resistance be evaluated?

4) Based upon published energy dissipation factors, can the heat generation in a given capacitor be predicted? If this can be done a meaningful figure of merit (thermal Q) for the capacitor can be predicted?

5) Using a simplified model, can an analysis be carried out which would permit one to correlate experimentally determined values for the foregoing items with the analysis?

6) What tests would be required to do the foregoing?

In order to answer these questions meaningfully it has been found necessary to suggest the following two tests.[4] The first is to obtain an empty case from the manufacturer and to install a resistor in the case and thermocouples on the case. The unit is then mounted in a vacuum chamber and operated at several steady power levels to the resistor while monitoring the thermocouples. Such a test has been conducted on a Maxwell capacitor case and it yields the effective emissivity of the case. The second test consists essentially of centrally mounting an internal thermocouple and also an external thermocouple on the capacitor. The steady state temperatures are monitored under various operating conditions. Based upon these two tests it becomes possible to immediately answer questions 1, 4 and 6.

A preliminary thermal analysis has been carried out for simplified slab and cylindrical models which indicate that questions 2, 3, and 5 can be answered in the affirmative when the analysis is combined with the two tests.

In addition it may be possible to correlate the electrical quality "Q" of a capacitor to the thermal "Q". It may also be possible to either explain or predict capacitor failures when the failure mechanism is thermal.

The thermal conductivity of a foil type capacitor can be very difficult to estimate from the knowledge of the materials used and their thicknesses

since there may be as many as a thousand interfaces per inch of capacitor, each having an unknown variable contact resistance. Assuming zero contact resistance and alternate foil layers in a semi-infinite slab type unit, an expression can be derived for the difference in temperature between the centerline and any part of the capacitor in steady state as a function of the volume heat generation, the thickness of each foil and their thermal conductivities. This analysis can be also extended to include thermal contact resistance and several foils in series. In addition to the slab geometry, a cylindrical geometry has also been analyzed and a recursion formula developed.

Based upon the simplified analysis presented below, it will be noted that an equivalent uniform thermal conductivity can be calculated which can be correlated to the materials and their thicknesses. From this, one can possibly estimate the thermal contact resistance, the heat generation, energy dissipation factor and a figure of merit for the capacitor. The inclusion of an internally mounted thermocouple therefore appears to be desirable as a technique for providing additional information to evaluate the macroscopic properties of a capacitor.

A. Slab Geometry

Assume the capacitor consists of alternate foils of thickness t_1 and αt_1 respectively. The construction is a slab infinite in the "y" direction and having a uniform heat generation in each of the heat generating plates (see Figure 18). Alternate plates generate heat. Consider the unit to be symmetrical with heat removal at $\pm x$. The volume heat generation will be denoted as q, temperature as T, thermal conductivities as K.

The governing heat transfer equations for the heat generating section are:

$$\nabla^2 T = -\frac{q}{K}$$

$$\frac{d^2T}{dx^2} = -\frac{q}{K}$$

and

$$\frac{dT}{dx} = -\frac{qx}{K} + C_1 \qquad \text{(a)}$$

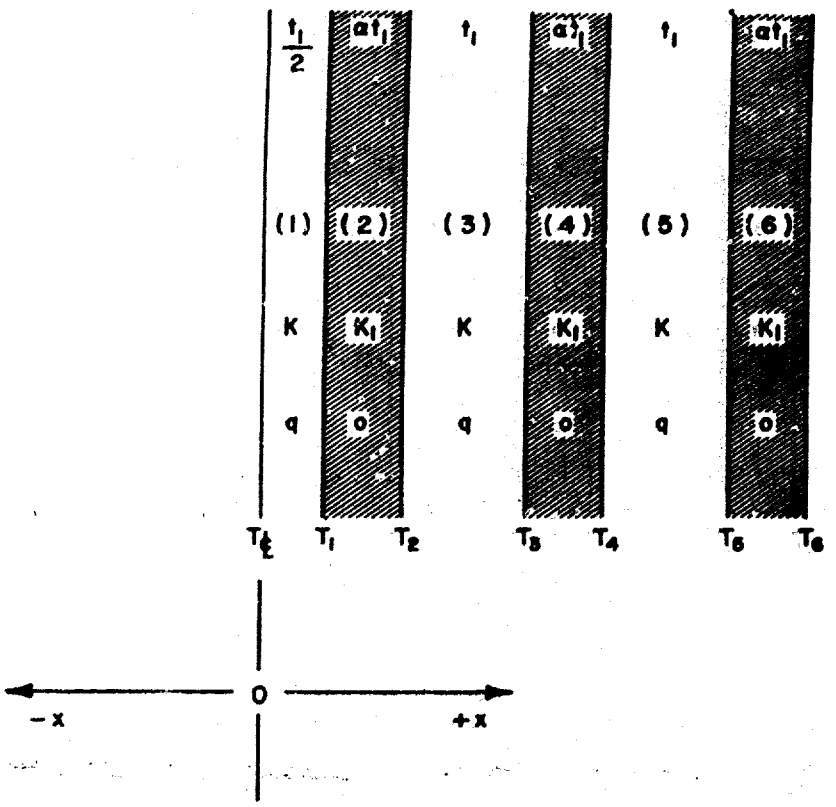

Figure 18. Slab Geometry Notation

For section (1)

$$\frac{dT}{dx} = 0 \text{ @ } x = 0 \quad \therefore C_1 = 0$$

$$T = \frac{qx^2}{2K} + C_2$$

$$\text{@ } x = 0, \quad T = T_{CL}$$

$$\therefore C_2 = T_{CL}$$

and,

$$T_1 = T_{CL} - \frac{qt_1^2}{8K} = T_{CL} - qt_1^2 \left(\frac{1}{8K}\right) \qquad (1)$$

All of the heat generated in section (1) must flow through section (2). Therefore,

$$Q_2 = \frac{qt_1}{2}$$

and $$T_1 - T_2 = \frac{\alpha q t_1^2}{2K_1}$$

Substituting from (1),

$$T_2 = T_{CL} - qt_1^2 \left(\frac{1}{8K} + \frac{\alpha}{2K_1} \right) \quad (2)$$

At any point in section (3) the heat flow is the heat generated in section (1) plus the heat generated to the point in question in section (3), i.e.,

$$Q = \frac{qt_1}{2} + qx_3$$

$$\frac{dt}{dx} = - \frac{\frac{qt_1}{2} + qx_3}{K} = - \frac{qx_3}{K} + C_1$$

where x_3 is the distance into section (3) from its edge,

and $$C_1 = - \frac{qt_1}{2K}$$

Thus,

$$\frac{dT}{dx} = - \frac{qx}{K} - \frac{qt_1}{2K}$$

and

$$T = - \frac{qx^2}{2K} - \frac{qt_1 x}{2K} + T_{CL} - \frac{qt_1^2}{8K} - \frac{\alpha q t_1^2}{2K_1}$$

Simplifying:

$$T_3 = T_{CL} - qt_1^2 \left(\frac{9}{8K} + \frac{\alpha}{2K_1} \right)$$

Continuing on, we establish T_4, T_5, and T_6. These temperatures are thus:

$$T_1 = T_{CL} - qt_1^2 \left(\frac{1}{8K} \right)$$

$$T_2 = T_{CL} - qt_1^2 \left(\frac{1}{8K} + \frac{\alpha}{2K_1} \right)$$

$$T_3 = T_{CL} - qt_1^2 \left(\frac{\alpha}{8K} + \frac{\alpha}{2K_1} \right)$$

$$T_4 = T_{CL} - qt_1^2 \left(\frac{9}{8K} + \frac{\alpha}{K_1} \right)$$

$$T_5 = T_{CL} - qt_1^2 \left(\frac{25}{8K} + \frac{\alpha}{K_1} \right)$$

$$T_6 = T_{CL} - qt_1^2 \left(\frac{25}{8K} + \frac{3}{2} \frac{\alpha}{K_1} \right)$$

Generalizing for odd and even sections,

Odd: $$T_N = T_{CL} - qt_1^2 \left[\frac{N^2}{8K} + \frac{N-1}{4} \frac{\alpha}{K_1} \right]$$

Even: $$T_N = T_{CL} - qt_1^2 \left[\frac{(N-1)^2}{8K} + \frac{N}{4} \frac{\alpha}{K_1} \right]$$

Since: $N >> 1$ $$T_N = T_{CL} - qt_1^2 \left[\frac{N^2}{8K} + \frac{N}{4} \frac{\alpha}{K_1} \right]$$

Simplifying: $$T_{CL} - T_N = q \left(\frac{Nt_1}{2} \right)^2 \left[\frac{1}{2K} + \frac{\alpha}{K_1} \right]$$

As a test, if $K_1 \to \infty$, $T_{CL} - T_N = \frac{q}{2K} \left(\frac{Nt_1}{2} \right)^2 = \frac{q(t)^2}{2K}$ where t is the half thickness of the slab. This corresponds to a homogeneous slab with uniform heat generation and this is the result usually found in standard texts.

If we wish to express the foregoing in terms of an "average" thermal conductivity, K_{avg},

$$\frac{1}{2K_{avg}} = \frac{1}{2K} + \frac{\alpha}{K_1}$$

and, $$K_{avg} = \frac{K K_1}{K_1 + \alpha (2K)}$$

as $\alpha \to 0$, $K_{avg} \to K$ as would be expected.

B. Cylindrical Geometry

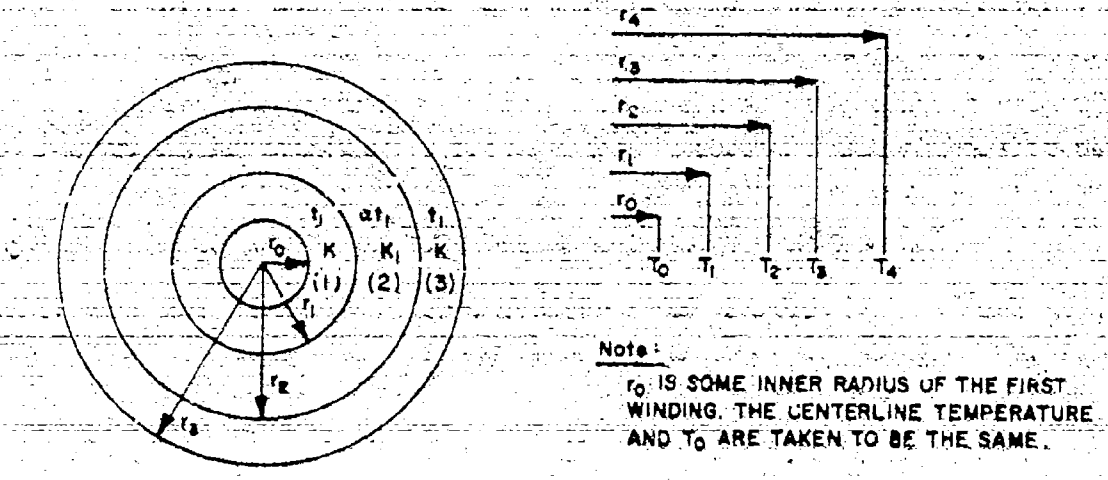

Figure 19. Cylindrical Geometry Notation

Section 1 - Heat Generation

$$\nabla^2 T = \frac{d^2T}{dr^2} + \frac{1}{r}\frac{dT}{dr} = -\frac{q}{K}$$

with $p = \frac{dT}{dr}$ this equation becomes:

$$\frac{dp}{dr} + \frac{p}{r} = -q/K$$

or, $p = C_1 r$

with $C_1 = -\frac{q}{2K}$

and $\frac{dT}{dr} = -\frac{qr}{2K}$

Hence, $T = -\frac{qr^2}{4K} + C_2$

Now, at $r = r_o$, $T = T_o$, therefore,

$$T_o = -\frac{qr_o^2}{4K} + C_2$$

$$C_2 = T_o + \frac{qr_o^2}{4K}$$

and, $T_o - T_1 = \frac{q}{4K}(r_1^2 - r_o^2) \simeq \frac{q}{2K} r_o t_1$

or, $T_1 = T_o - \frac{qr_o t_1}{2K}$

Section 2 - No Heat Generation - Conduction Only.

$$\Delta T = T_1 - T_2 = \frac{Q}{2\pi K_1} \ln \frac{r_2}{r_1} = \frac{2\pi r_o t_1 q}{2\pi K_1} \ln \frac{r_2}{r_1} \simeq \frac{qr_o t_1}{K_1} \left(\frac{\alpha t_1}{r_1}\right)$$

but, $T_1 = T_o - \frac{qr_o t_1}{2K}$

Therefore, $T_2 = T_o - qr_o t_1 \left(\frac{1}{2K} + \frac{1}{K_1} \frac{\alpha t_1}{r_1}\right)$

Note: $r_2 = r_1 + \alpha t_1$

$$\frac{r_2}{r_1} = 1 + \frac{\alpha t_1}{r_1} \quad \text{and} \quad \ell n \frac{r_2}{r_1} \simeq \frac{\alpha t_1}{r_1}$$

Section 3 - Heat Generation and Conduction from Section 1

$$(\Delta T) \text{ Heat generation} = \frac{q}{4K} (r_3^2 - r_3^2) = \frac{q}{2K} r_2 t_1$$

$$(\Delta T) \text{ conduction} = \frac{q}{K} r_o t_1 \frac{t_1}{r_2}$$

Total: $$\Delta T = \frac{q}{2K} r_2 t_1 + \frac{q}{K} r_o t_1 \frac{t_1}{r_2} = q r_o t_1 \left(\frac{t_1}{r_2 K} + \frac{r_2}{2K r_o} \right)$$

$$\therefore T_3 = T_o - q r_o t_1 \left[\frac{1}{2K} + \frac{1}{K_1} \frac{\alpha t_1}{r_1} + \frac{t_1}{r_2 K} + \frac{r_2}{r_o} \left(\frac{1}{2K} \right) \right]$$

Section 4 - No Heat Generation - Conduction Only

$$Q = 2\pi r_o t_1 q + 2\pi r_2 t_1 q = 2\pi t_1 q (r_o + r_2)$$

$$\therefore T = \frac{Q}{2\pi K_1} \ell n \frac{r_4}{r_3} = \frac{t_1 q (r_o + r_2)}{K_1} \left(\frac{\alpha t_1}{r_3} \right)$$

Note: $$r_4 = r_3 + \alpha t_1; \quad \frac{r_4}{r_3} = 1 + \frac{\alpha t_1}{r_3} \quad \text{and} \quad \ell n \frac{r_4}{r_3} = \frac{\alpha t_1}{r_3}$$

$$\therefore T_4 = T_o - q r_o t_1 \left[\frac{1}{2K} + \frac{1}{K} \frac{\alpha t_1}{r_1} + \frac{t_1}{r_2 K} + \frac{r_2}{r_o} \left(\frac{1}{2K} \right) + \frac{1}{K_1} \left(\frac{r_o + r_2}{r_o} \right) \frac{\alpha t_1}{r_3} \right]$$

Section 5 - Heat Generation and Conduction from Sections (1) and (3)

$$(\Delta T)\ \text{Heat generated} = \frac{q}{4K}(r_o^2 - r_4^2) = \frac{q}{2K} r_4 t_1$$

$$(\Delta T)\ \text{Conduction} = \frac{t_1 q (r_o + r_2)}{K_1} \frac{t_1}{r_4}$$

$$T_5 = T_o - q r_o t_1 \left[\frac{1}{2K} + \frac{1}{K_1} \frac{\alpha t_1}{r_1} + \frac{t_1}{r_2 K} + \frac{r_2}{r_o}\left(\frac{1}{2K}\right) + \frac{1}{K_1}\left(\frac{r_o + r_2}{r_o}\right) \frac{\alpha t_1}{r_3} + \frac{r_4}{r_o} \frac{1}{2K} + \frac{1}{K}\left(\frac{r_2 + r_o}{r_o}\right) \frac{t_1}{r_4} \right]$$

Section 6 -

$$\Delta T = \frac{Q}{2\pi K_1} \ln \frac{r_6}{r_5} = \frac{t_1 q (r_o + r_2 + r_4)}{K_1} \frac{\alpha t_1}{r_5}$$

Summarizing the foregoing, one has:

1) at r_o; $T = T_o$

2) at r_1; $T_1 = T_o - q r_o t_1 \left(\frac{1}{2K}\right)$

3) at r_2; $T_2 = T_o - q r_o t_1 \left[\frac{1}{2K} + \frac{1}{K_1} \frac{\alpha t_1}{r_1} \right]$

4) at r_3; $T_3 = T_o - q r_o t_1 \left[\frac{1}{2K} + \frac{1}{K_1} \frac{\alpha t_1}{r_1} + \frac{1}{2K} \left(\frac{r_2}{r_o}\right) + \frac{t_1}{r_2 K} \right]$

5) at r_4; $T_4 = T_o - q r_o t_1 \left[\frac{1}{2K} + \frac{1}{K_1} \frac{\alpha t_1}{r_1} + \frac{1}{2K}\left(\frac{r_2}{r_o}\right) + \frac{t_1}{r_2 K} + \frac{1}{K_1}\left(\frac{r_o + r_2}{r_o}\right) \frac{\alpha t_1}{r_3} \right]$

6) at r_5; $T_5 = T_o - q r_o t_1 \left[\frac{1}{2K} + \frac{1}{K_1} \frac{\alpha t_1}{r_1} + \frac{1}{2K}\left(\frac{r_2}{r_o}\right) + \frac{t_1}{r_2 K} + \frac{1}{K_1}\left(\frac{r_o + r_2}{r_o}\right) \frac{\alpha t_1}{r_3} + \frac{1}{2K}\left(\frac{r_4}{r_o}\right) + \frac{1}{K}\left(\frac{r_o + r_2}{r_o}\right) \frac{t_1}{r_4} \right]$

or, alternately:

1) at r_o: $T = T_o$

2) at r_1: $T_1 = T_o - qr_o t_1 \quad \frac{1}{2K}$

3) at r_2: $T_2 = T_1 - qr_o t_1 \quad \frac{\alpha t_1}{K_1 r_1}$

4) at r_3: $T_3 = T_2 - qr_o t_1 \left(\frac{1}{2K} \quad \frac{r_2}{r_o} + \frac{t_1}{r_2 K} \right)$

5) at r_4: $T_4 = T_3 - qr_o t_1 \left[\frac{1}{K_1} \left(\frac{r_o + r_2}{r_o} \right) \quad \frac{\alpha t_1}{r_3} \right]$

6) at r_5: $T_5 = T_4 - qr_o t_1 \left[\frac{1}{2K} \quad \frac{r_4}{r_o} + \frac{1}{K} \left(\frac{r_o + r_2}{r_o} \right) \quad \frac{t_1}{r_4} \right.$

Expressed as a series, one therefore finds:

"N" ODD; $T_N = T_{N-1} - qr_o t_1 \left[\frac{1}{2K} \left(\frac{r_{N-1}}{r_o} \right) + \frac{t_1}{K} \left(\frac{1}{r_{N-1}} \right) \left(\frac{\Sigma r_{N-3}}{r_o} \right) \right]$

"N" EVEN; $T_N = T_{N-1} - qr_o t_1 \left[\frac{\alpha t_1}{r_{N-1} K_1} \quad \left(\frac{\Sigma r_{N-2}}{r_o} \right) \right]$

These summations could be very tedious and could readily be carried out on a computer if it is found to be warranted. Otherwise, a "homogeneous" solution could be carried out to determine an equivalent set of properties or else the slab could be used as a first approximation.

Motivated by the above considerations, a thermocouple was imbedded in the windings of a capacitor during its manufacture.

2.2.1c Capacitor Quality Q by Thermal Tests

When a manufacturer quotes the "Q" of a capacitor it is usually a number derived from the testing of a small test coupon under conditions that may widely differ from the actual conditions that prevail during use of the capacitor. A steady state thermal method [5] can be used to evaluate a meaningful figure of merit (effective Q) for capacitors. The proposed method consists simply of evaluating the steady state heat loss from the capacitor under a given set of operating conditions. This method can be used for bench tests as well as under operating conditions in a vacuum. In addition to both air and vacuum operation being amenable to a simple analysis, calibrations can be performed with relative ease for both modes of operation. No special equipment is required and these tests can be performed using thermocouples, a high voltage probe, and a resistor (or light bulb). The detailed considerations and typical data reduction for the recent tests with a Maxwell capacitor are given below.

a. General Consideration

The proposed figure of merit Q is defined as follows:

$$Q = \frac{\text{energy stored in capacitor}}{\text{energy lost per discharge}} = \frac{\text{power stored in capacitor}}{\text{power lost in capacitor}}$$

In the steady state all of the heat generated within the unit must be radiated and/or convected away from the outside of the capacitor. Therefore,

$$Q = \frac{\text{power stored in capacitor}}{\text{heat lost}}$$

and

$$Q = \frac{n\,(1/2\,CV^2)}{q} \quad \text{(after steady state is achieved)}$$

where
- n = discharge rate - pulses/sec.
- C = capacitance
- V = voltage
- q = total heat loss rate per unit time

B. Bench Tests in Air

Let us assume that a capacitor is bench tested to discharge into a simulated load of extremely low resistance and inductance. After several hours of operation a steady outer case temperature will be attained which we will denote as T_e and which one can monitor with thermocouples. The full charge voltage and discharge rate will also be monitored. Using the definition of Q given in A,

$$Q = \frac{n\,(1/2\,CV^2)}{q} \qquad \frac{n\,(1/2\,(CV^2)}{UA\,(T_e - T_o)}$$

where: U = Overall coefficient of heat transfer including radiation and convection

A = Surface Area

T_o = Ambient temperature

For the temperature range of interest U can be taken as 2.1 Btu/hr ft^2°F for the cylindrical portion of the capacitor and 1.7 Btu/hr ft^2°F for the base of the capacitor[6]. Since the arrangement at the top of the capacitor is relatively complicated and since the top may actually be a heat source due to the nozzle configuration, it will be neglected at this time.

As an example of the procedure let us take a Maxwell capacitor operating in air at a discharge rate of 1 pps and having an average case temperature of 120°F. This unit is a cylinder 2-5/8" diameter x 6-1/2" long. It has a C ~ 18.9 μf and let us further assume it is operated at 1500 volts. Therefore,

$$1/2\,CV^2 = 21.3 \text{ joules}$$

$$q = UA\,(T_e - T_o)_{cyl} + UA\,(T_e - T_o)_{base} = 42.3 \text{ Btu/hr}$$

and

$$Q = 1.72$$

If the equilibrium temperature had been measured as 160°F under these conditions, Q would have been calculated 0.955 which is not meaningful since Q cannot (by definition) be less than unity. A typical plot of Q versus capacitor temperature in air might be as shown below for the Maxwell capacitor used in this illustration.

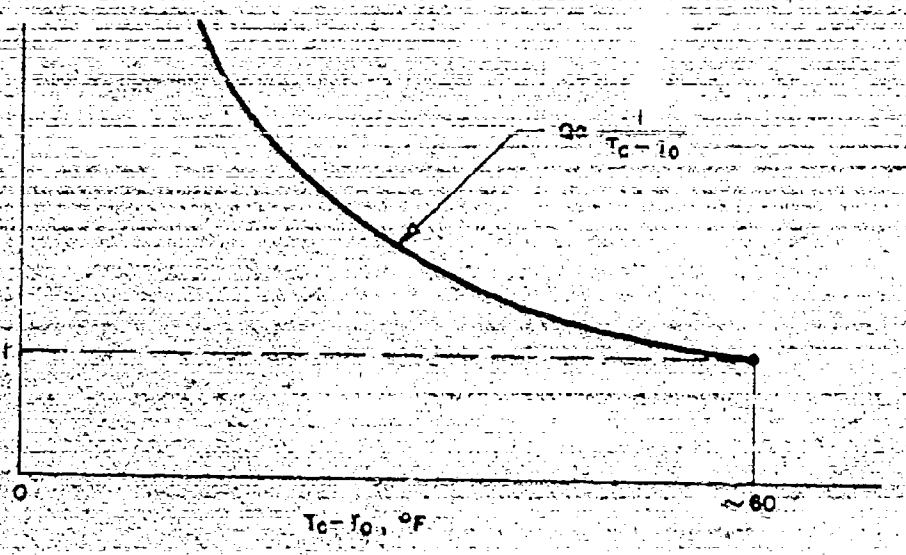

Figure 20. Schematic Q Variation

In addition to the calculation performed above, it should also be a simple matter to calibrate Q by experimentally determining q versus T_c. If the capacitor has a case we need only obtain a hollow case and using a light bulb or a resistor to measure the case temperature as a function of the power to the load inside the case. At this point q is plotted as a function of case temperature and Q is evaluated from the test as before. This gives an independent check on both q and Q and it would be expected that the agreement between the calibrated and calculated values of Q would agree to within ± 20%.

C. Tests in Vacuum

During testing the temperature of the capacitor can be monitored and it is observed that equilibrium temperatures are usually achieved after 2-5 hours of steady testing. In a vacuum chamber the predominating mechanism of heat transfer is radiation and q becomes:

$$Q = \sigma A \varepsilon (T_c^4 - T_o^4)$$

where: σ = Stefan-Boltzmann constant

ε = Effective emissivity

and T's = Absolute temperatures.

The effective emissivity is a function of the painted coating on the capacitor. Based upon the data in Hsu and Kern[7], a reasonable value to use is ~0.5. Obviously, if the manufacturer knows the emissivity or it can be established from test (as will be indicated later on), this would be preferable.

In a recent test with the Maxwell capacitor, it was estimated that the case temperature was 140°F at equilibrium when the engine was pulsed at 1 pps. Using this figure,

$$q = 1728 \times 10^{-12} \times .5 \left[\frac{\pi (2.625)(6.5)}{144} + \frac{\pi}{4} \frac{(2.625)^2}{144} \right] \left[\frac{}{(600)}^4 - \frac{}{530}^4 \right]$$

$$q = 17.9 \text{ Btu/hr radiated}$$

$$\therefore Q = 4.05$$

Carrying out this calculation for $Q = 1$ yields $T_c = 270°F$. A typical plot of Q versus T_c for this case would be of the form shown below.

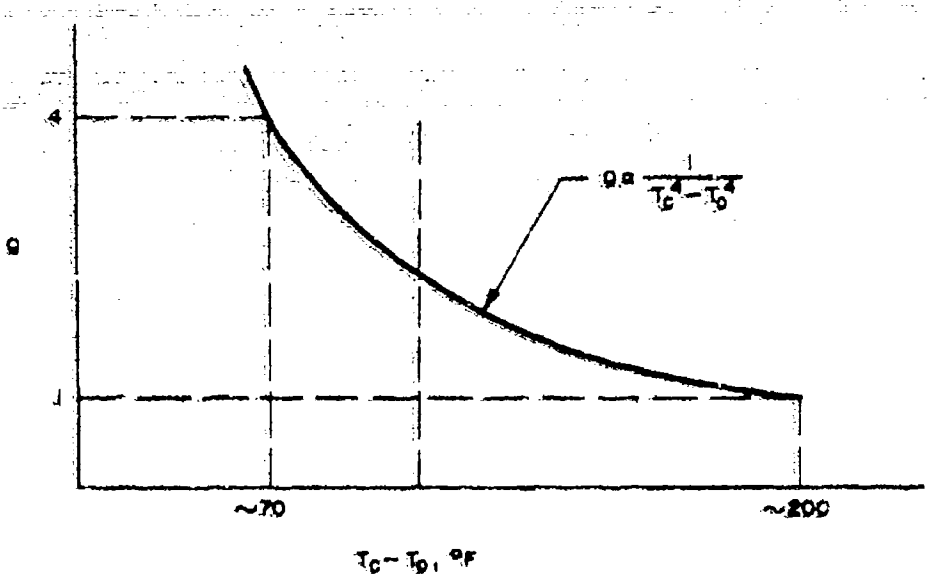

Figure 21. Schematic Q Variation

A calibration for vacuum operation can be performed as was done for the "air case" considered and the data reduced in the same manner as previously noted. The effective emissivity of 0.5 assumed appears to be a good estimate for this quantity but it is possible to be in error due to this assumption. It is estimated that the maximum error to be ± 6% in this value.

If the capacitor has no case, a thermocouple can be attached to its outside and Q estimated using the foregoing methods. Also a calibration can be performed by using the outer winding material as a case and inserting a heat source inside the hollow shape made of this material to the shape of the capacitor to perform the calibration as has been previously indicated.

It is believed that the foregoing method of testing capacitors will yield the most meaningful figure of merit for actual operation of capacitors in a pulsed microthruster. It is recommended that a comparison of the results as obtained by the method proposed be made with results quoted by capacitor manufacturers using bench testing techniques.

2.3 POWER CONDITIONING SUBSYSTEM

2.3.1 General

The power conditioner must perform two functions. It has to accept a low d.c. voltage (typically 16 to 28 volts) and convert it to a high voltage (typically 1000 to 1500 volts) and it must also transfer energy as efficiently as possible into the thruster energy storage capacitor. Ordinary dc-dc converters are readily available which have a conversion efficiency of about 50%. If ordinary RC charging is used, then the capacitor charging efficiency will be limited to about 50%. Hence by unsophisticated techniques one arrives at an overall power conditioning efficiency of only about 25%. Obviously a 25% efficiency is unacceptable. For this reason considerable analytic and experimental studies were carried out at Republic Aviation prior to the present program for the purpose of improving this efficiency. Prior to the present program a solid state power converter was developed at Republic which had experimentally realized an overall efficiency of 64%. Since the present program called for examining charging and conversion techniques with an overall efficiency of 50% to 60%, it was believed

that the upper value of the target efficiency might be realizable. Indeed, the state-of-the-art of the power conditioning subsystem for the pulsed plasma microthruster has by the present effort been advanced to experimentally realize an overall efficiency from 78 to 80%! If weight and volume were not also prime considerations, it is estimated that an efficiency of 92% could be arrived at as the upper practical limit by the present techniques employed.

The power conditioning subsystem was designed and built by Wilmore Electronics, Inc. to specifications of Fairchild Hiller, Republic Aviation Division. The technique has been discussed in some detail in References 8 and 9. Basically, small energy bits are switched at a rate of from 5Kc to 20 Kc into the primary of a transformer. The secondary winding of this energy storage transformer, the "flyback" circuit, appears as a current source rather than a voltage source, thus enabling it to deliver energy efficiently to the thruster energy storage capacitor. Since the source and the load are never directly coupled to each other the primary circuit becomes protected from load short circuits such as occur during pulsed operation of the thruster.

2.3.2 Analysis

The Wilmore Electronics method of power conditioning involves a two part process by which energy is transferred from a low voltage fixed voltage source to a capacitor charge at high voltage with high efficiency. In the first half of the repetitive process energy is stored in an inductance (the primary winding of the main power transformer). When this energy reaches a predetermined level, the primary connection to the low voltage source is opened and the resultant inductively stored energy is switched to the secondary of the main power transformer which is connected to the capacitor load through a diode in such a polarity that the diode is forward biased to the resultant secondary current flow. Charging current flows until the diode is back biased (or until the current reaches zero). This basic charge cycle is repeated periodically until the capacitor is charged to the desired level.

Because of the fact that a predetermined stored energy is switched each cycle of the charging process, the process has been described as constant power charging. If a fixed repetition rate is maintained, then the cyclic average

power drain on the low voltage source will be constant. This does not imply, however, that the rate of energy transfer to the load will be constant. An analysis has been performed [10] to determine expressions for the efficiencies of the above outlined capacitor charging process. In any given charge cycle, there will be an initial current I(o) flowing in the secondary circuit which will be the same for all charge cycles. There will be an initial charge on the load capacitance which we denote as Q(o). This will vary from zero at the first cycle of the charging process to approximately $V_F C$ at the start of the last cycle of the charge process.

In the accompanying analysis expressions have been derived for the efficiency of energy storage in the primary of the power transformer and criteria for this efficiency to be high are established, and, for the efficiency of capacitor charging in an R, L, C, circuit where the initial current is I(o) and the initial charge on the capacitor is Q(o). Algebraic expressions for efficiency are given for critically-damped parameters and for under-damped parameters. Several indicative numerical examples are presented.

Energy transfer from the low voltage power source to the primary of the power transformer is considered first,

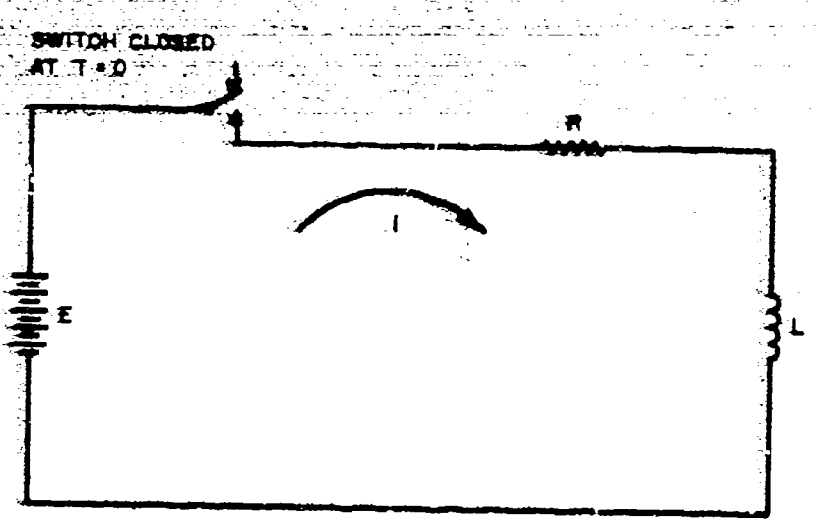

Figure 22. Equivalent Circuit Schematic

Current in the above circuit is given by:

$$i = \frac{E}{R}\left(1 - \epsilon^{-\frac{R}{L}t}\right) \qquad (1)$$

Efficiency is defined by:

$$\eta_1 = \frac{\text{energy stored in inductor (L)}}{\text{energy extracted from low voltage source E}}$$

$$\eta_1 = \frac{\frac{1}{2} L\, i\,(t)^2}{\int_0^t E\, i\,(\tau)\, d\tau} \qquad (2)$$

Substituting (1) in (2) there results:

$$\eta_1 = \frac{L}{2R} \frac{\left(1 - \epsilon^{-\frac{R}{L}t}\right)^2}{\left[t - \frac{L}{R}\left(1 - \epsilon^{-\frac{R}{L}t}\right)\right]} \qquad (3)$$

We next make the assumption that $\frac{R}{L}t \ll 1$ for with $\frac{R}{L}t$ large in (3), η_1 is small; this is of course not desired. Thus, with $\frac{R}{L}t$ small we approximate the exponentials in (3) by several terms in the series expansion:

$$1 - \epsilon^{-\frac{R}{L}t} = \frac{R}{L}t - \frac{R^2 t^2}{2L^2} + \frac{R^3 t^3}{6L^3} - \cdots$$

Substituting this result in (3) and upon appropriate simplifications yields:

$$\therefore \eta_1 \approx 1 - \frac{2Rt}{3L} + \frac{13\, R^2 t^2}{36\, L^2} - \cdots \qquad (4)$$

It is seen from (4) that if t, the time at which the switch is opened, is chosen short compared to the basic time constant L/R of the circuit, high efficiencies for the first part of the energy conversion process can be obtained.

The second part of the energy conversion process consists in transferring the energy stored in the first part with some efficiency, η_2, to the capacitor which is the load on the power conditioner. The circuit is shown in Figure 23.

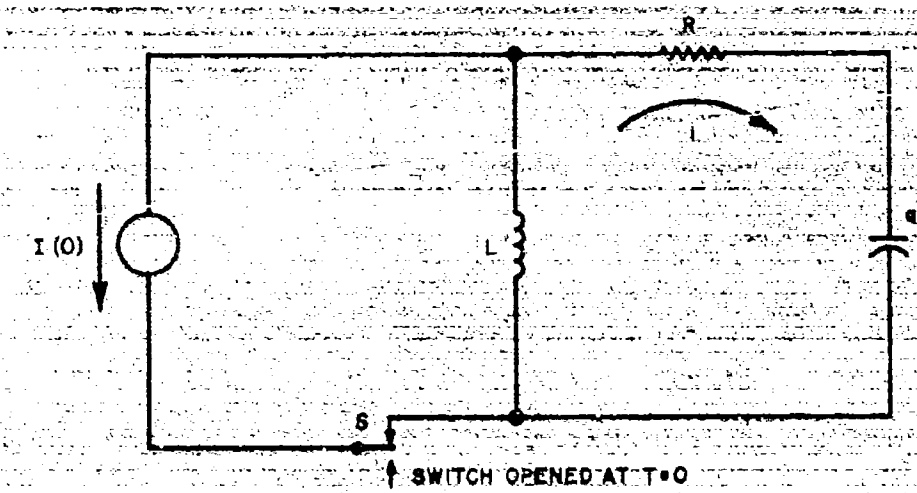

Figure 23. Equivalent Circuit Schematic, Continued

In the circuit of Figure 23 it is assumed that prior to t=0 the current I(o) is established in inductance L. At t=0 the switch S is opened and a charging current i(t) flows in a manner governed by R, L, C, and I(o), Q(o), the initial values of i(t) and q(t) the charge on the capacitor, respectively. The process is assumed to continue, until the current i(t) crosses 0 at which time due to the presence of a series diode in the actual circuit, the second part of the energy transfer process is completed. Below, expressions are first developed for i(t). Then efficiency for the second half of the charging process is defined. Results for i(t) are applied to the efficiency expression and expressions are developed for efficiency in terms of R, L, C, I(o), and Q(o).

In the time domain for the circuit of Figure 23, once the switch opens we have the following differential equation governing current in the circuit:

$$L\frac{di}{dt} + Ri + \frac{q}{C} = 0 \qquad (5)$$

or, in terms solely of the variable q ($i = \frac{dq}{dt}$) (5) becomes:

$$L\frac{d^2q}{dt^2} + R\frac{dq}{dt} + \frac{q}{C} = 0 \qquad (6)$$

To facilitate prompt solution we take the Laplace Transform of both sides of (6). Letting the Laplace Transform of q(t) be Q (p) we arrive at the following:

$$\mathcal{L}\left\{\frac{d^2q}{dt^2}\right\} = p^2 Q(p) - pQ(o) - I(o) \qquad (7)$$

From (7), (6) there results:

$$Q(p) = \frac{(R + L_p)\, Q(o) + L\, I(o)}{Lp^2 + Rp + \frac{1}{C}} \qquad (8)$$

Now in order to convert (8) to the Laplace Transform of the current we take note of the following:

$$I(p) = \mathcal{L}\{i(t)\} = \mathcal{L}\left\{\frac{dq}{dt}\right\} = pQ(p) - Q(o) \qquad (9)$$

When substituted into (8), equation (9) becomes:

$$I(p) = \frac{pI(o) - \frac{Q(o)}{LC}}{\left\{p + \frac{R}{2L}\left(1 - \sqrt{1 - \frac{4L}{R^2C}}\right)\right\}\left\{p + \frac{R}{2L}\left(1 + \sqrt{1 - \frac{4L}{R^2C}}\right)\right\}} \qquad (10)$$

In order to take the Inverse Laplace Transform of (10), it is necessary to stipulate to a degree, the parameter $4L/R^2C$. If $4L/R^2C \neq 1$ we get by partial fraction expansion of (10)

$$I(p) = \frac{\frac{I(o)}{2} - \frac{\frac{2Q(o)}{RC} + I(o)}{2\sqrt{1 - 4L/R^2C}}}{p + \frac{R}{2L}\left(1 - \sqrt{1 - \frac{4L}{R^2C}}\right)} + \frac{\frac{I(o)}{2} + \frac{\frac{2Q(o)}{RC} + I(o)}{2\sqrt{1 - 4L/R^2C}}}{p + \frac{R}{2L}\left(1 + \sqrt{1 - \frac{4L}{R^2C}}\right)} \qquad (11)$$

The Inverse Laplace Transform of a function of the form

$\frac{A}{p+\omega_o}$, is given by:

$$\mathcal{L}^{-1}\left\{\frac{A}{p+\omega_o}\right\} = A\,\epsilon^{-\omega_o t} \qquad (12)$$

Applying (12) to (11) and making use of the property that the Inverse Laplace Transform of the sum is the sum of the Inverse Laplace Transforms, we get, for $4L/R^2C \neq 1$

$$I(t) = I(o)\,\epsilon^{-\frac{R}{2L}t}\cosh\frac{R}{2L}t\sqrt{1-\frac{4L}{R^2C}} - \frac{\left[\frac{2Q(o)}{RC}+I(o)\right]}{\sqrt{1-\frac{4L}{R^2C}}}\,\epsilon^{-\frac{R}{2L}t}\sinh\frac{R}{2L}t\sqrt{1-\frac{4L}{R^2C}} \qquad (13)$$

If, on the other hand, $4L/R^2C = 1$, (10) becomes:

$$I(p) = \frac{pI(o) - \frac{Q(o)}{LC}}{\left(p+\frac{R}{2L}\right)^2} \qquad (14)$$

The Inverse Laplace Transform of a function of the form:

$$\frac{F(p)}{(p+\omega_o)^2} = \left.\frac{\partial\left[F(p)\,\epsilon^{pt}\right]}{\partial p}\right|_{p=-\omega_o} \qquad (15)$$

Applying (15) to (14) where $F(p) = pI(o) - \frac{Q(o)}{LC}$ and $\omega_o = \frac{R}{2L}$, we get:

$$I(t) = e^{-\frac{R}{2L}t}\left[I(o) - t\left(\frac{RI(o)}{2L} + \frac{Q(o)}{LC}\right)\right] \tag{16}$$

The next important determination is the time, t_o, when the current drops to zero following its initial value of I(o). As mentioned above, at this point the cycle is halted by the action of a series diode in the Wilmore charging circuit.

By (13) the case $4L/R^2C \neq 1$ becomes:

$$\frac{\sinh \frac{R}{2L} t_o \sqrt{1 - \frac{4L}{R^2C}}}{\cosh \frac{R}{2L} t_o \sqrt{1 - \frac{4L}{R^2C}} - \frac{2Q(o)}{RC} \frac{1}{I(o)}} = \frac{I(o)\sqrt{1 - \frac{4L}{R^2C}}}{} \tag{17}$$

The second case $(4L/R^2C = 1)$ yields, by (16):

$$t_o = \frac{2LC\, I(o)}{I(o)\, RC + 2Q(o)} \tag{18}$$

We next proceed to the efficiency calculations. The efficiency of energy transfer during the period $0 \leq t \leq t_o$ will be given by the ratio of the energy gained in the capacitance stored energy to the energy initially stored in the inductance L. Thus, for this, the second part of the charging process:

$$\eta_2 = \frac{\frac{1}{2C}\left[Q_{to}^2 - Q(o)^2\right]}{\frac{1}{2} L\, I(o)^2} \tag{19}$$

where Q_{to} is defined by:

$$Q_{to} = Q(o) + \int_o^{t_o} i\,(t)\ dt \qquad (20)$$

Efficiency expressions have been derived for the cases $4L/R^2C > 1$ (under-damped) and $rL/R^2C = 1$ (critically-damped). As evidenced by (20) is necessary to compute

$$\int_o^{t_o} i\,(t)\ dt$$

For $4L/R^2C > 1$, (13) becomes:

$$i(t) = I(o)\ \epsilon^{-\frac{R}{2L}} \cos \frac{R}{2L} t \sqrt{\frac{4L}{R^2C} - 1} - \frac{\left[\frac{2Q(o)}{RC} + I(o)\right] \epsilon^{-\frac{R}{2L} t}}{\sqrt{\frac{4L}{R^2C} - 1}} \sin \frac{R}{2L} t \sqrt{\frac{4L}{R^2C} - 1} \qquad (21)$$

Evaluation of $\int_o^{t_o} i(t)\ dt$ for (21) yields:

$$\int_o^{t_o} i(t)\ dt = \frac{I(o) 2L\ \epsilon^{-\frac{R}{2L} t_o}}{R\sqrt{\frac{4L}{R^2C} - 1}} \left[\sin \frac{R}{2L}\ t_o \sqrt{\frac{4L}{R^2C} - 1} \right]$$

$$+ Q(o)\ \epsilon^{-\frac{R}{2L} t_o} \left[\cos \frac{R}{2L}\ t_o \sqrt{\frac{4L}{R^2C} - 1} + \frac{\sin \frac{R}{2L}\ t_o \sqrt{\frac{4L}{R^2C} - 1}}{\sqrt{\frac{4L}{R^2C} - 1}} \right]$$

$$- Q(o) \qquad (22)$$

and by (20)

$$Q_{to} = \frac{I(o)\,2L\,\epsilon^{-\frac{R}{2L}t_o}}{R\sqrt{\frac{4L}{R^2C}-1}}\left[\sin\frac{R}{2L}t_o\sqrt{\frac{4L}{R^2C}-1}\right]$$

$$+Q(o)\epsilon^{-\frac{R}{2L}t_o}\left[\cos\frac{R}{2L}t_o\sqrt{\frac{4L}{R^2C}-1}+\frac{\sin\frac{R}{2L}t_o\sqrt{\frac{4L}{R^2C}-1}}{\sqrt{\frac{4L}{R^2C}-1}}\right] \qquad (23)$$

Substitution of (23) into (19) yields, after several manipulations:

$$\eta_2 = \frac{1}{LC}\left(\frac{Q(o)}{I(o)}\right)^2\left[\epsilon^{-\frac{R}{L}t_o}\left(\cos\frac{R}{2L}t_o\sqrt{\frac{4L}{R^2C}-1}+\frac{\sin\frac{R}{2L}t_o\sqrt{\frac{4L}{R^2C}-1}}{\sqrt{\frac{4L}{R^2C}-1}}\right)^2-1\right]$$

$$+\frac{1}{LC}\epsilon^{-\frac{R}{L}t_o}\left[\frac{4L^2}{R^2}\,\frac{\sin^2\frac{R}{2L}t_o\sqrt{\frac{4L}{R^2C}-1}}{\frac{4L}{R^2C}-1}\right]$$

$$+\left(\frac{Q(o)}{I(o)}\right)\frac{4\epsilon^{-\frac{R}{L}t_o}}{RC\sqrt{\frac{4L}{R^2C}-1}}\left[\sin\frac{R}{2L}t_o\sqrt{\frac{4L}{R^2C}-1}\right]\left[\cos\frac{R}{2L}t_o\sqrt{\frac{4L}{R^2C}-1}+\frac{\sin\frac{R}{2L}t_o\sqrt{\frac{4L}{R^2C}-1}}{\sqrt{\frac{4L}{R^2C}-1}}\right] \qquad (24)$$

Now, by making use of (17) as applied to the case $4L/R^2C > 1$ one can show that:

$$= \frac{\frac{LC}{2}\,\epsilon^{-\frac{R}{L}t_o}}{\left(\frac{Q(o)}{I(o)}\right)^2 + RC\left(\frac{Q(o)}{I(o)}\right) - LC} + 2\,\frac{Q(o)}{I(o)}\,\frac{\epsilon^{-\frac{R}{L}t_o}\left[\frac{RC}{2} + \frac{Q(o)}{I(o)}\right]}{\left[\left(\frac{Q(o)}{I(o)}\right)^2 + RC\,\frac{Q(o)}{I(o)} + LC\right]}$$

$$+ \frac{1}{LC}\left(\frac{Q(o)}{I(o)}\right)^2\left[\epsilon^{-\frac{R}{L}t_o}\left(\frac{\left(\frac{Q(o)}{I(o)}\right)^2 + 2RC\,\frac{Q(o)}{I(o)} + R^2C^2}{\left(\frac{Q(o)}{I(o)}\right)^2 + RC\,\frac{Q(o)}{I(o)} + LC}\right) - 1\right] \tag{25}$$

We next perform the efficiency calculation for the case $4L/R^2C = 1$. In this case, by (16)

$$\int_o^{t_o} I(t)\,dt = \left[1 - \epsilon^{-\frac{R}{2L}t_o}\right]\left[\frac{2L}{R}\right]I(o) - \frac{4L^2}{R^2}\left(\frac{RI(o)}{2L} + \frac{Q(o)}{LC}\right)\left[1 - \epsilon^{-\frac{R}{2L}t_o}\right]$$

$$+ \frac{2L}{R}\left[\frac{RI(o)}{2L} + \frac{Q(o)}{LC}\right]t_o\,\epsilon^{-\frac{R}{2L}t_o} \tag{26}$$

Substitution of (18) into (26) and making use of the fact that $4L/R^2C = 1$, yields:

$$\int_o^{t_o} I(t)\,dt = -Q(o) + Q(o)\,\epsilon^{-\frac{R}{2L}t_o} + \frac{2L}{R}I(o)\,\epsilon^{-\frac{R}{2L}t_o} \tag{27}$$

and by (20)

$$Q_{to} = \left[Q(o) + \frac{2L}{R}I(o)\right]\epsilon^{-\frac{R}{2L}t_o} \tag{28}$$

Substitution of (28) into (19) results in the following efficiency expression for the critically damped case:

$$\eta_2 = \frac{1}{LC}\left\{\frac{2L}{R}\left(\frac{L}{R}+\frac{Q(o)}{I(o)}\right)\epsilon^{-\frac{I(o)}{\frac{I(o)}{2}+\frac{Q(o)}{RC}}} - \left(\frac{Q(o)}{I(o)}\right)^2\left(1-\epsilon^{-\frac{I(o)}{\frac{I(o)}{2}\frac{Q(o)}{RC}}}\right)\right\} \qquad (29)$$

2.3.2a Numerical Examples

The main results of the preceding section are the efficiency expressions (4), (25), and (29).

Equation (4) needs no numerical interpretation; Equations (25) and (29) however, are somewhat more difficult to access by inspection.

As exemplary calculations, two sets of more or less realistic parameters are chosen, one under-damped and one critically damped. Since efficiency is seen to vary with initial conditions two extremes for each case are calculated and the results documented. For the under-damped case we choose $L = 2.5$ henries, $C = 10\ \mu f$, $R = 500$ ohms and for the critically damped case we choose $L = 2.5$ henries, $C = 10\ \mu f$, and $R = 1000$ ohms. $I(o)$ is assumed equal to 10 ma in all cases and $Q(o)$ is allowed to assume two values in each case, -0 and 10^{-2} coulombs (corresponding to 1000 volts on a $10\mu f$ thruster capacitor). The purpose is to compare with a minimum computation the incremental efficiencies at both extremes of the charge cycle.

For $Q(o) = 0$, Equation (25) becomes:

$$\eta_2 = \epsilon^{-\frac{R}{L}t_o} \qquad (30)$$

where t_o is given by:

$$\sin \frac{R}{2L} t_o \sqrt{\frac{4L}{R^2C} - 1} = \sqrt{1 - \frac{R^2C}{4L}} \qquad (31)$$

If we let $C = .10^{-5}$, $L = 2.5$, $R = 500$, we get:

$$t_o = \frac{\pi}{3.3\,(100)} = .00604 \text{ seconds} \qquad (32)$$

and by (30),

$$\eta_2 = 29.8\% \qquad (33)$$

For $Q(o) = 10^{-2}$, numerical substitution into (25) requires performing computations to 6 or 7 decimal places. When this was done, the result for efficiency at the latter end of the charge cycle was,

$$\eta_2 = 97.35\% \qquad (34)$$

The corresponding calculations using (29) and the critical damped case parameters yielded for $Q(o) = 0$,

$$\eta_2 = 18.5\% \qquad (35)$$

and for $Q(o) = 10^{-2}$, again with lengthy computations,

$$\eta_2 = 96\% \qquad (36)$$

From these few examples it is seen that a) efficiencies run higher in the under-damped case, b) incremental efficiencies are lowest when the capacitor is uncharged and reach very high values for the final charge cycles, and c) the time t_o, is a variable which depends on the initial charge $Q(o)$, in this particular numerical example ranging from 5 milliseconds for the $Q(o) = 0$ charge cycle to 0.25 milli-seconds for the $Q(o) = 10^{-2}$ coulombs charge cycle. This latter result suggests that in order to build up the capacitor charge in minimum time, using the method

outlined, a variable repetition rate should be employed controllable by the time t_o. The results also suggest that should the power conditioner load capacitance only be partially discharged into its particular load, higher charging efficiencies could be realized.

In conclusion, general expressions have been developed for capacitor charging efficiencies using a constant energy per cycle power conditioner similar to the Wilmore method. More complete numerical results on optimization can be obtained using a computer to make the numerous lengthy numerical calculations needed for this additional work.

2.3.3 Experimental Studies

In order to experimentally determine actual power conditioning overall efficiency and its life, several power conditioners were procured from Wilmore Electronics, Inc. in accordance with specifications furnished by Fairchild Hiller/Republic Aviation Division. In particular, three different models were designed, built, and tested:

Model	Description
1032	Breadboard circuit to charge a 20 joule capacitor to 1 KV ± 5% at a rate up to 4 Hz, or any combination of pulse frequency and discharge energy which results in 20 watts of output power at 1KV.
B032-1	Same as Model 1032, but packaged to produce the highest possible component density.
1035	Breadboard circuit to charge a 20 joule capacitor to 1.5KV ±5% at a rate up to 2 Hz, or any combination of pulse frequency and discharge energy which results in 40 watts of output power at 1.5 KV. A 500 volt output was also provided capable of charging up to 0.1 μfd in unison with the main output.

All three models had an input power of 28V d.c. Figures 24 and 25 show Models 1035 and B032-1 respectively.

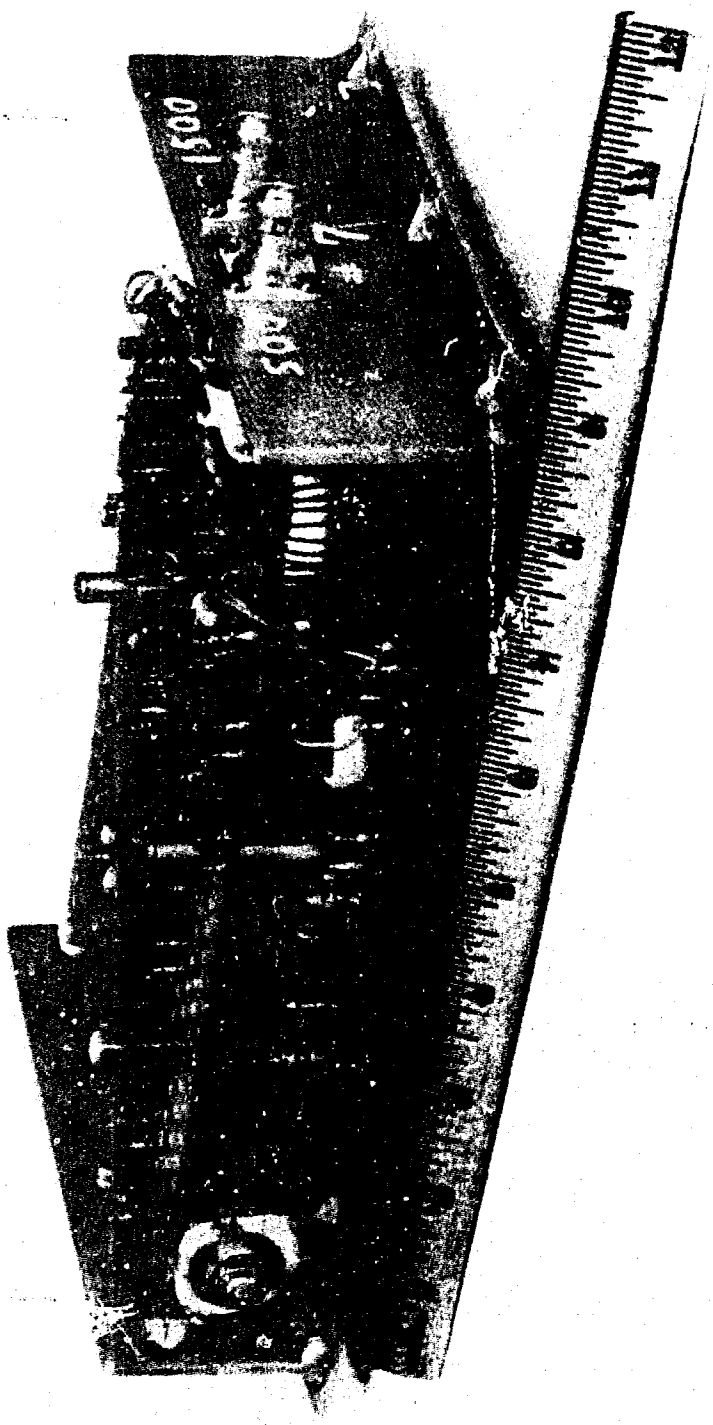

Figure 24. 40 Watt Breadboard Power Conditioner

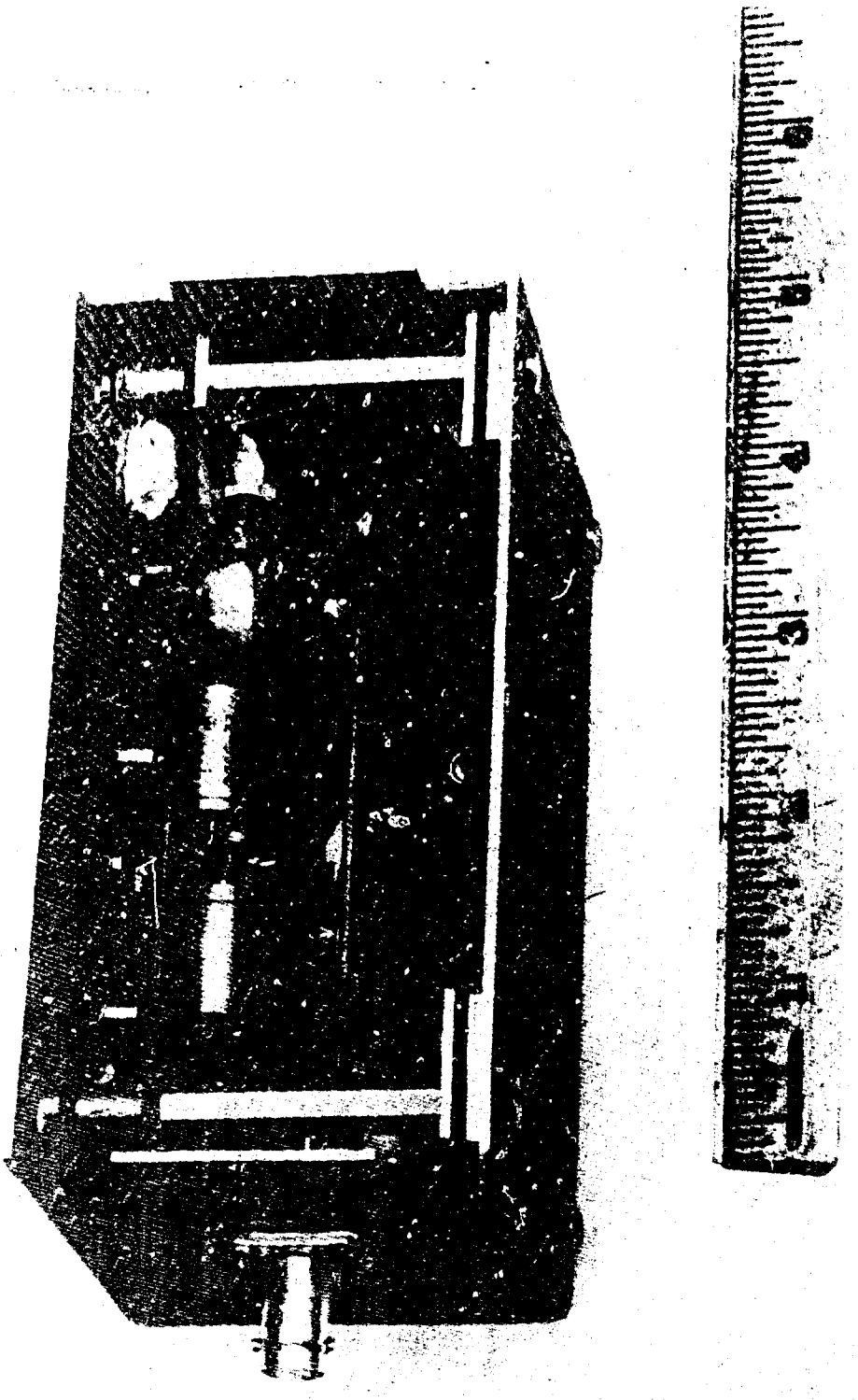

Figure 25. 20 Watt Packaged Power Conditioner

2.3.3a Life Tests

It was highly desirable to life test the power conditioners under conditions which represent those occurring while powering a thruster. Therefore, two approaches were taken in life testing of power conditioners. In one case, a given power conditioner was used to power thrusters undergoing tests. A running record was maintained of the total accumulated number of discharges to which the power conditioner was subjected. In the second case, a discharge simulator was designed, built, and used to life test a power conditioner[11]. To perform this latter testing, a thruster was operated and the discharge current and voltage waveforms were recorded. From these, equivalent fixed values of resistance and inductance at the same capacitance were calculated which would produce the same voltage and current shapes in an equivalent series LCR circuit. Then, this equivalent circuit (the "discharge simulator") was used instead of a thruster. Figure 26 shows one of the simulators that was used during power conditioner life tests. With this technique it was possible to keep the power conditioner in an evacuated bell jar while the simulator remained in air.

Table 5 presents some of the results that have been obtained with the three different models. Model 1032 was operated for 4.26×10^7 discharges before it was accidentally damaged. Model B032-1 has accumulated 3.54×10^7 discharges and is still operational. Using a nominal figure of 3.5 μ lb-sec/joule for the impulse bit of a typical thruster and noting that each discharge was at the 5 joule level, it is readily seen that the life of model 1032 was equivalent to 745 lb-sec of total impulse at a thrust level of 17.5 μ lbs before it was accidentally damaged by venting the test facility to air before input power was removed. Several other power conditioners were also accidentally damaged while testing. These failures are attributed to the fact that elements of the power conditioner will fail if the output load is removed while input power is supplied. While the Wilmore power conditioners are protected against short circuits, they were not protected against open circuits. While it is a simple matter to place a small auxiliary protective capacitor across the output of the power conditioner to preclude such accidents, the few percent loss in efficiency was considered undesirable.

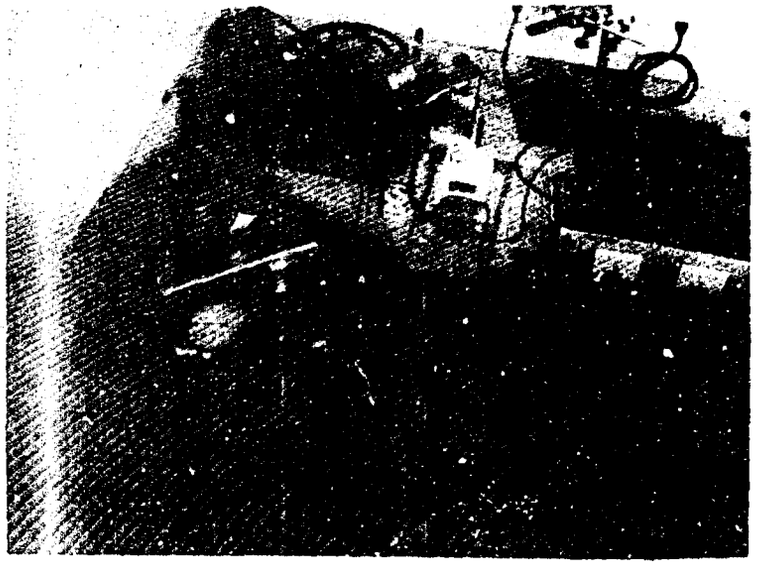

Figure 26. Power Conditioner Discharge Simulator

TABLE 5. POWER CONDITIONER LIFE TEST STUDIES

Description	Model	Serial No.	Simulated Discharges		Thruster Discharges		
			PC in Air	PC in Vacuum	PC in Air	PC in Vacuum	Total on Unit
5 j Breadboard	1032	10/13/66	19,423,714	24,033,042	3,496,659	0	46,953,415*
5 j Breadboard	B032-1	BO 32-1	23,700,016	0	11,784,933	0	35,484,949
20 j Breadboard	1035	1035BB-2	516	0	8,052,840	815,529	8,868,885***
20 j Breadboard	1035	1035BB-3	1,334,097	442,700	3,115,060+	567	4,892,424*
20 j Breadboard	1035	1035BB-4	617	0	1,743,366	0	1,743,983****
20 j Breadboard	1035	1035BB-5	7,547	3,085,509	1,247,464	0	4,341,020
20 j Breadboard	1035	1035BB-6	2,688,555	0	360,997	0	3,049,052**
20 j Breadboard	1035	1035BB-7	1,988	0	703,569	0	705,557

* 4.26×10^7 discharges were carried out before unit was repaired due to accidental damage
** Returned to manufacturer for repair after 2,688,555 discharges
*** Damaged due to vacuum failure (has been repaired
**** Damaged during test
\+ Plus discharges accumulated at A.F.A.P.L.

In no case has a limiting factor been established which suggests that a life of 10^8 discharges could not be realized if given sufficient testing time.

2.3.3b Efficiency Measurements

Three alternate efficiency measurements have been made on the Wilmore power conditioners:

1. A well regulated voltage source was used to drive the Wilmore unit. The current delivered by this source was monitored by a d.c. ammeter. The varying meter reading was used to estimate an average current. The efficiency was then calculated using the relation

$$\eta = \frac{\frac{1}{2}CV^2f}{E_{bb}I_{av}} = \frac{\frac{1}{2} \times 10^{-5} \times 10^6 \times 4}{28 \times 0.92} = 77.6\%$$

The resistance in the capacitor discharge circuit for this test was 0.5 ohm, a value for under-damped discharge.

2. It was felt that an unknown margin of error was being encountered in the estimate of the average current above, so an alternate method of efficiency computation was used.

A small 0.3 ohm resistor was placed in series with the floating return of the 28 volt power supply. An oscillogram of the repetitive voltage appearing across this resistor served to give the current waveform as drawn by the Wilmore unit. Utilizing this oscillogram, a graphical integration was performed to ascertain the true average current. The efficiency was then recomputed, subtracting a small loss for the 0.3 ohm resistor from the input power. The efficiency was computed in the above manner for an under-damped discharge (load resistance = 0.25 ohms) and an under-damped discharge (load resistance = 0.5 ohms). Due to varying eye interpretation of the oscillograms, a range of efficiencies were computed based on different readings. The computed efficiencies were:

(a) 76.9% to 78.1% for a load resistance of 0.25 ohms

(b) 78.2% to 78.3% for a load resistance of 0.5 ohms

In the first case a negative voltage of approximately 200 V was on the 10.02 μf load capacitance at the start of the charge period while in the second under-damped case a slight negative voltage of approximately -80 volts was on the capacitor at the start of the charge period thus accounting for the slightly higher efficiency readings observed in the 0.5 ohm load resistor case. In the 0.25 ohm resistance case the power conditioner is supplying 0.651 watts more power than in the 0.5 ohm case. In an actual thruster operation the capacitor is charged from 0 volts and therefore the better estimate of efficiency in this case is in the range of 78.2% to 78.3%.

These efficiencies represent the best estimates available as of this date. These values check closely with the original estimate of 80% supplied by Wilmore.

2.3.3c Weight

No particular attempt was made to minimize the weight of Models 1032 or 1035. These weighed 1152 grams and 1492 grams, respectively. Model B032-1 weighed 720 grams. Quite generally, Wilmore Electronics Inc. claims that the weight of densely packaged power conditioners will depend upon the power level of operation in accordance with the values cited in Table 6.

TABLE 6. Power Conditioner Weight

Power Level	Weight
Below 200 watts	500 grams plus 11 grams/watt
Above 200 watts	500 grams plus 5 grams/watt

As a check, it is seen that the actual weight of 760 grams of Model B032-1 is very close to the calculated weight of 720 grams. Since the packaged weight of Model B032-1 weighs 66% of the breadboard Model 1032, one can assume that a packaged version of Model 1035 will be roughly 66% of the breadboard weight, or 985 grams. According to Table 6, a weight of 940 grams is predicted. It may, therefore, be safely assumed that the weight of state-of-the-art packaged power conditioners for pulsed plasma microthrusters will be in accordance with the schedule presented in Table 6. It is perhaps interesting to note at this point that the specific weight of power conditioning for the pulsed plasma microthruster system appears to equal the best values quoted for the state-of-the-art ion engine systems.

2.4 Discharge Initiation Subsystem

2.4.1 General

The discharge initiating subsystem is comprised of a pulse frequency control circuit (driver), an ignition circuit, and surface igniter plugs. The interrelationship of these components is shown in Figure 27. The function of the surface igniter plug is to create a microdischarge within the thruster nozzle for releasing the main thruster discharge. The energy for the microdischarge is provided by the ignition circuit which is powered by a roughly 500 V d.c. power supply and triggered by a driver. The driver enables the thruster to operate on a single pulse basis, a train of pulses or uninterrupted thrusting. Two typical laboratory drivers are shown in Figures 28 and 29 respectively. The time lapse between the release of a triggering pulse by the driver until the occurrence of an impulse bit has been measured to be roughly 0.2μ seconds with the main thruster capacitor and ignition circuit previously energized.

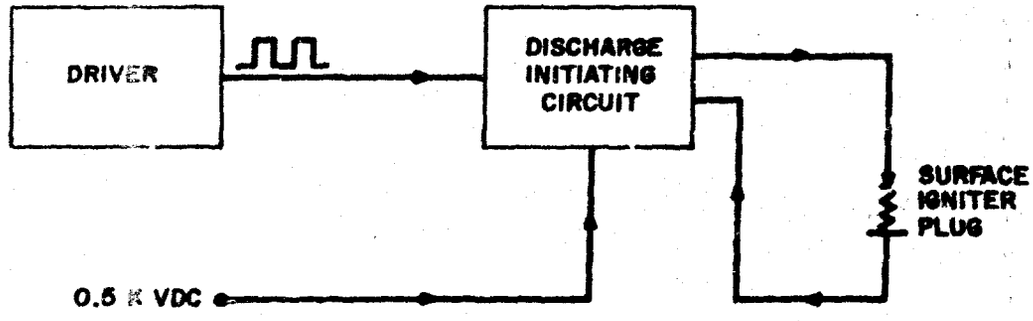

Figure 27. Discharge Initiation Subsystem Block Diagram

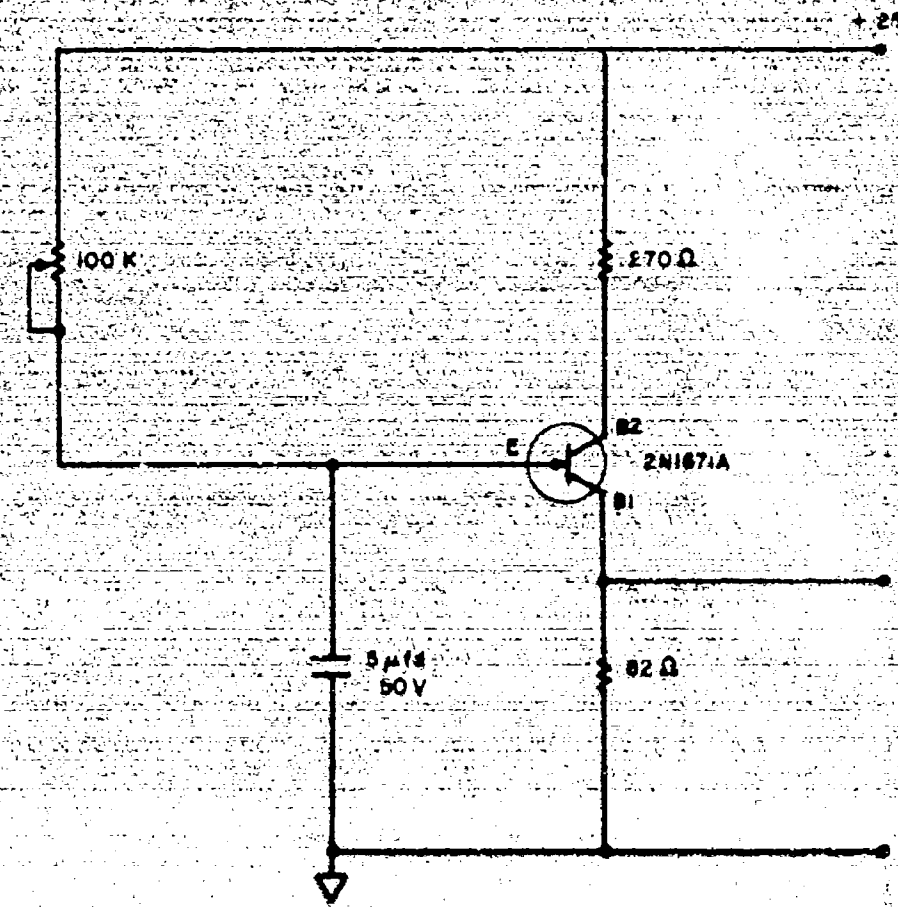

Figure 28. Single Frequency Laboratory Driver

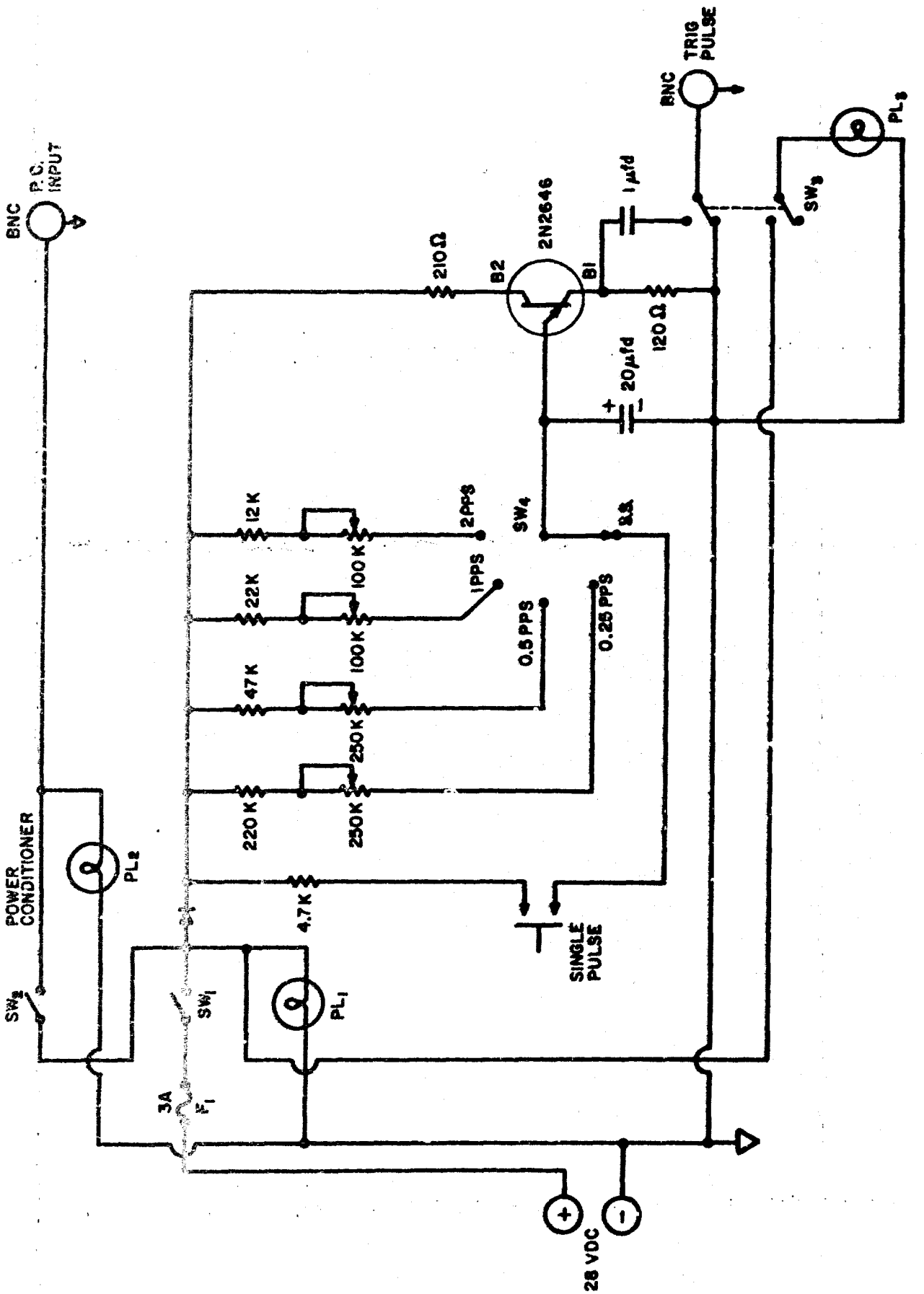

Figure 29. Variable Frequency Laboratory Driver

2.4.2 Ignition Circuit

Three different ignition circuits were developed during the course of the present program each representing a substantial improvement over the previous design. These three systems are denoted as the Krytron ignition system, the spark gap ignition system, and the transformer system, respectively.

2.4.2a Krytron Ignition System

The Krytron is an EG&G four-element (grid, anode, cathode, and keep-alive) cold cathode gas filled switch tube, designed to operate in an arc discharge mode. A column of ionized gas, appearing in the glow mode, and maintained by a "keep-alive" current, provides an initial source of plasma. This "keep-alive" current prevents the tube from conducting until a positive pulse is applied to the grid.

In the Krytron ignition circuit (Figure 30) capacitor C_1 is charged up to 4 KV through R_1. Resistor R_2 provides the Krytron with 40 μ A, of "keep-alive" current. When a positive pulse from the driver is applied to the gate of the SCR it conducts the discharge C_2 through the primary of T_1. This produces an 800V pulse on the grid of the Krytron which discharges C_1 through the igniter plug causing it to fire.

The Krytron used in this system is a special version of a standard tube. This Krytron has a high gas fill pressure which increases the life of the tube in this application to 1.3×10^7 shots, a factor of 30 over that of the standard tube.

A prototype of the above system (see Figure 31) was built in a volume of four cubic inches and weighed 193 grams. This weight included, for test purposes, a 10 pps generator which was used to fire the ignition system. This system was tested in a vacuum environment and performed reliably throughout its life of 1.3×10^7 shots. Other life tests of this circuit are presented in Table 7.

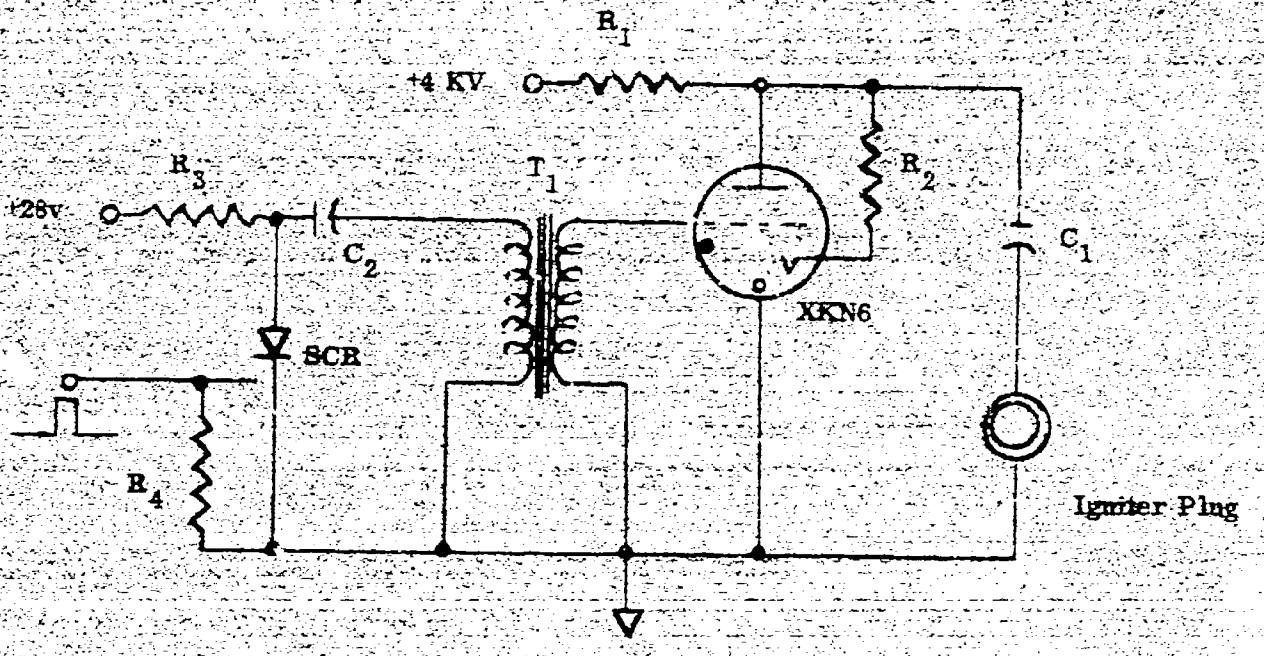

Figure 30. Krytron Ignition System

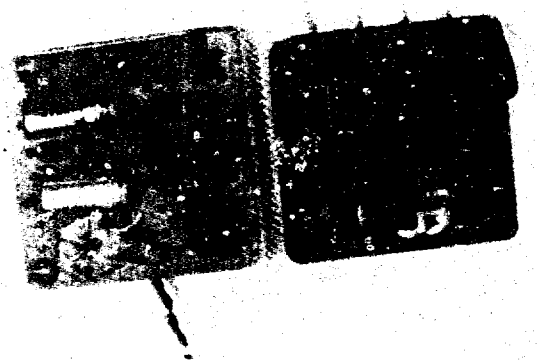

Figure 31. Prototype Krytron Ignition System

TABLE 7. DISCHARGE INITIATION SUBSYSTEM COMPARISON

Model	Manufacturer	Energy/Discharge, Joules	Life	Current	C, V	
					μ fd.	KV
Krytron XKN6	EGG	0.016	1.3×10^7	47 ohm current limiter	0.002	4.0
Krytron XKN6	EGG	0.024	1×10^6	No current limiter	0.003	4.0
Krytron XKN6	EGG	0.024	1.2×10^6	No current limiter	0.003	4.0
Sparkgap TG107	Signalite	0.00915	6×10^7	No current limiter	0.0015	3.5
Sparkgap TG107	Signalite	0.0915	TIP ($> 3.6 \times 10^6$)	No current limiter	0.015	3.5
Sparkgap TG16	Signalite	0.00915	1.5×10^8	No current limiter	0.0015	3.5
X-1	Transformer	0.125	$> 1.85 \times 10^{7*}$	No current limiter		1.5
1	Transformer	0.125	$> 1.75 \times 10^{6*}$	No current limiter		1.5
2	Transformer	0.125	$> 2.52 \times 10^{6*}$	No current limiter		1.5

*Tests are conducted with thrusters and are still in progress.

This system had the inherent disadvantage of reduced life because of the limited life of the Krytron. A substantial improvement in life was achieved by the spark gap ignition system.

2.4.2b Spark-Gap Ignition System

This system was designed, built, and tested in an effort to eliminate the requirements of the 4 KV supply of the Krytron system, and to extend the life of the discharge initiating subsystem beyond the life of 1.3×10^7 discharges of a Krytron system using a single Krytron tube. The spark-gap ignition system utilizes a Signalite sealed spark-gap as the main switching element.

Figure 32 shows this system in block form while Figure 33 shows a breadboard system that was life tested. The principle of operation is as follows. A command pulse is sent to a silicon controlled switch (SWS) turning it on. The SCS in turn, turns on a 28 V d.c. to 4 KV converter which charges up a capacitor. When the voltage on the capacitor reaches 3.5 KV the sealed spark gap breaks down and discharges the capacitor across the igniter plug causing it to fire. When this happens a reset pulse is fed back to the SCS which turns the system off until it receives the next command pulse. The total "on-time" of this system is 0.03 seconds per pulse. A schematic of this system is shown in Figure 34. The breadboard circuit shown in Figure 34 accepts 28V d.c. at 40 ma and operates at a design pulse rate of 10Hz.

The voltage at which the spark gap breaks down as a function of continuous discharges is shown in Figure 35. The test in this case was arbitrarily terminated at 1.54×10^8 discharges when the conductivity of the gap had increased to the point where a 25% smaller energy would be delivered to the load. Such a reduction in energy would not have been sufficient to interfere with normal thruster operation.

2.4.2c Transformer Ignition System

This ignition system is an all solid state device and uses a step-up transformer to achieve the desired initiating pulse.

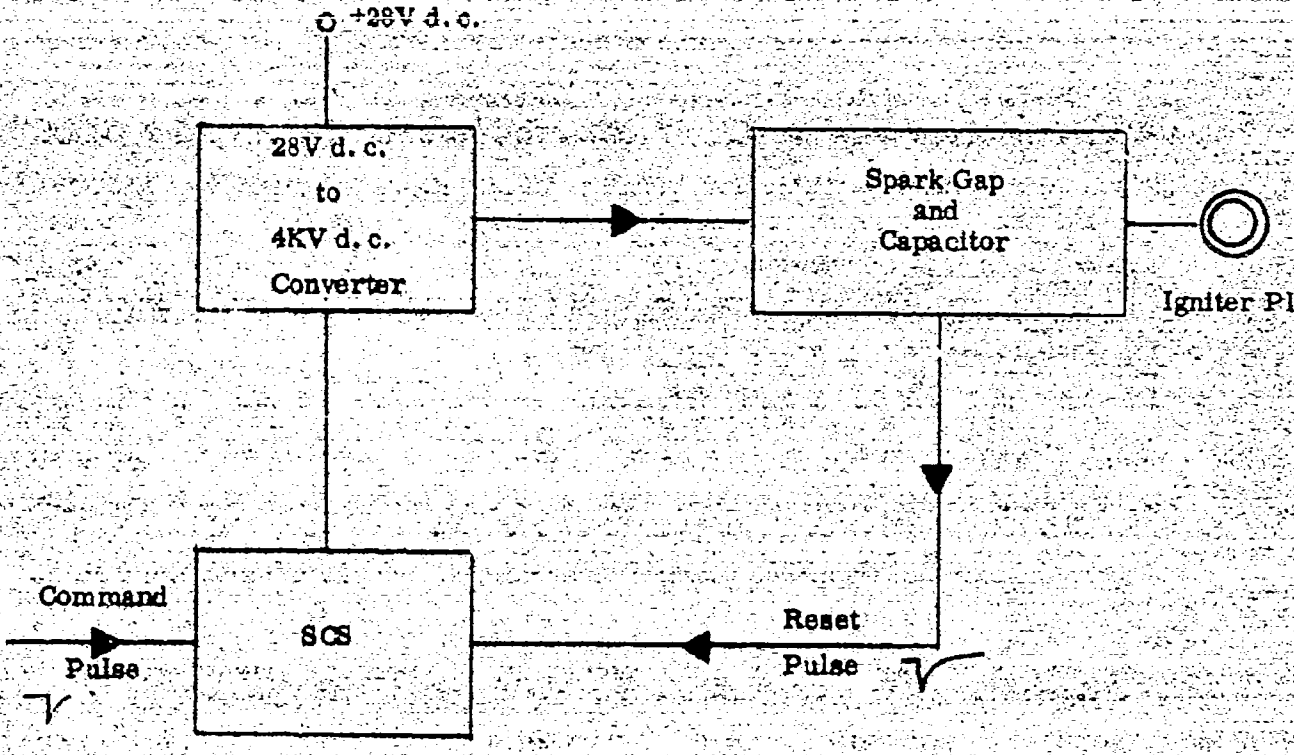

Figure 32. Block Diagram Spark Gap Ignition System

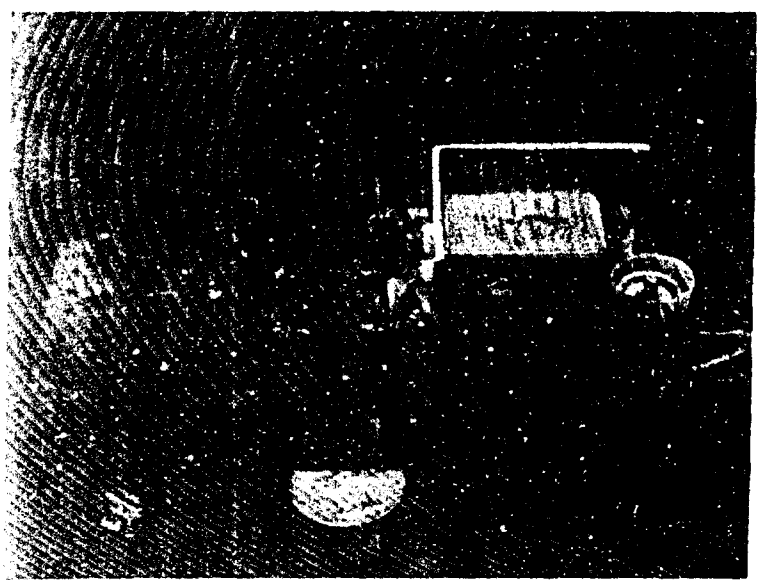

Figure 33. Spark Gap Ignition System

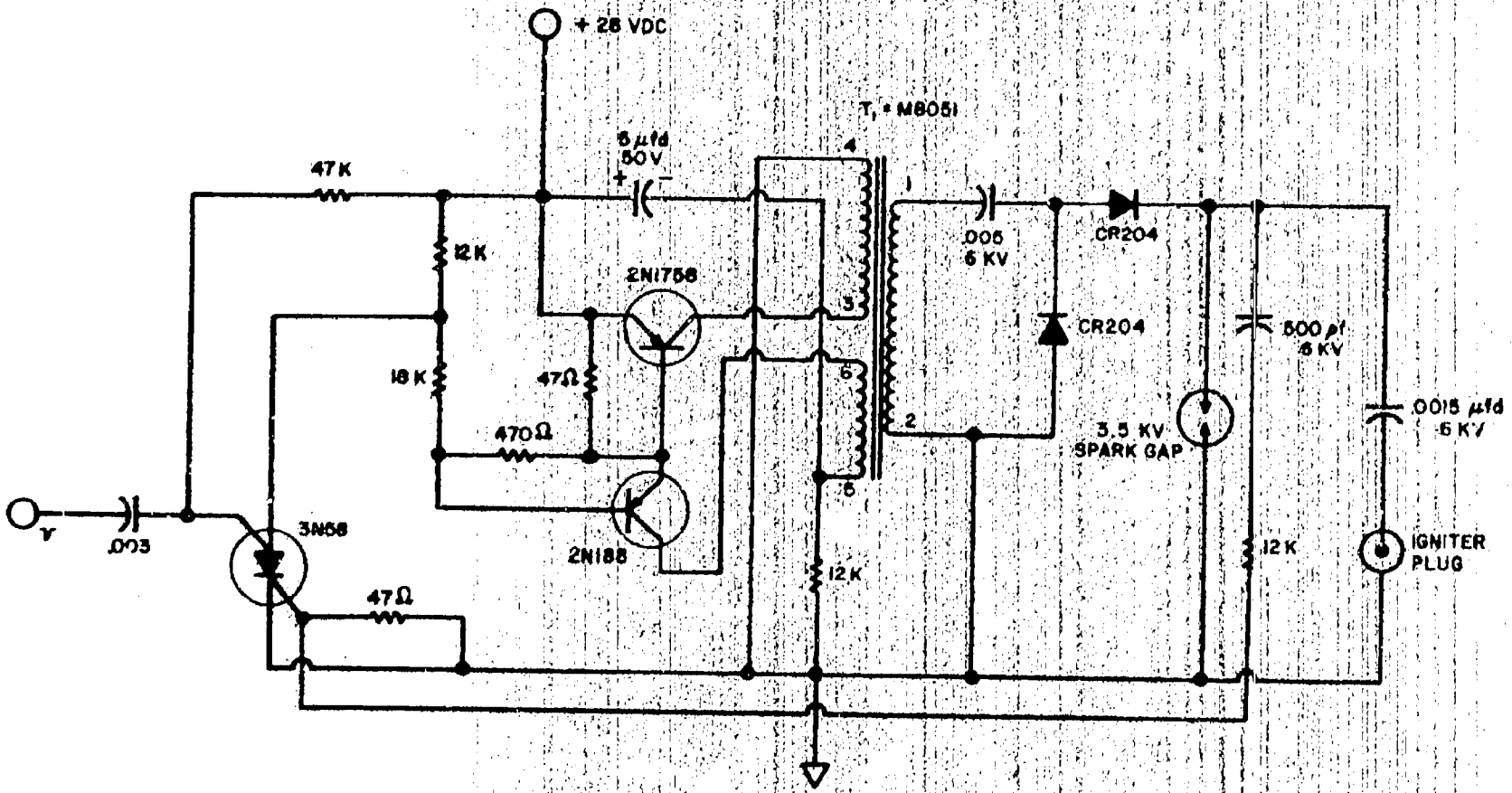

Figure 34. Spark Gap Ignition System Schematic

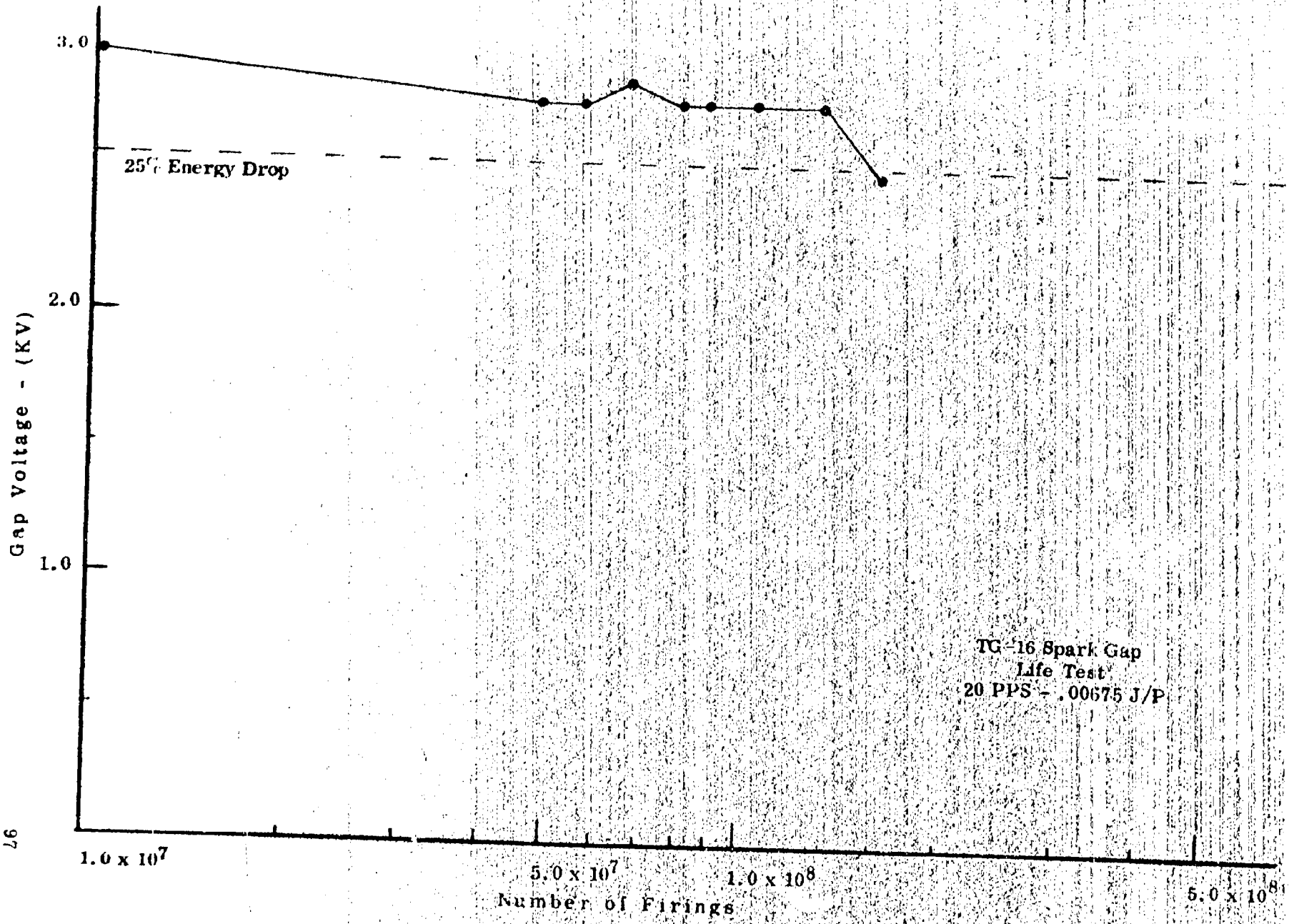

Figure 35. Spark Gap Ignition System Life Test

In this transformer circuit (see Figure 36) a capacitor (C_1) is charged from 500 to 550 volts by the main power conditioner. This capacitor is then discharged through an SCR into the primary of a 3:1 turns ratio pulse transformer. The discharge is accomplished by turning the SCR on with a trigger pulse from the driver. The transformer output of about 1100 volts is fed directly to the ignitar plugs. The SCR in the circuit turns itself off when the capacitor is fully discharged. The circuit is now ready for a repeat of the foregoing cycle.

The simplicity of the transformer network and the inherent life and reliability of it justified that further improvements and life tests of the spark gap ignition system be terminated. All thrusters are now operated with transformer ignition systems. Two typical dual transformer ignition systems which drive two thruster nozzles are shown in Figures 49 and 57 respectively.

A transformer discharge system was checked for high temperature and low temperature operation at a pulse rate of 5 Hz. All testing at temperatures above room ambient temperature was carried out in an oven with the temperature monitored by a thermocouple attached to the chassis of the discharge initiating circuit. Low temperature operation was carried out by lowering the discharge initiating network into an insulated container which was held several inches above the level of liquid nitrogen located in the container. The temperature of the circuit was regulated by controlling the distance between the transformer circuit being tested and the free surface of the liquid nitrogen. The temperature cycle experimentally investigated is shown in Figure 37. During the test three parameters were monitored: output voltage across a fixed load of 50 ohms, minimum trigger level, and total leakage of the circuit.

The results of this thermal test indicated no noticeable change of output pulse throughout the temperature cycle. The typical output pulse at temperature is shown in Figure 38. The total leakage current of the unit varied from 80μ amps at 100°C to less than 1μ amp at -80°C. The minimum trigger level varied from 2 volts at 100°C to 2.9 V at -80°C indicating that a trigger voltage of 3.5 volts would be adequate to fire the circuit under all conditions of temperature variation likely to be encountered in practice.

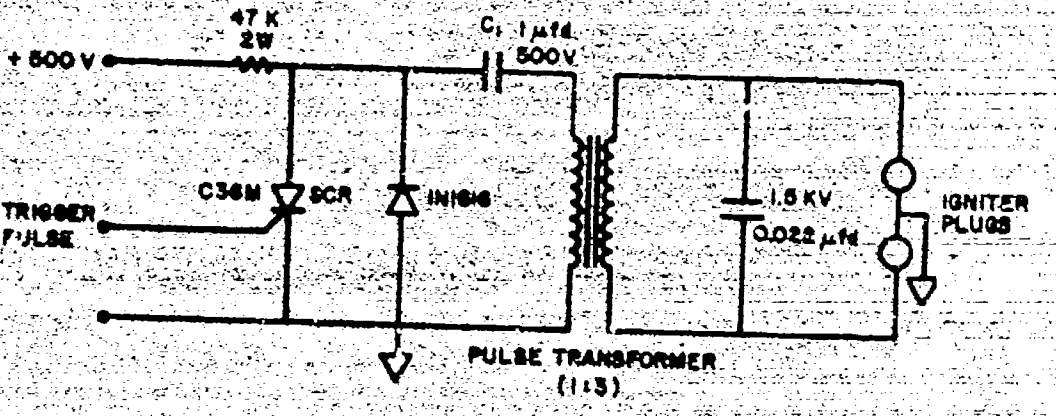

Figure 36. Transformer Discharge Initiating Network

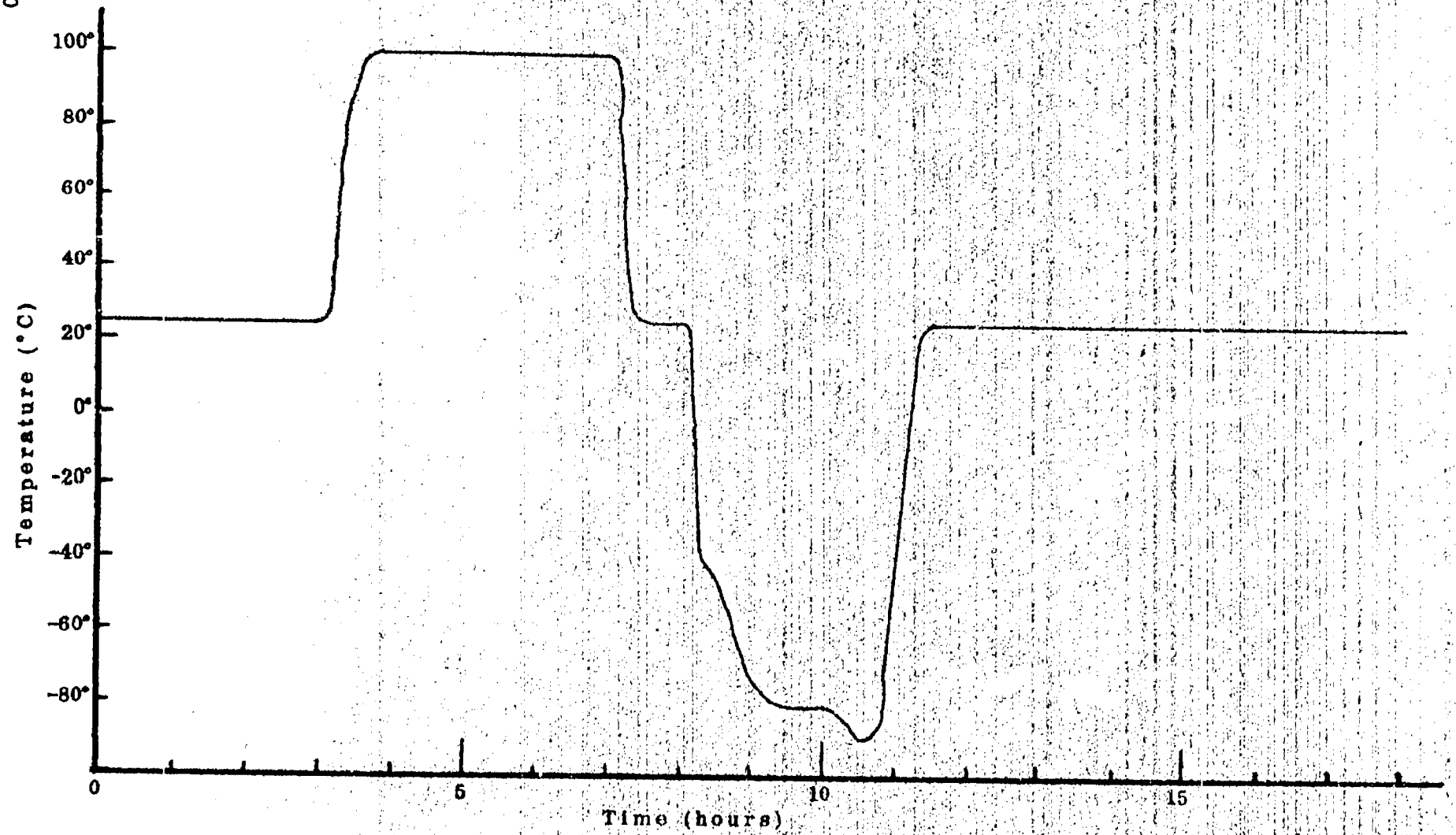

Figure 37. Temperature Cycle - Discharge Initiating Circuit -Thermal Test at 5 Hz

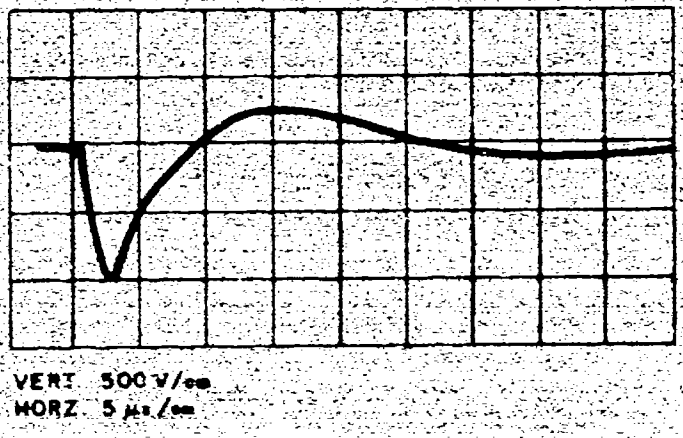

Figure 38. Typical Output Pulse

2.4.3 Surface Igniter Plug

The function of the igniter plug is to generate a microdischarge within the interelectrode region in order to release the main thruster capacitor.

Two basic mechanisms are possible for starting an electric discharge between two infinitely extending electrodes which are separated by a "perfect" vacuum and which are connected across the terminals of a charged capacitor. One of these mechanisms is to electrostatically draw particles from the electrode surface into the interelectrode region (see Reference 12, for example). The second mechanism is to inject either neutral or charged particles into the interelectrode spacing from a source other than the electrodes. If one considers a more realistic case where the two electrodes are joined to each other (i.e., are not extended infinity long) by a third element, then a discharge may be initiated in a perfect vacuum by either:

1) Injecting particles from the third element with the interelectrode region, or,
2) By switching voltage across the surface of the third element in the case where it is a conductor, or
3) Using auxiliary means for injecting particles into the interelectrode spacing in cases where the third element is normally nonconducting.

Since Teflon does not carry surface circuits which can be used to initiate the main thruster discharge, surface igniter plugs are used to inject particles into the interelectrode spacing*. The igniter plugs that are used are of a coaxial configuration with the interelectrode spacing filled with a semiconductor. In a vacuum environment a sliding discharge occurs across the semiconductor bridging the two igniter plug electrodes. A typical igniter plug which has been used for 5×10^6 discharges is shown in Figure 33. In a number of tests of a 20 joule/discharge thruster operated at 2 Hz, a given pair of igniter plugs have undergone

---

* The use of a pulsed heated filament similar to that reported in Reference 13 was also tried early in this program. The igniter plug technique was found to be more reliable.

a total of 1.25×10^7 discharges with no serious erosion of the cathode surface of the igniter plug. In terms of thruster performance this total number of discharges is equivalent to a total impulse of 760 lb-sec for the 130μ lb thrust level thruster in which the tests were carried out. It is believed that the basic life of a surface igniter plug which is electrically insulated (i.e., "floats" relative to the cathode via a resistor) is well within the life of the state-of-the-art of the remaining thruster components.

In one diagnostic test, a clean igniter plug was inserted in an ion pump vacuum facility (i.e., no possibility of oil contamination) and evacuated to 8×10^{-7} Torr. The plug was then operated and no rise in the vacuum background pressure could be observed.

An analytic study of the energy transfer efficiency into an igniter plug has been carried out and is presented below. In this analysis the energy absorbed by a semiconductor igniter plug is assumed to be related to its fixed d.c. resistance measured across its terminals*. The equivalent circuit of the existing transformer coupled discharge initiator circuit that was used to obtain quantitative estimates of the energy delivered to the igniter plug as a function of its d.c. resistance is shown in Figure 40. This d.c. resistance was allowed to vary between 0.01 ohms and 100 ohms in computations on the IBM 7094 and the in-house IBM "Quiktran" connection. It was assumed that the energy initially stored in the 1μ fd discharge capacitor was constant at 5 millijoules for each value of plug resistance used. This energy corresponds to the lower level of energy being used in thruster tests (normally about 125 millijoules are used in life tests of thrusters).

The circuit under consideration is shown in Figure 40. Prior to $t = 0$ a charge Q_o has been stored on capacitor C. At $t=0$ the switch is closed and the capacitor C is discharged through the primary of transformer T resulting

---

* In any actual case the resistance will be some time dependent function, the form of which is not yet known. See Reference 14, for example.

Figure 39. Surface Igniter Plug After 5×10^6 Discharges

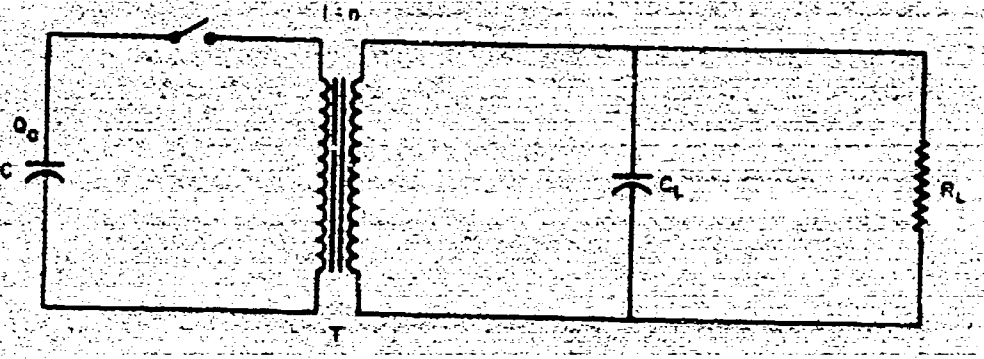

Figure 40. Discharge Initiating Circuit and Surface Igniter Plug

in a transfer of energy to load resistor R_L. A calculation for the energy transferred to load resistor R_L has been based on the circuit approximation to Figure 40 given in Figure 41, wherein the capacitor C has been reflected to the secondary of transformer T and the transformer has been replaced by an equivalent series inductance resistance combination L_T, R_T. If we apply Kirchoff's Law to the two loops in Figure 41, we get:

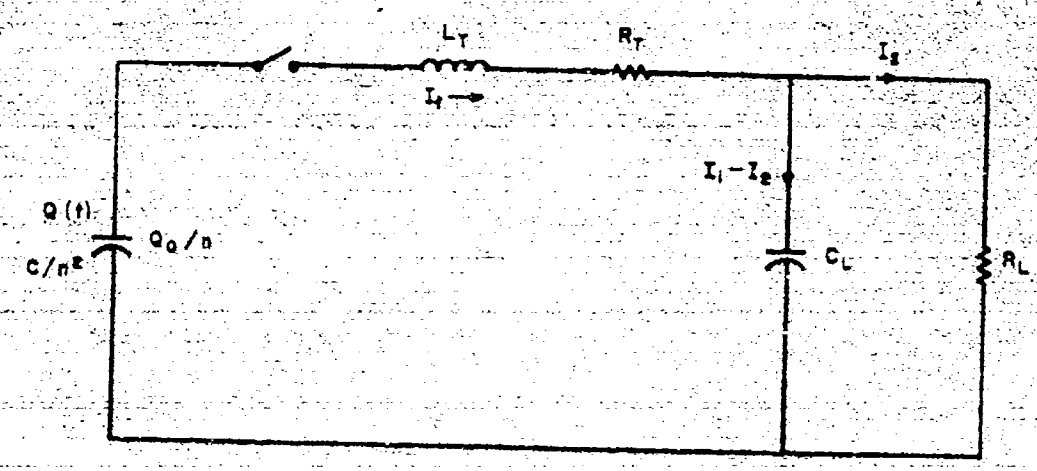

Figure 41. Equivalent Circuit

$$\frac{n^2 Q(t)}{C} - L_T \frac{dI_1}{dt} - R_T I_1 - \frac{1}{C_L} \int (I_1 - I_2)\, dt = 0 \qquad \text{(A-1)}$$

$$\frac{1}{C_L} \int (I_1 - I_2)\, dt = R_L I_2 \qquad \text{(A-2)}$$

assuming the initial charge on C_L is 0. The charge on capacitor C/n^2 is given by:

$$Q(t) = \frac{Q_o}{n} - \int I_1 (t)\, dt \qquad \text{(A-3)}$$

Substituting A-3 into A-1, one obtains,

$$L_T \frac{dI_1}{dt} + R_T I_1 + \frac{1}{C_L} \int (I_1 - I_2)\, dt - \frac{n^2}{C} \int I_1\, dt = \frac{Q_o n}{C} \qquad (A-4)$$

from which one finds an expression for the current $I_2(t)$.

Now the energy delivered to the load resistance R_L, is given by:

$$E_L = \int_o^\infty I_2^2(t)\, R_L\, dt \qquad (A-5)$$

Upon substituting the expression for the current $I_2(t)$ enables one to evaluate the energy delivered into the resistive load R_L.

For the purpose of a preliminary calculation the circuit parameters corresponding to the diagnostic thruster studies of the present program have been assumed:

R_T = 1.0 ohm

L_T = 1.20×10^{-4} henries

C_L = 2.0×10^{-8} farads

C = 1.0×10^{-6} farads

n = 3.0

Q_o = 10^{-4} coulombs

Results of machine calculations are presented in Figure 42. For the example evaluated it is seen that a large transfer of the stored energy gets delivered to the semiconductor igniter plug if its d.c. resistance is above roughly 10 ohms. While the initial d.c. resistance of most igniter plugs is above 10 ohms, its resistance will rapidly drop as the plug "sparks". Once the plug becomes conducting it is possible that transfer of energy with the "spark" becomes insufficient. This latter situation has not yet been analyzed.

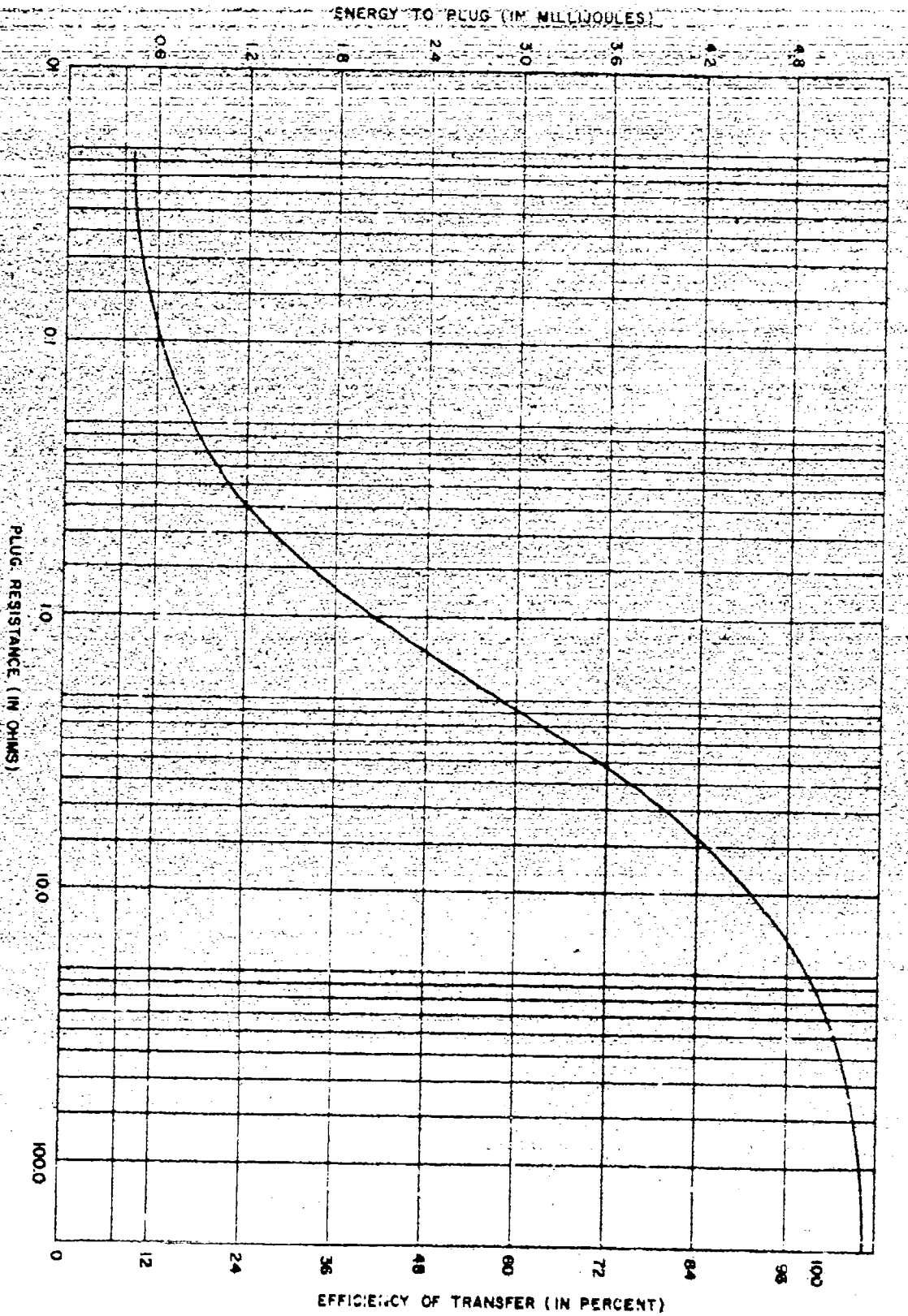

Figure 42. Plug Energy vs Plug Resistance

2.5 Other Pertinent Studies

2.5.1 Propellant Studies

Some of the requirements of an ideal solid propellant for a pulsed plasma thruster are:

a) That it be stable in a vacuum environment and at cryogenic temperatures; i.e., that it not sublime, outgas or decompose while stored directly in a vacuum.

b) That it be non-char forming upon being energized and that mass emittance be rapidly self-extinguishing upon removal of energy.

c) That it have a relatively high density and preferably be inert and non-toxic to facilitate handling and storage.

d) That it can be easily converted to a plasma with a minimum amount of energy addition.

Prior to the present program it was found that many low melting point metals met many of the above requirements. Indeed, exploratory experiments carried out at Republic Aviation early in 1966 were encouraging. Since most of the metals that were used acted as energy absorbing heat sinks, the experiments were discontinued.* Upon a complete review of suitable propellants meeting the above requirements, it was concluded that solid fluorocarbon compositions, notably Teflon, appeared to be better suited for the intended purpose. While most of the studies of this program were carried out with Teflon, other fluorocarbons and plastics that were investigated are listed in Table 8.

---

* Studies of a pulsed plasma thruster using metallic propellants have been studied elsewhere. (See for example, A.S. Gilmour, Jr., "Concerning the Feasibility of a Vacuum Arc Thruster," AIAA Paper No. 66-202 and the review of solid propellant thruster concepts presented in W.J. Guman and P.E. Peko, "Solid Propellant Pulsed Plasma Microthruster Studies," AIAA Paper 68-85, 1968).

TABLE 8. FLUOROCARBON AND PLASTIC PROPELLANTS

Chemical Composition	Formula	Trade Name	Company
Polytetrafluoroethylene	$(-CF_2-CF_2-)_n$	Teflon - TFE	duPont deNemours
Copolymer of tetrafluoroethylene and hexafluoropropylene	$(-CF_2CF_2-CF_2CF-CF_3-)_n$	Teflon - FEP	duPont deNemours
Polyvinylidene fluoride	$(-CH_2-CF_2-)_n$	Kynar	Penn Salt
Copolymer of vinylidene fluoride and hexafluoropropylene	$(-CF_2CH_2CF_2CF-)$ CF_{3n}	Viton Fluorel	duPont deNemours Firestone
Polytrifluorochloroethylene	$(-CF_2CFCl-)_n$	Kel-F81X Genetron X	Minnesota Mining General Chemical
Copolymer of vinylidene fluoride and trifluorochloroethylene	$(CF_2CH_2CF_2CFCl-)_n$	Halon Kel-F Elastomer Genetron VK	Allied Chemical Minnesota Mining General Chemical
Polyethylene resins	$(-CH_2CH_2-)_n$	Polythene, etc.	
Acetal resins	$(-CH_2O-)_n$	Delrin	duPont deNemours

Teflon is duPont deNemours registered trademark for its fluorocarbon resins, including TFE (tetrafluoroethylene) resins and FEP (fluorinated ethylene propylene) resins.

Teflon is an ideal propellant in that it meets all of the requirements listed above. With almost negligible energy (for microthrusters) it depolymerizes directly from a solid to a gas, this process terminating upon removal of energy. This feature is advantageous to the action of a propellant shut-off valve. It has a relatively high mass density and can be stored directly in a vacuum without tankage, (See Figures 1 and 2). These two latter aspects eliminate the necessity of developing a propellant subsystem which can reliably operate in temperature sufficiently above ambient conditions to be encountered in space, its polymer chain "unzips" (depolymerizes) and gaseous monomers are emitted. The energy required to convert the solid into gaseous form is evaluated from its heat of vaporization,

$$h_v = cp \Delta T + h_f + h_d$$

where

i) the enthalpy term $C_p \Delta T = 12.3$ K cal/mole

ii) the phase transition $h_f = 1.4$ K cal/mole

iii) the heat of depolymerization $h_d = 37$ K cal/mole

or

$h_v = 52$ K cal/mole or 9.9×10^5 joules/lb of propellant.

For a thruster delivering 10 micropounds of thrust at a specific impulse of 1000 seconds, only 9.9×10^{-3} watts of energy are required to convert the solid propellant directly into gaseous form. Additional energy, however, is required to ionize the gas and accelerate the resulting plasma. While the power requirements to ionize the monomers cannot be readily evaluated, the smallest power P to accelerate the plasma to generate thrust T at a specific impulse I_{sp} will be $P = g T I_{sp}/2$ with g the gravitational constant. For a 10 micropound thruster operating at a specific impulse of 1000 seconds at least 0.44 watts will be required to accelerate the plasma besides the energy required for ionization and other thermal losses that will be encountered due to radiation and conduction. In order to keep the ionization energy at a minimum, additives which have a low ionization potential (Lithium, etc.) may be incorporated in the Teflon. Besides this approach, additives may be incorporated which produce an exothermic reaction. This latter approach also reduces electric energy requirements for generating a

particular thruster performance. Teflon with Lithium Hydride was obtained for evaluation as well as Teflon with oxidizers and additives stable in a vacuum, but capable of producing an exothermic reaction when energized* The additive Lithium Hydride is interesting for several reasons. Not only does Lithium have a relatively low ionization potential, but it spontaneously reacts with fluorine which is present in Teflon. The heat of reaction which is about 5.6 K cal per gram is roughly equal to the heat of vaporization required to convert solid Teflon into gaseous monomers. It is therefore anticipated that some improvement in thruster efficiency can be expected.

With the exception of the extensive results that have been obtained with virgin Teflon, inconclusive results other than diagnostic evaluations of other propellants exist for inclusion in this final report.

In a comparison of Teflon with CTFE-2300 by Allied Chemical it was found that the CTFE-2300 upon depolymerization evidently undergoes the transition through a liquid phase before being emitted as a gas. Figure 43 shows a microphotograph (magnified 122x) of the surface of CTFE after being used in a thruster for a number of hours. Small globules which evidently form while the liquid phase congeals are evident. A similar photograph at the same magnification showed the surface of Teflon to be smooth and photomicrographically appeared as a white surface. While the specific thrust was found to be the same with either composition the specific impulse of Teflon was about 11 percent higher than that of the CTFE.

Some additional diagnostic results with propellants other than Teflon (TFE), are compared with Teflon in Table 9. All of these results were obtained with a given thruster operating at the same initial conditions.

---

* A number of samples containing Teflon, Viton, Potassium perchlorate, Ammonium perchlorate, Boron, and Magnesium were obtained for evaluation. These have not been tested as of this time.

Figure 43. CTFE 2300 Magnified 122x

Table 9. Diagnostic Comparison of Propellants

Propellant	Specific Impulse, sec	Specific thrust, lb/w	Thrust Efficiency, %
TFE	1085	3.48	8.25
FEP	985	3.59	7.7
Halon	1010	3.48	7.66
KEL F-81	947	3.00	6.2
Polyethylene	2410	1.74	9.15
Polypropylene		Char Forming	
Delrin 500	1315	2.92	8.4
Delrin-AF		Char Forming	
Kynar		Char Forming	

2.5.2 Preliminary RFI Studies

Preliminary RFI tests were performed on an experimental laboratory type 5 joule per discharge pulsed plasma thruster operating at four (4) pulses per second (about 70μ lb thrust level). No precautions were taken to reduce RFI in the thruster by either isolating the thruster from the thruster casing or by using RFI suppression filters. The tests were made in the 200-300 mc band with an Empire Device NF-105. The inherent noise (RFI) measuring circuitry in the instrument was not utilized due to the narrow pulse width of the radiatod pulse signal emitted by the thruster and the presence of extremely large amplitude unwanted interfering pulses originating from all extraneous laboratory sources through the spectrum.

Examination of the interference signal was made by examining the receiver i.f. amplifier output pulsed r.f. pulsed packet or waveform on a Tektronix Model 555 oscilloscope synchronized to the plasma thruster trigger input. By this means, a synchronized examination of the radiated RFI waveform could be examined in detail without inclusion of the extraneous unwanted outside equipment pulsed radiation present in the laboratory.

The calibration or measurement of the absolute intensity of the radiated pulsed r.f. signal was performed by the substitution method, i.e., injecting a calibrated signal generator (HP-608) r.f. C.W. signal in place of the intercept dipole and varying the generator output until the signal height as seen on the oscilloscope screen was the same height as the plasma thruster radiated signal.

The thruster with exhaust cone pointed forward was mounted in an "L" type pyrex glass tubular evacuated chamber. An external resonated dipole was mounted just outside the evacuated test chamber, approximately 2 feet in front of the thruster horn assembly.

Measurements made at 230 mc indicate that the signal generator level equals the average of the plasma RFI pulses (as viewed on the oscilloscope) which was 50 microvolts. This corresponds to an equivalent input across a 50 ohm source impedance of -75 dbm.

The measurement receiver (Empire Devices NF-105) had an i.f. bandwidth of 250 KC.

The results of the present exploratory study can be examined with regard to a typical mission. For example, the following parameters pertaining to an existing satellite were used:

Transponder	
Carrier Frequency Range	: 250 mc ± 30 mc
Noise Figure	: 3 db
Bandwidth	: 100 KC
Threshold	: -120 dbm

Calculations on the equivalent noise power of the above transponder receiver based upon the above receiver characteristics indicate that:

$$E_n^2 = 4\,K\,T\,B\,\Delta f$$

$$P_n = E^2/R = \frac{4KTB\,\Delta f}{R}$$

$$P_m = -122 \text{ dbm}$$

It is presumed that the transponder receiver aboard the satellite is of the FM type. The threshold for a receiver of this type is approximately 12 db. Since this is a multi-loop system it is necessary that the input C/N ratio be extremely high, possibly 25-30 db above the inherent equivalent noise power of the receiver, in order to provide a clean useable re-transmitted video signal. Based upon this hypothesis, the actual received signal should be approximately:

$$P_m = -122 + 30 = -92 \text{ dbm}$$

The measured RFI pulse produced by the thruster was about -75 dbm, at a distance of two feet from the thruster exit nozzle. The calibration data for the NF 105 dipole antenna stated that the effective gain was 8 db (over that of direct input to the receiver).

Applying the inverse square law to reduce the antenna separation from the dipole to the thruster from 2 feet to 1 foot (the desired measurement distance) produces an equivalent increase in signal intensity of + 6db.

- 8 db + 6 db = - 2 db.

Applying the above correction factor to the RFI pulse input:

RFI pulse power = - 15 + (-2)

= - 77 dbm

An additional correction factor has to be taken into consideration; the ratio of the RFI receiver bandwidth to the transponder receiver bandwidth.

$$\text{BW Ratio} = \frac{\text{RFI Rcior}}{\text{Xponder R COT}} = \frac{250\ \text{KC}}{100\ \text{KC}}$$

$$= 2.5$$

This means that the noise power improvement gained by using the transponder receiver is approximately 4 db.

Applying this correction factor to the measured pulsed plasma noise power values:

Corrected Noise Power = - 77 - (4)

= - 81 dbm

Thus an excess noise power is generated during thrusting. The magnitude of this excess noise power is equal to:

Noise Power Excess = - 77 - (-92) = + 15 dbm.

It should be mentioned that observation of the thruster RFI pulses revealed that the character, width, and amplitude of the observed pulse varied from pulse to pulse. The variation in width ranged from 2 to 5 microseconds. The amplitude varied approximately 3 to 1. Since these tests were carried out with an early thruster model it is recommended that measurements be repeated with an updated thruster model.

In order to appreciate the observed pulse r.f. response, comparison tests were made employing a pulse signal generator. It was observed that the same type of observed pulse r.f. carries pulse i.f. output signal obtained by slightly detuning the receiver from the signal generator frequency setting. This indicated that the plasma thruster radiated pulse harmonic response produced infinitely large numbers of harmonics with pulsed spectral response and which were slightly jittery in the frequency and time domain.

It is believed that the RFI signal level while large should not cause excessive trouble due to the narrow transponder receiver bandwidth employed (which in turn indicates a low digital bit rate, i.e., wide pulse widths) and the narrow pulse width of the RFI generated pulses (2-5 micro seconds).

Brief tests indicated that the RFI measured values were essentially constant over the frequency band 200-300 mc; and that the radiation seemed to be hemispherical, in other words, that the thruster radiation was essentially isotropic.

In any practical application the thruster will be isolated from the thruster enclosure and RFI suppression filtering will be used on all power and signal leads to the thruster. The effect of such isolation has not yet been examined in the laboratory.

2.5.3 Exhaust Beam Observations

In a pulsed plasma thruster one distinguishes the time for the capacitor to discharge its energy and also the life of the plasma that exists within the thruster nozzle. The former quantity depends significantly upon the inductance and capacitance of the discharge circuit. Either a Rogoswsky coil or a voltage probe can be used to measure the energy deposition time. The life time of plasma will depend upon many factors. Some of these are dependent upon the properties of the plasma while others depend upon geometry and environmental factors. Nevertheless, it was of interest to examine these two times as seen by a voltage probe and a calibrated vacuum phototube (RCA tube 1P42 - this tube has a wavelength of maximum response of 4800 ± 500 angstrom). The phototube was positioned to look along the thrust axis directly into the thruster nozzle. The voltage probe recorded the discharge voltage waveform. The test was carried out for a thruster which

has been operated at the 22 μ lb thrust level for an extensive period of time. Figure 44 presents the results of this measurement. The capacitor is seen to be discharged in about 2.2 μ sec. The plasma is seen to persist a little over 10 μ sec with a peak intensity roughly 1.45 μ sec after energy deposition starts. These results show that for the 20 μlb thruster the impulse bits that are generated are comprised of extremely short bursts of plasma. Figure 45 shows the exhaust plume generated by a typical parallel rail thruster while operating in a vacuum environment. The column of highest luminosity is seen to undergo only a minor expansion and not to subsist any great distance downstream of the thruster nozzle exit plane.

Even though highly luminous plasma does not apoear to be present downstream of the thruster, this does not imply the absence of a high velocity exhaust stream. As a matter of fact, it has been observed that the exhaust beam appears to be comprised of a flux of mass which appears to have the properties of a beam of particles rather than a volume of gas. It has been repeatedly observed that an object placed in the exhaust beam will block the beam and shade any region downstream of the object from the exhaust beam. Indeed, it even appears that a slight diffraction pattern is formed by the edges of the interspersed object upon a plane downstream of the object. A true gaseous efflux would tend to expand around the interspersed object and fill any void spaces in the exhaust downstream of the object. Figures 46 and 47 show these observations. Figure 46 shows the image projected onto the hinged end flange of the vacuum chamber of a support stand, clamp and mirror that was in the exhaust of a Teflon propelled pulsed microthruster. The void in the exhaust stream produced by these objects and the diffraction patterns of the edge are seen more clearly in Figure 47. These observations suggest that the exhaust beam of a Teflon propelled pulsed microthruster behaves as a flux of particles rather than a gaseous cloud*. If the exhaust is indeed comprised of discrete particles as the results suggest, then it would be a simple matter to protect surfaces extending from a satellite (solar panels, gravity gradient booms, etc.) from the impingement of these particles by small fences.

* It is not believed that the exhaust beam is entraining oil vapor contamination and depositing it on the walls of the vacuum chamber such as reported elsewhere, Reference 15.

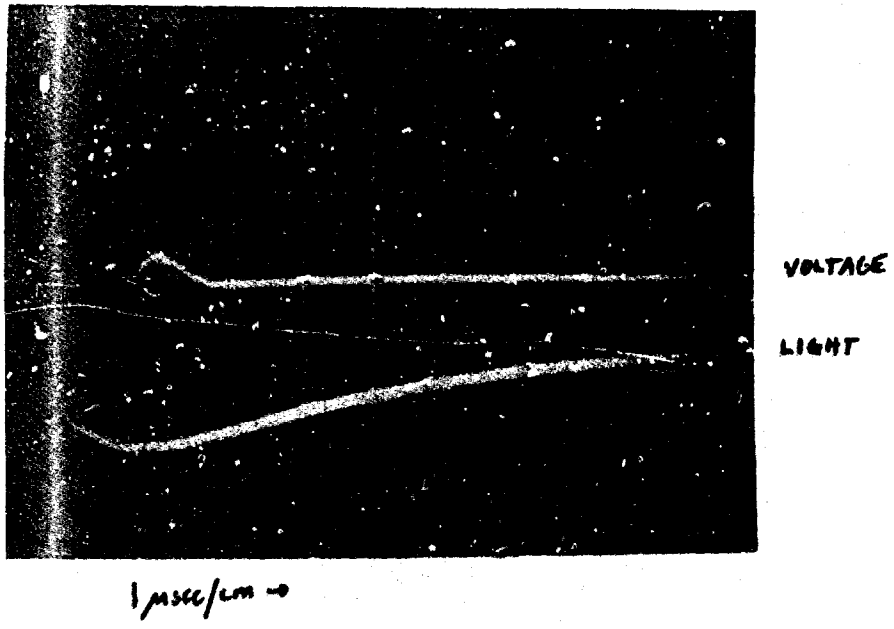

Figure 44. Discharge Voltage and Exhaust Phototube Measurements

Figure 45. Typical Vacuum Exhaust Plume of a Parallel Rail Thruster

Figure 46. Exhaust Pattern on Vacuum Chamber End Flange

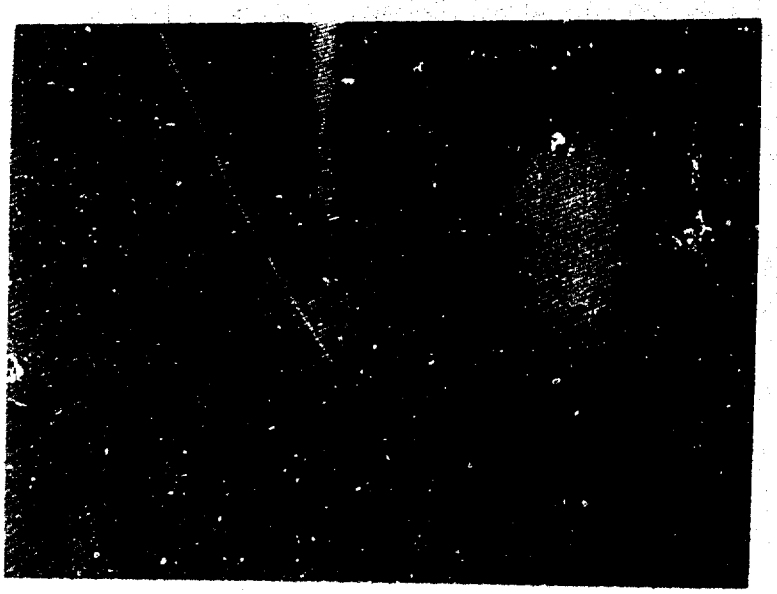

Figure 47. Void Pattern in Exhaust Beam Projected onto End Flange

SECTION III

MICROTHRUSTER SYSTEM TESTS

3.1 Extended Tests

A number of system life tests have been carried out during the course of the present study. These life tests included the thruster with its capacitor, the self-contained propellant system, a discharge initiation network, and either a power conditioner or a high voltage d.c. power supply. This latter, when used, was located external to the vacuum chamber. Safety interlocks were introduced in the testing facilities which removed thruster power in cases when

a) An external power plant failure occurred.

b) Overheating of the diffusion pumps due to a low water flow rate or an elevated water temperature occurs.

During the life tests the thruster would be operated around-the-clock until failure. The only momentary deliberate removal of power (lasting a few minutes) occurred during thrust stand calibrations. Thrust data and calibrations were generally recorded once per day. An event counter was used to record accumulated discharges.

The results and pertinent data of the thruster system tests that have operated continuously for more than 100 hours at the indicated thrust level are presented in Tables 10, 11, and 12, respectively. Two typical thruster systems that have been tested are shown in Figures 1, 2, 48, and 49, respectively.

It is significant to observe that the total impulse generated, the total hours of thruster system operation, as well as the specific thrust generated during most of the tests presented in Tables 10, 11, and 12 significantly exceed values reported by any other electrical microthruster system in the comparable range of performance.

It should also be observed at this point that the recorded number of hours of any given test are at the indicated thrust level. Since the thrust level of a pulsed plasma thruster is derived from periodically generated impulse bits,

TABLE 10. EXTENDED THRUSTER TESTS

(Above 100 hours of uninterrupted operation and 50 lb-sec total impulse)

> 50 lb-sec

Log Number	76	79/81	85	88E-5	94E-1	89D-7-1	89D-9
Date of Test	May 1967	June/Dec '67	Aug. 1967	Sept. 1967	Oct. 1967	Nov. 1967	Nov/Dec '67
Total Discharges of Test	1,952,039	13,637,764	1,811,069	2,307,387	951,523	1,351,553	939,240
Average Thrust Level, μ lb	68	50 (aver.)	48.5	142	138	136	106
Impulse/Discharge, μ lb-sec	65	50 (aver.)	48.5	71	69	68	53
Total Impulse of Test, lb-sec	124.9	658	87.9	162.3	66.8	92	49.9
I_{sp}, sec.	1300	1227(aver.)	994	640	560	1100 (est.)	875
T/P, μ lb/watt	3.06	2.38	2.2	3.38	3.3	2.58	2.36
Thrusting Time, hours	342	3800	222	321	132	188	130
Joules/Discharge	20.8	21	20.8	21	20.8	26.3	22.5
Capacitor Model	AX-0019	AX-0019	X-0008	5C20MN-AS	X-0009	1625	1970
Capacitor Manufacturer	Bendix	Bendix	Bendix	Maxwell	Bendix	Sprague	Sprague
Capacitor spec. wgt, j/lb	2.7	2.7	2.7	8.1	2.7	9.9	8.5
Capacitor, spec. wgt, watt/lb	2.7	2.7	2.7	16.2	2.7	19.8	16.8
Pulse Frequency, Hz	1	1	1	2	2	2	2
Fuel Size, inches	3/8 x 3/4	3/8 x 3/4	3/8 x 3/4	1 x 1	1.00 x 1.06	3/4 x 3/4	3/4 x 3/4
Voltage of Test, Kv	1.5		1.5	1.5	1.5	1.5	1.5
Reason for Termination	Intermittent firing	Inability to initiate discharge	Power plant failure	Capacitor failure	Electrical short	Capacitor failure	Capacitor failure
Refueled	Yes	Yes	No	No	No	No	No
Power Conditioner	Yes	No	No	No	No		No

TABLE 11. EXTENDED THRUSTER TESTS

(Above 100 hours of uninterrupted operation)

> 50 lb-sec

Log Number	98E-3	98E-4	98E-5	98E-6	104E-1	104E-5
Date of Test	Dec/Jan '68	Jan. 1968	Jan. 1968	Feb/Mar '68	Apr/May '68	June -
Total Discharges of Test	3,112,979	890,173	2,970,873	4,180,267	2,265,660	1,926,586
Average Thrust Level, μ lb	103	134	136	131	140	140 (est.)
Impulse/Discharge, μ lb-sec	51.5	67	68	65.5	140	140 (est.)
Total Impulse of Test, lb-sec	160.5	60	202	273.7	317.2	270
I_{sp}, sec	458	600	600	550	1070	1070 (est.)
T/P, μ lb/watt	2.64	2.75	3.24	3.28	3.5	3.5
Thrusting Time, hours	433	124	413	582	630	535
Joules/Discharge	19.3	22.1	21	21	40	40
Capacitor Model	W 1968	W 1968	W 2091	W 2091	W 2108	W 2106
Capacitor Manufacturer	Sprague	Sprague	Sprague	Sprague	Sprague	Sprague
Capacitor spec. wgt, j/lb	7.45	8.55	7.68	7.68	7.78	7.78
Capacitor, spec. wgt, watt/lb	14.8	17.1	15.4	16.1	7.78	7.78
Pulse Frequency, Hz	2	2	2	2.1	1	1
Fuel Size, inches	1.06 x 1.06	1.06 x 1.06	1.06 x 1.06	1.06 x 1.06	1.06 x 1.06	1.06 x 1.06
Voltage of Test, Kv	1.4	1.5	1.38 x 1.40	1.4	1.4	1.4
Reason for Termination	Fuel hung-up	Capacitor failure	Electrical short	Capacitor failure	One igniter plug inoperative	Electrodes shorted
Refueled	No	No	No	No	No	No
Power Conditioner	No	Yes	Yes	Yes	Yes	Yes

TABLE 12. EXTENDED THRUSTER TESTS

Log Number	96A	96B	96D	101A	101X-8
Date of Test	10/27 - 11/21/67	11/22 - 12/19/67	1/16 - 2/23/68	2/21 - 5/9/68	8/19 -
Total Discharges of Test	2,125,424	2,270,898	11,013,986	8,744,227	2,230,385 +
Average Thrust Level, μ lb	5.86	7.1	Not on stand	8.04	1.0
Impulse/Discharge, μlb-sec	5.86	7.1	~ 5.08	5.36	6.0
Total Impulse of Test, lb-sec	12.4	16.1	56	46.9	
I_{sp}, sec	215	251	~ 220	308	220
T/P, μ lb/watt	3.15	3.81	2.73	2.86	3.24
Thrusting Time, hours	590	630	760	1600	2050 +
Joules/Discharge	1.86	1.86	1.85	1.86	1.86
Capacitor Manufacturer	Dearborn	Dearborn	Dearborn	Dearborn	Dearborn
Pulse Frequency, Hz	1	1	4	1.5	0.166
Voltage of Test, Kv	1.36	1.36	1.36	1.36	1.36
Reason for Termination	(Propellant covered the Igniter Plug)		Capacitor failure*	Intermittent	In progress

*After 14,665,281 discharges

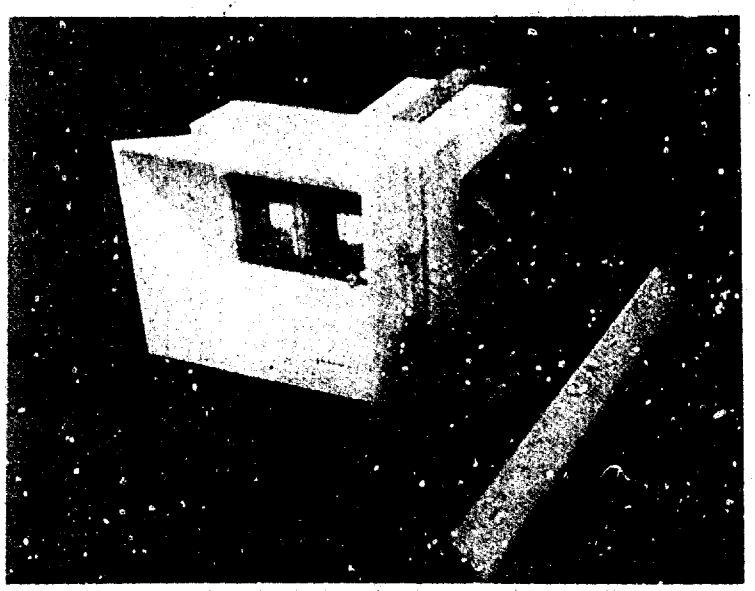

Figure 48. Dual Nozzle Thruster System

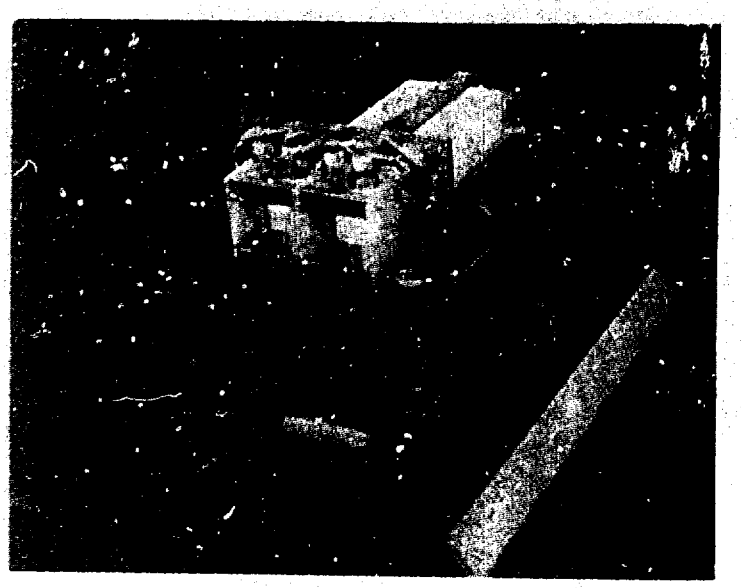

Figure 49. Thruster System Electronics

operation of a pulsed plasma thruster at half the indicated pulse rate will produce half the thrust level, but exhibit twice the indicated lifetime in hours! This trade-off between thrust level and pulse frequency is a feature unique to the pulsed plasma thruster.

The total impulse capability that has been demonstrated encompasses the range required of many of the power limited smaller satellites.

With the exception of the two tests denoted as Log 76 and 79/81, respectively, all tests were carried out without refueling. With the exception of the tests utilizing Bendix capacitors, all tests were carried out at the highest power density (watts/lb) considered compatible with desired life. It is for this reason that most tests were terminated because of a capacitor failure. These failures were analyzed and modifications were subsequently incorporated to achieve greater capacitor longevity at the same power density rather than simply derating the capacitor. In cases when the life test was terminated because of an electrical short, it was found that a conducting deposit would bridge the two electrodes even though re-entrant cavities were incorporated in the insulator assembly. A very high degree of correlation has been found between vacuum oil back streaming (due to external power or water failures) and the appearance of such highly conducting deposits. It is strongly suspected that a reaction occurs between the plasma and back-streamed oil vapor like that reported in reference 15. In a controlled experiment it has also been found that the interaction of the plasma with outgassed material of a recently cured epoxy will form a heavy layer of deposit even on the face of the Teflon being depolymerized. This deposit would subsequently act as a "heat shield" severely hindering the depolymerization of Teflon below it. It has, therefore, been found essential to thoroughly cure epoxies before use to preclude deposit formation by the interaction of the plasma with outgassed material. Since all of the vacuum facilities in which the life tests were carried out did not have liquid nitrogen traps, it was not possible to preclude oil back streaming. It is believed that the laboratory vacuum pumping system should be comprised of ion pumps with sorption roughing rather than oil diffusion pumps for truly establishing maximum life capability of the thruster system. Of course, such reactions between the plasma and oil vapor cannot occur in space.

Figures 50, 51, and 52 were taken of the thruster denoted as Log 79/81 in Table 10 after 3800 hours of operation. Figure 50 is a view looking at the nozzle along the thrust producing axis. As indicated in Table 10 this test was terminated because of the inability of the igniter system to initiate a discharge due to deposit formation on the electrode surfaces. It can be seen that the Teflon propellant remained white (i.e., non-charring) while a residue formed on the insulating sidewalls as well as on the electrodes. The cross-section of the nozzle shown in Figure 50 was initially rectangular (3/8-inch wide by 3/4-inch high). In Figure 50 it is seen that deposit formations on the lower parts of the side insulator reduced the nozzle efflux area. Figure 51 shows the deposit formation on the cathode while Figure 52 shows a 7X magnification of the same surface. The surface was very nearly completely covered with the exception of small craters which extended to the electrode surface. It is most important to note that actual electrode erosion below the deposit was insignificant. Figure 53 shows a cathode from which the deposit has been removed so as to expose the erosion beneath the deposit. It is estimated that electrode erosion would be of no problem even for an order-of-magnitude larger time of operation at the same power and thrust level. At no time would difficulty be anticipated due to erosion of the fuel retaining shoulder.

As indicated in Table 10, the 3800 hour test was carried out with refueling. Figure 54 shows the 3/8 x 3/4-inch Teflon propellant end pieces after each refueling and exactly as removed from the thruster. In all cases it was found that the depolymerized Teflon surface remained perfectly white. The slight nonplanar condition of the surface represents the shape after roughly 2-1/4-inches of Teflon of each rod was consumed. In no case has this slight irregularity of the surface been found to affect the thrust level.

Figure 55 shows the thruster nozzle at the end of the test denoted as Log 104-E-5. This test lasted for 535 hours at the 140 μ lb thrust level and generated 270 lb-sec of total impulse at a specific impulse of about 1070 seconds. The formation of a small amount of deposit can be seen on the lower electrode in Figure 55, whereas the face of the Teflon propellant remained perfectly white. Figure 56 shows the propellant rod of Figure 55 upon removal from the thruster. After consuming 3 inches of Teflon the roughly 1 square inch frontal area is seen to be still very nearly planar.

Figure 50. View Looking Into Thruster After 3800 Hours of Operation

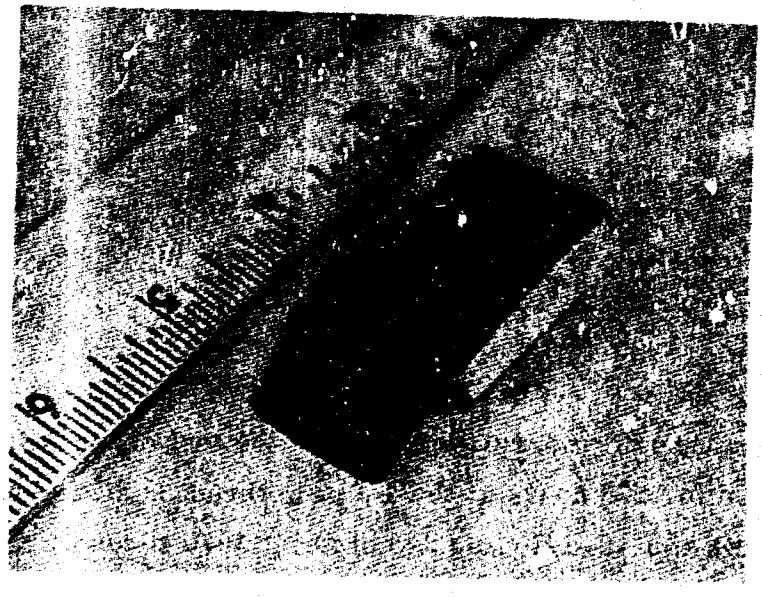

Figure 51. Cathode After 3800 Hours of Operation

Figure 52. 7X Magnification of Cathode Surfaces After 3800 Hours of Operation

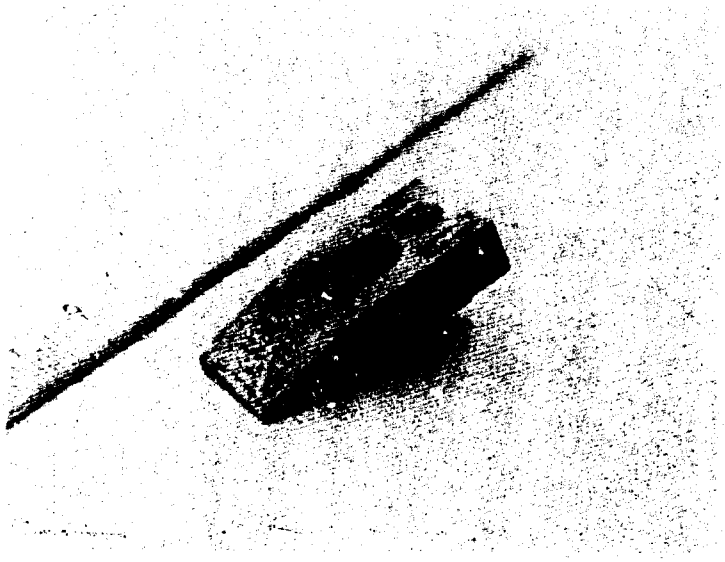

Figure 53. Cathode Erosion Below Deposit

Figure 54. Propellant Remnants After Each Refueling

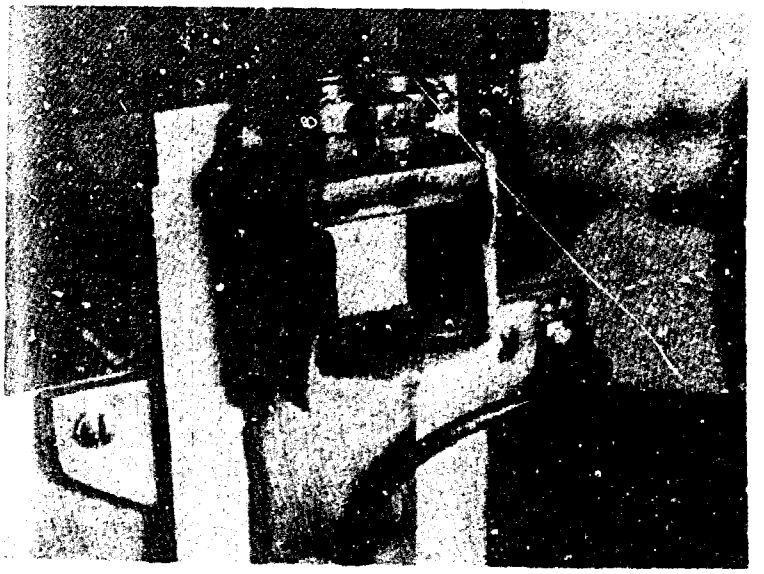

Figure 55. Thruster of Log 104-E-5

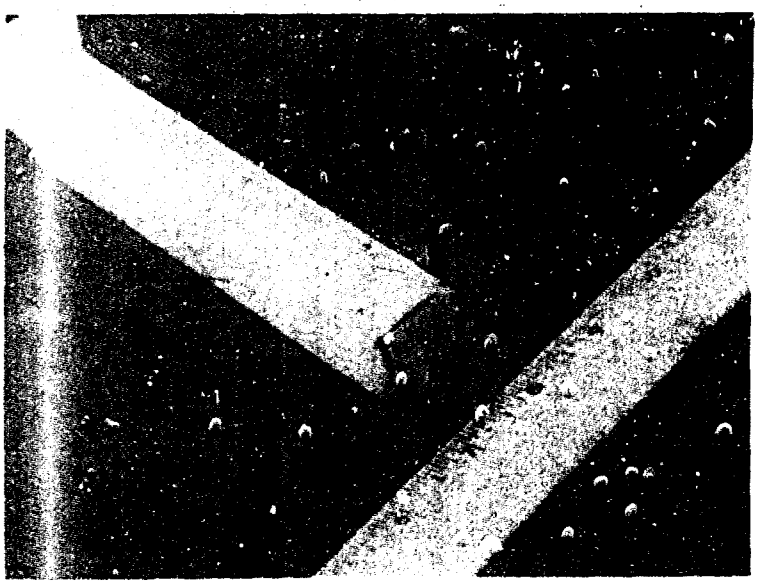

Figure 56. Propellant of Log 104-E-5 After 535 Hours at 140 μ lb

The thruster system life tests carried out show that the performance and life capability in terms of total impulse meet many of the mission requirements of power-limited satellites requiring microthrusters. Under a separately supported program a pulsed plasma microthruster and power conditioner were designed, built, flight qualified, and delivered to the contractor for installation on a satellite. Figures 57 and 58 show this flight hardware. Some of the test results of laboratory versions of this system are presented in Table 12.

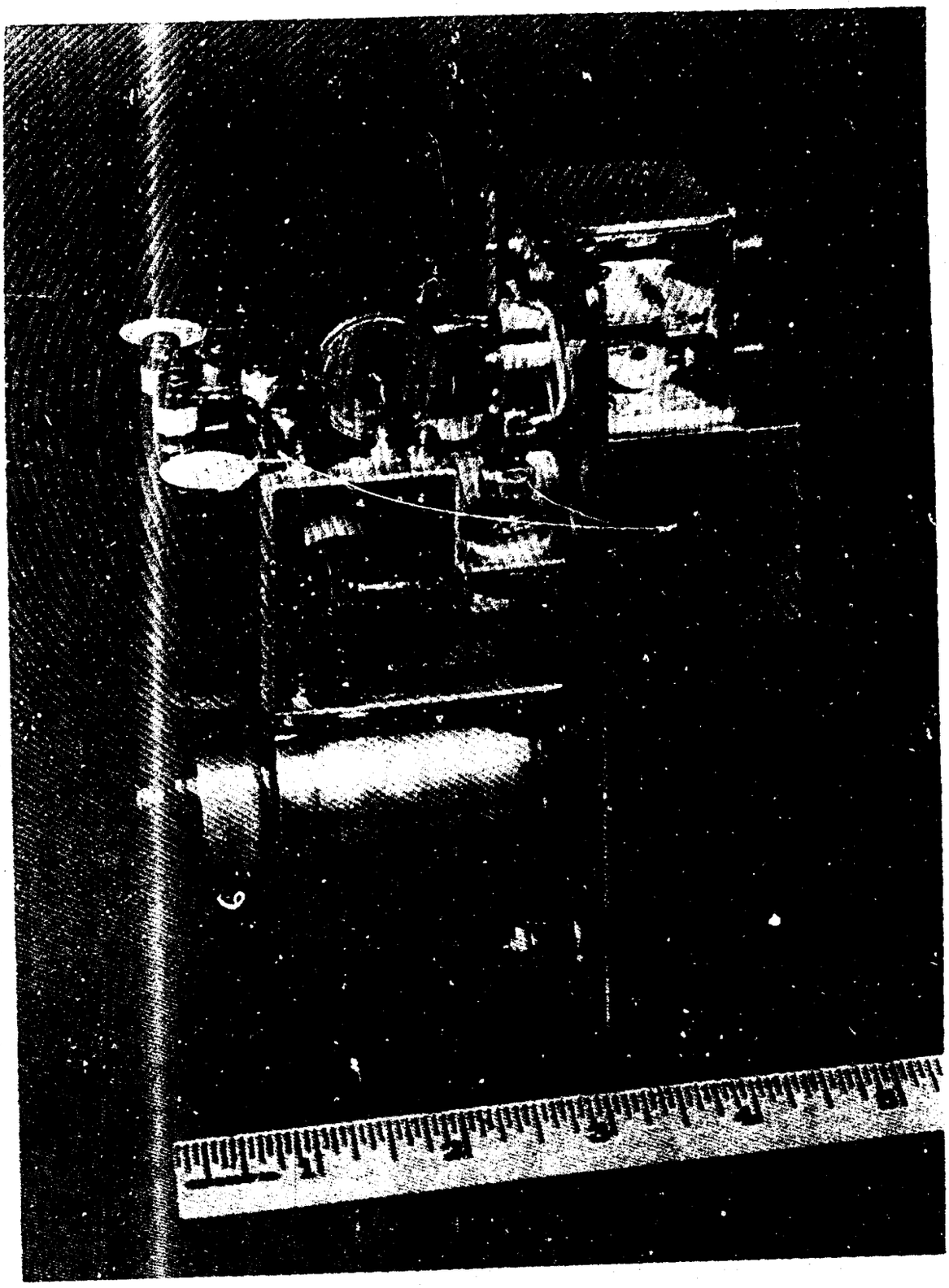

Figure 57. Flight Qualified Pulsed Plasma Microthruster

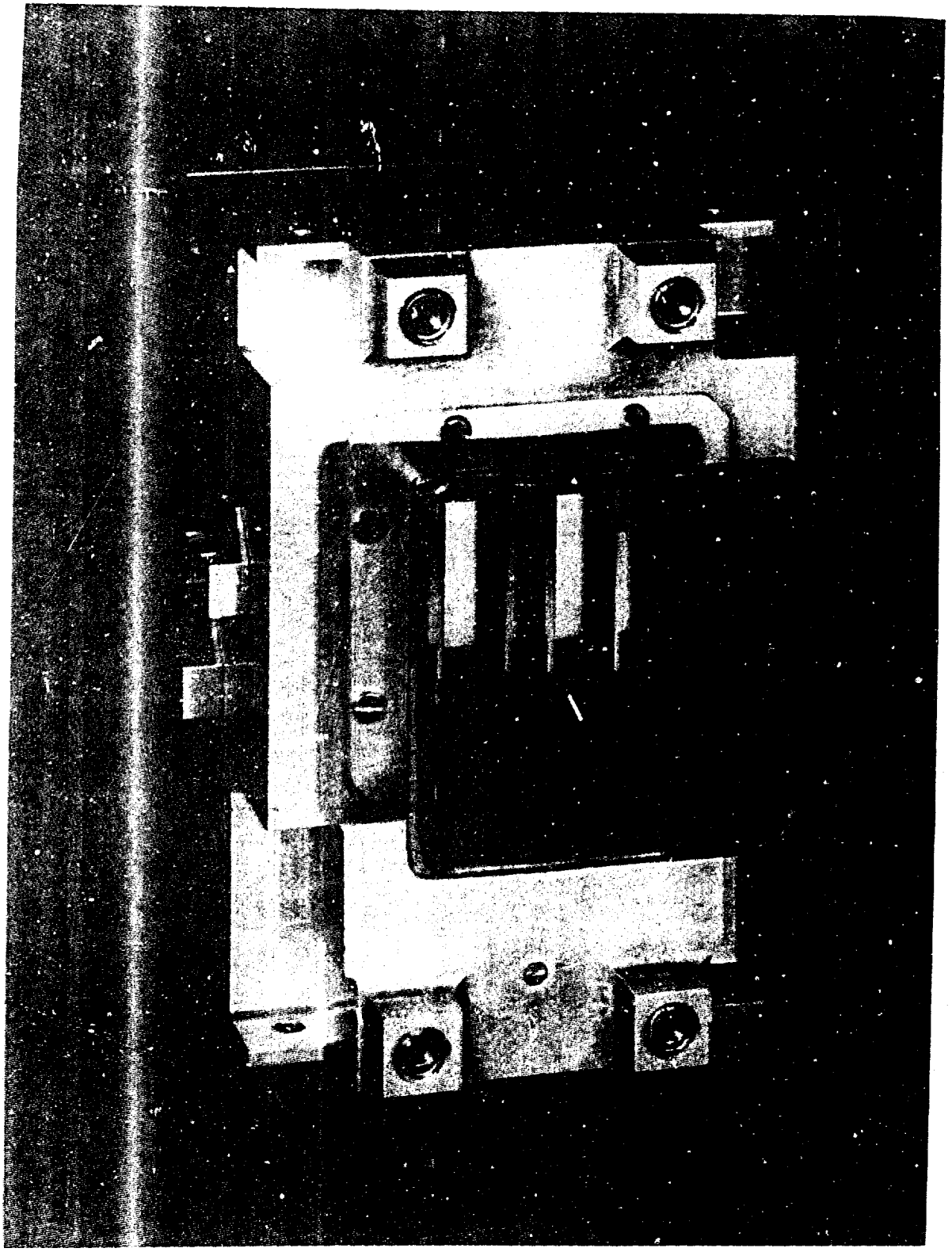

Figure 58. **Flight Qualified Pulsed Plasma Microthruster**

SECTION IV

THRUST BALANCE

4.1 General Description

The measurement of thrust from pulsed plasma thrusters operating in the range of 1 - 100 micropounds thrust imposes certain unusual requirements on the thrust measuring system. Among these are vacuum chamber shift during pump down, external movements in the vicinity of the vacuum chamber, building motions, and vibration due to mechanical equipment. It is also necessary to be able to carry out calibrations of the stand remotely in the vacuum chamber during engine operation.

The principle used for Republic's thrust measuring system illustrated in Figure 59 is that of the seismic pendulum. In this system the thruster package is supported from an arm pivoting about a vertical axis. The pivot axis is given a slight inclination to the vertical which results in a low point in the thruster's circle of movement around the pivot, such that the engine will always return to this low point if displaced. For small angles of inclination the movable arm will have relatively large displacements for small vertical rises. Thus for low thrusts in the horizontal direction large displacements are obtained and the system will have a low natural frequency enabling one to measure a single pulse or to integrate relatively low frequency pulsed operation of a microthruster. The sensitivity of the overall system is controlled by the weight of the moving mass, the angle of inclination and the read-out system used to make the measurements. The combination of the angle of inclination with the measuring system used for this stand makes the system very versatile over the desired range of operation.

The thrust measurement is a function of the displacement of the thrust arm from its zero position and for the small angular movements of the arm which is the normal operating regime of the thrust stand, this relationship is linear. The sensing of this small motion is accomplished using a capacitive measuring technique developed by Republic and previously applied to other sensitive force and displacement measuring systems. Capacitive systems have been produced that are capable of resolving 3×10^{-9} inches with a response in excess of 8000 Hz.

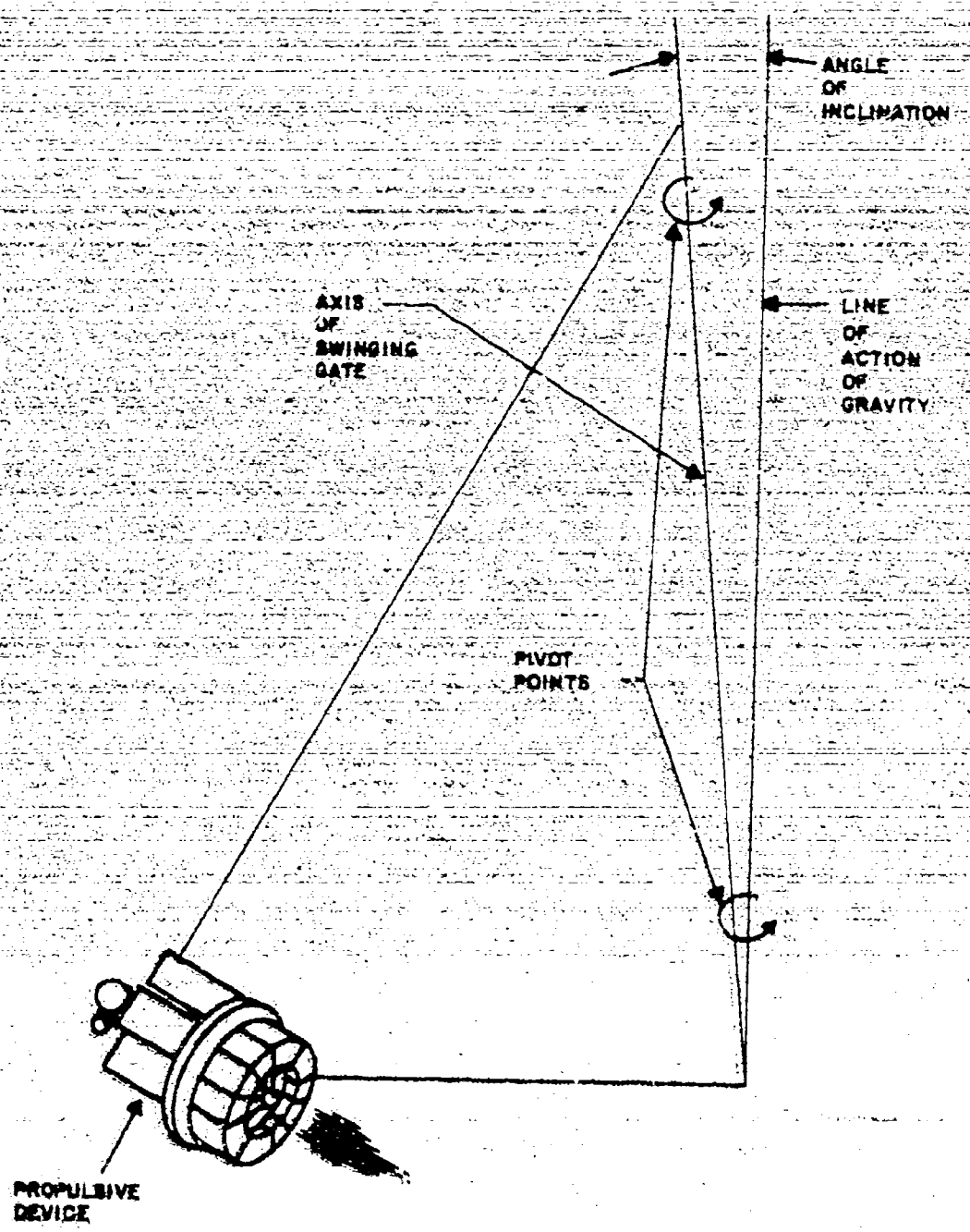

Figure 59. Principle of Seismic Pendulum

The principle of the displacement measuring transducer is based upon two back-to-back capacitors whose complementary out-of-balance is detected by means of an a.c. bridge circuit. The basic schematic of this unit is depicted in Figure 60. The transducer unit is equipped with 4 capacitor plates to form the variable capacitors C_1 and C_2 in the schematic (Figure 60). Two of the plates are combined to form the center portion of the bridge and are carried on a single plastic block attached to, and moving with, the package carrying plate. The two outer capacitor plates are attached to, and remain fixed with, the base plate of the transducer. As the package moves, the capacitances at C_1 and C_2 are increased and decreased or decreased and increased respectively, thus unbalancing the bridge circuit.

The read out for the system falls into two modes, a direct reading or a bridge balance operation. In the direct reading mode, the displacement is read on the self-contained meter on the face of the console or by connecting the output to a suitable recorder. The thrust is then obtained by a comparison with either the impulse or steady state calibrators. In the bridge balance mode the micro-thruster is operated and the bridge is nulled by operating the steady state calibrator to zero read-out of the self-contained meter or a recording oscillograph.

Figure 61 shows the thrust stand, the pivot arm steady state calibrator, impulse calibrator, standard weight calibrator, and capacitive motion transducer. For repetitive pulsing the thrust measurement is achieved using the null balance method indicated above. The balancing force is produced by the steady state calibrator which consists of a standard weight which can be remotely positioned by means of a motor driven lead screw. The turns of the screw are monitored by an encoder unit feeding into an electronic digital counter. This steady state calibrator can be checked by the application of thrust forces on the thrust stand arm by means of standard weights acting through a built-in bell crank lever shown in Figure 61.

The impulse calibrator imparts an impulse to the thrust stand by rolling a steel ball down an inclined plane and impacting the ball on the thrust arm. The rebounding ball is caught in a hopper and returned by a screw elevator to the top of the incline. The angle of the plane is set at 7°-12' and the frequency of the

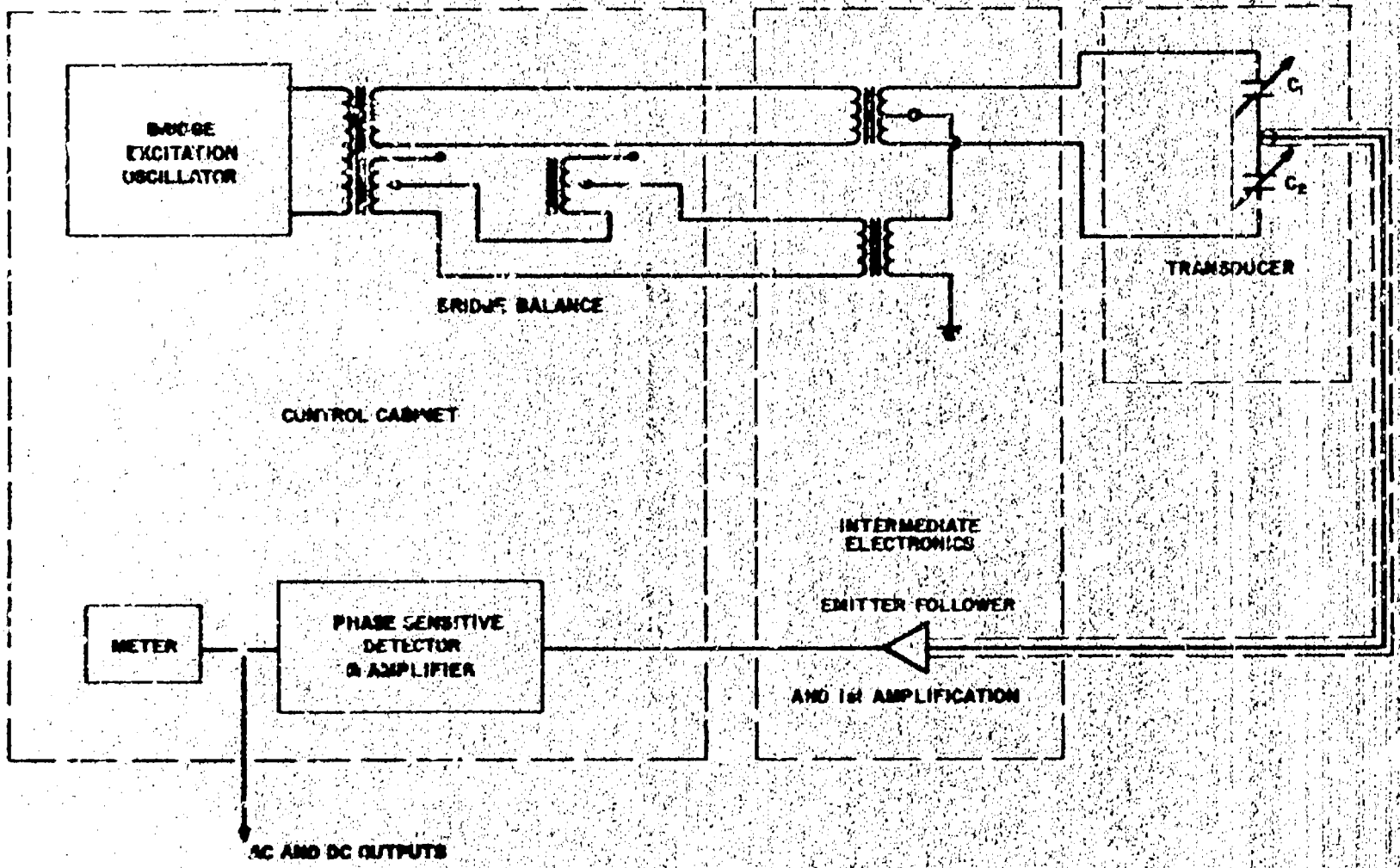

Figure 60. Thrust Measuring System Schematic

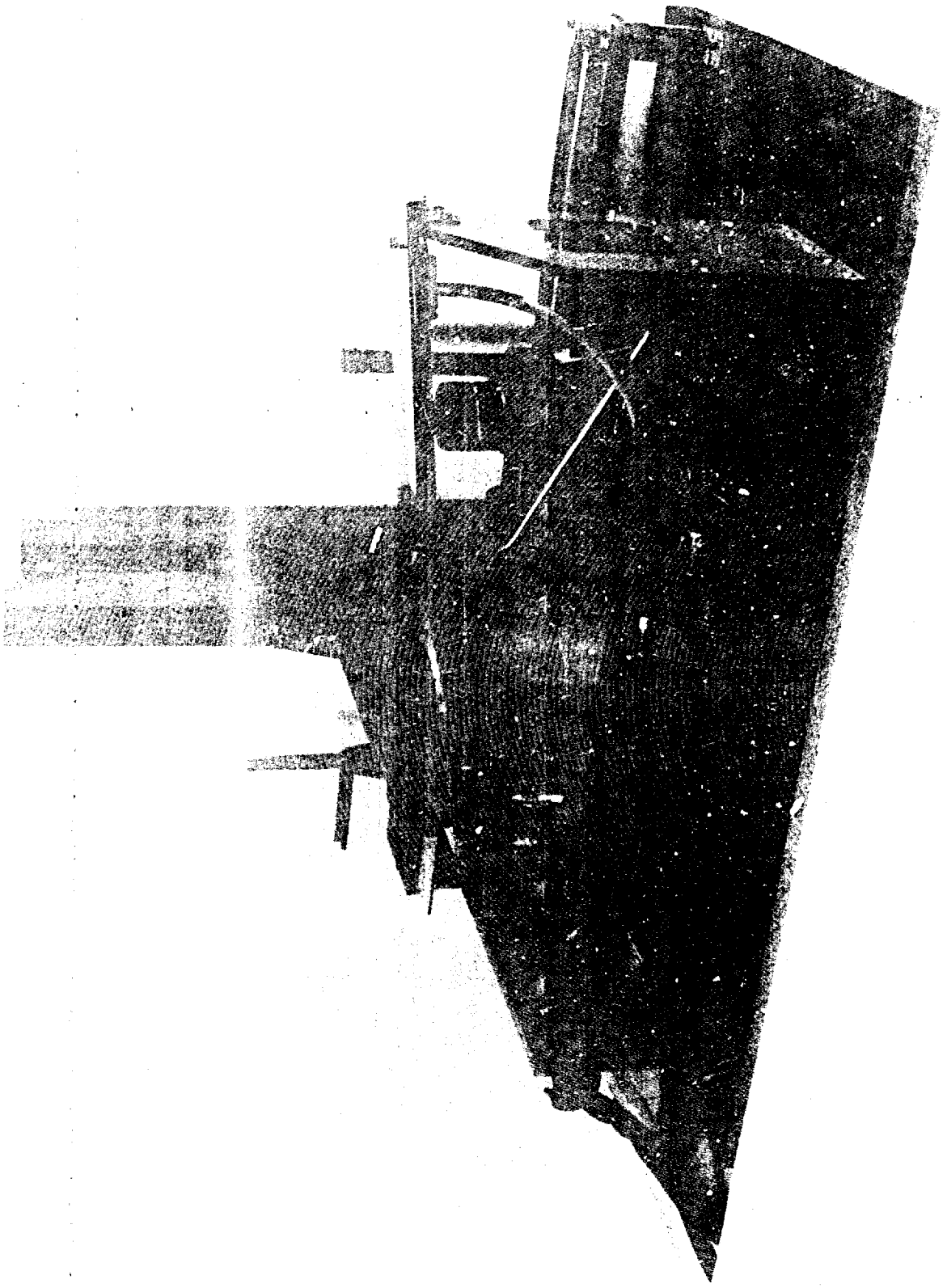

Figure 61. Thrust Stand

balls is preset to 1 Hz. By simply flicking the ball calibrator actuating switch it is also possible to have a single ball impact the stand. Since the natural frequency of the stand is much lower than 1 Hz its response to frequencies of 1 Hz or greater is linear with frequency. The impulse of a signle shot can also be readily obtained by comparison with the impulse of a single ball since the stand response is linear to a single impulse too.

Thrust read out is obtained from an electronic counter built into the control console (Figure 62). As noted above either a direct read out or null balacing can be used.

Two other features of the stand are noted at this point. The first is the damping provided by a paddle in a silicon oil bath to remove extraneous mechanical noise from the system. The silicon oil is suitable for the vacuum environment and the degree of damping can be controlled by varying the viscosity of the oil, the depth of the paddle immersed in the oil bath or the angle of the paddle to the direction of motion. The oil used is outgassed Dow Corning type 200 silicon oil of the appropriate viscosity. In addition remote leveling is provided by means of a motor positioned jack on the stand. This feature permits the operator to compensate for attitude changes in the test chamber, and changes in the center of gravity of the test package.

A separate control console contains all of the operating controls for the thrust measuring system. A recording oscillograph or electrical filtering of the output signal are used to obtain a permanent record of outputs.

4.2 Typical Results

Figures 63 and 64 show a typical 20 μ lb thrust stand calibration signal and a record of the output of a 7.6 μ lb thrust level thruster, respectively. The paper speed was 1 mm/sec in both cases. It is seen that the thrust balance can be calibrated within 1 minute and that thruster records can also be had within one minute. Small oscillations of the zero baseline are due to random background vibration of the vacuum chamber which are induced by ground movements of the building, nearby machinery, and traffic. These records show that thrust level measurements down to a few micropounds can readily be made. Results such as shown in Figures 63 and 64 have been repeatedly made over a period of weeks without the necessity of maintenance, particular precautions, or adjustments requiring more than a few minutes to carry out.

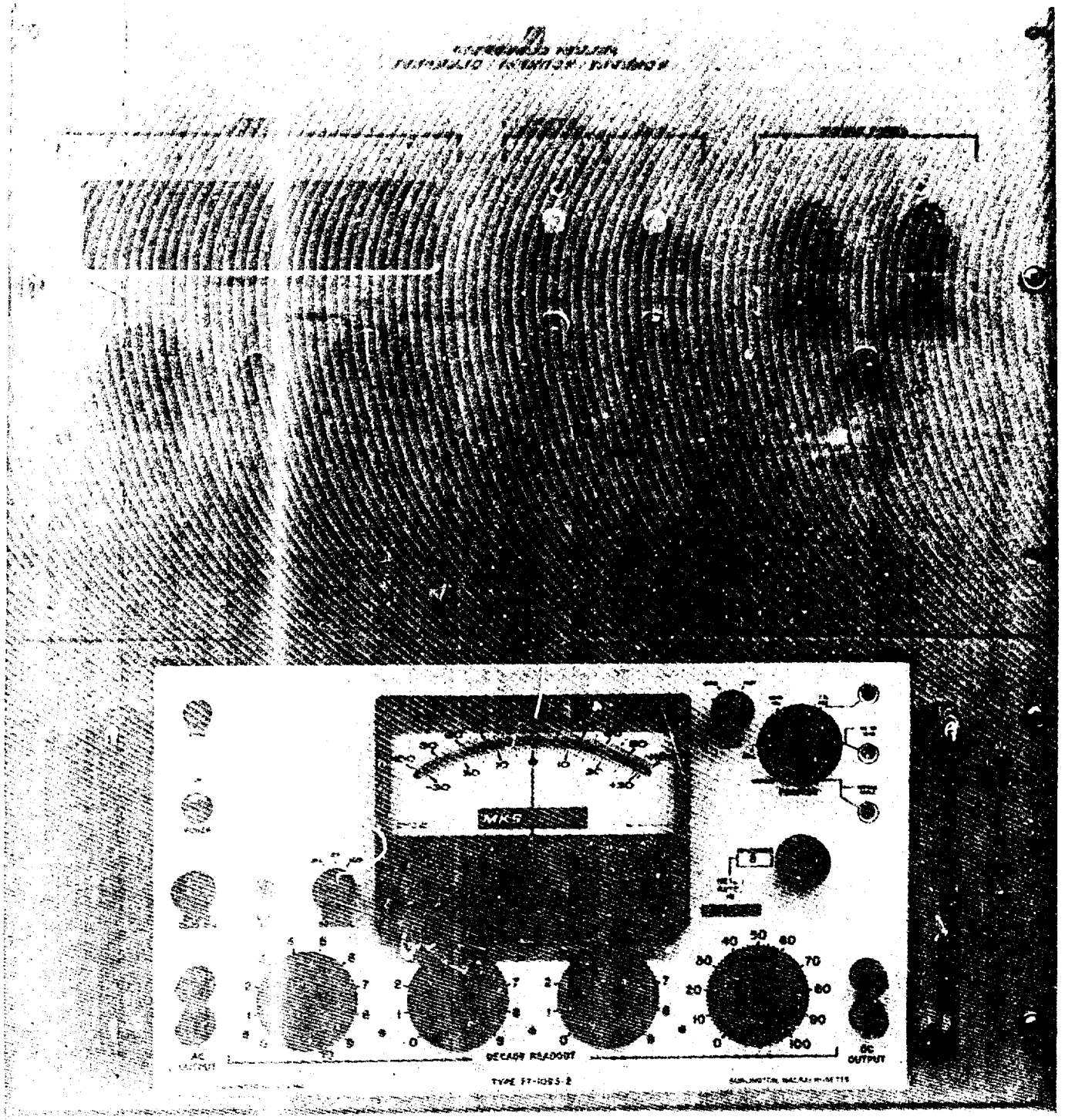

Figure 62. Control Console

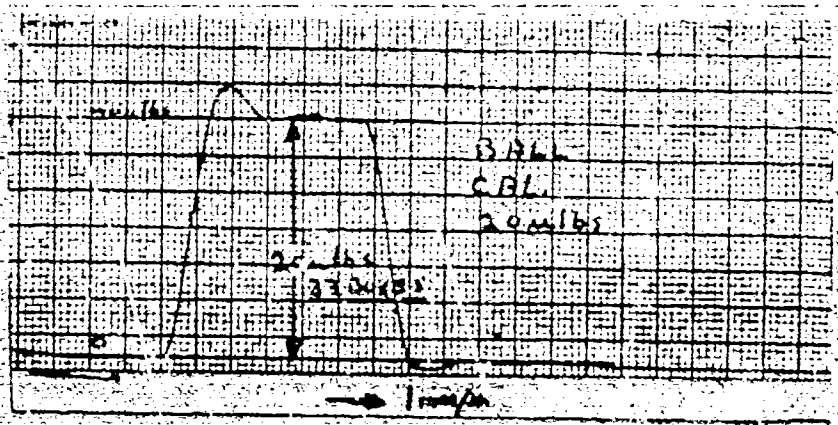

Figure 63. Ball Calibrator Output of 20 μ lb

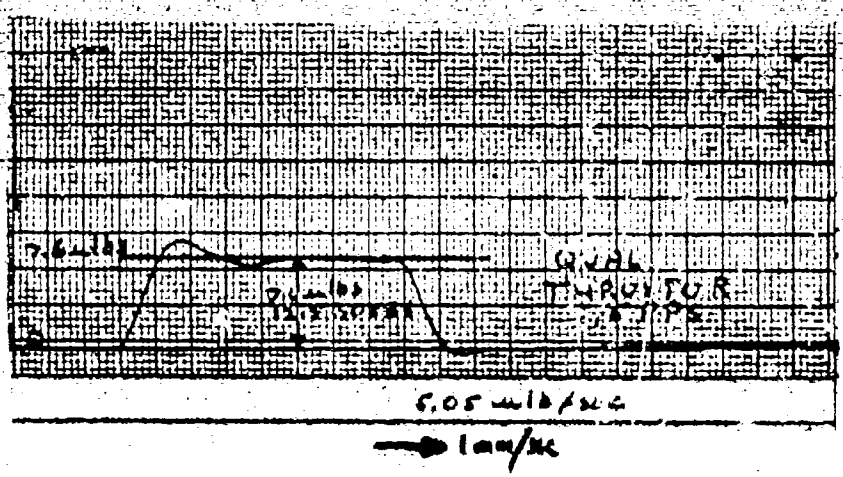

Figure 64. Thruster Output of 7.6 μ lb Thrust Level

SECTION V

APPLICATION STUDIES

5.1 General Applicability

The purpose of this section is to indicate the areas of applicability of the microthruster system that has been developed, and to provide guidelines in preliminary design for inclusion of this thruster system for meeting mission requirements.

One of the features that should be evident from the foregoing sections is that a vast flexibility in design parameters exists with this thruster system. Because of the simplicity of the system it is possible to easily custom design a thruster system to meet specific requirements that are imposed because of power, weight, volume, geometry, or performance constraints. Besides these constraints, it is also essential that the system perform reliably throughout its intended life. The reliability and thruster weight for pulsed plasma thruster systems are very closely related to each other. This interrelationship arises because of the energy storage capacitor. It is a well known fact that a capacitor can be derated to provide a particular life with essentially perfect reliability. Increasing the degree of reliability for a given life of a given capacitor is had at the expense of capacitor specific weight (expressed in terms of pounds/watt). This latter statement is evident from the voltage power law* (at constant temperature) and the fact that specific weight of a given capacitor in terms of pounds/joule is directly proportional to the square of the operating voltage.

The range of applicability of a single nozzle pulsed plasma microthruster to carry out EW or NS stationkeeping requirements of a synchronous orbit satellite

---

* This law states that $L_1/L_2 = (V_2/V_1)^n$ where L_1 is life at voltage V_1 and L_2 is life at voltage V_2, respectively. Exponent n is a function of capacitor material and is about 6 for the present purpose.

is seen from Table 13. This table has been calculated assuming that EW requirements are 7 fps ΔV per year and 150 fps ΔV per year in the NS plane.

From the calculated results presented in Table 13 it is seen that the pulsed plasma microthruster is capable of meeting the thrust requirements for EW stationkeeping for satellites weighing up to 7000 pounds. However, the microthruster would be considered applicable for NS stationkeeping requirements only for satellites weighing up to a maximum of about 2500 pounds. With regard to total impulse requirements, it is clear at the time of this writing that the demonstrated total impulse of the microthruster has not yet exceeded 658 lb-sec, or only the five-year EW impulse requirements of satellites weighing up to about 600 pounds. The NS requirements are more demanding and presently only NS total impulse requirement for a little over one year of the lightest satellite has been demonstrated by the microthruster. It is important to point out that the large values of total impulse demonstrated by ion engines (or resistojets) were not demonstrated by small microthrusters, but by bigger engines designed to operate in the millipound range! Clearly it is desirable that further life tests of more recent designs of solid propellant pulsed plasma microthrusters be carried out to determine the range of applicability of such thrusters. As indicated elsewhere in this report, it would be almost essential to perform such life tests in vacuum chambers in which it would be impossible for the plasma to interact with diffusion pump oil (i.e., preferably to carry out life tests in ion pumped vacuum chambers having sorption roughing).

The general considerations presented above considered EW and NS requirements of synchronous orbit satellites. For other applications, i.e.,

drag compensation
station changes
orbit acquisition
spin axis precession
inversion maneuvers
attitude maintenance or changes
pointing accuracies, etc.

the pulsed plasma microthruster would appear in many cases to be completely compatible with the requirements.

TABLE 13. APPLICABILITY TABULATION

A. IMPULSE REQUIREMENTS

Satellite Weight (lbs)	EW Impulse Rqts/Yr (lb-sec)	NS Impulse Rqts/Yr (lb-sec)
85 - 500	$18.5 < I < 108$	$396 < I < 2,330$
500 - 1500	$108 < I < 326$	$2,330 < I < 7,000$
1500 - 2500	$326 < I < 543$	$7,000 < I < 11,680$
2500 - 7000	$543 < I < 1520$	$11,650 < I < 32,600$

B. THRUST REQUIREMENTS, 100% DUTY CYCLE

Satellite Weight (lbs)	EW Thrust/Thruster (μ lb)	NS for 2 Thrusters (μ lb)	NS per Thruster (μ lb)
85 - 500	$0.587 < \bar{T} < 3.43$	$12.5 < \bar{T} < 73.6$	$6.25 < \bar{T} < 36.8$
500 - 1500	$3.43 < \bar{T} < 10.3$	$73.6 < \bar{T} < 222$	$36.8 < \bar{T} < 111$
1500 - 2500	$10.3 < \bar{T} < 17.2$	$222 < \bar{T} < 370$	$111 < \bar{T} < 185$
2500 - 7000	$17.2 < \bar{T} < 48.2$	$370 < \bar{T} < 1103$	$185 < \bar{T} < 556$

C. THRUST REQUIREMENTS, 25% DUTY CYCLE

Satellite Weight (lbs)	EW Thrust/Thruster (μ lb)	NS per Thruster (μ lb)
85 - 500	$2.34 < \bar{T} < 13.7$	$25 < \bar{T} < 147$
500 - 1500	$13.7 < \bar{T} < 41.2$	$147 < \bar{T} < 444$
1500 - 2500	$41.2 < \bar{T} < 68.9$	$444 < \bar{T} < 740$
2500 - 7000	$68.9 < \bar{T} < 193$	$740 < \bar{T} < 2220$

For the latter requirements, it is useful to think in terms of the pulsed microthruster system as depicted in Figure 1 of this report with the option that the power conditioner may be used to power one or more thrusters and discharge initiating circuits. Furthermore, as will be shown, it is many times more advantageous to operate more than one thruster nozzle which are discharging either in the same or in different directions.

For purposes of generalized calculations following data is representative of existing hardware:

The thrust to power ratio is evaluated by noting from Figure 16 that an impulse (I) of about 4 μ lb-sec is generated for each joule of electric energy (E), i.e.,

$$I = 4E$$

with I the impulse bit in μ lb-sec, E the energy in joules. If the thruster is operated at a pulse rate (f) pulses/sec, the average thrust (T) will then be:

$$T = 4fE = 4P$$

with P the power in watts delivered to the capacitor. This delivered power is about 80% of the input power to the power conditioner. No stand-by power is consumed when the system is not operating, nor is power consumed to prepare the system for operation, yet maintaining essentially instantaneous dynamic response.

The specific impulse is found to depend upon the discharge energy per unit frontal area (see Section 2.1.3b). Experimentally it is possible to realize a relation between specific impulse (I_{sp}) and discharge energy (see Reference 16) given by:

$$I_{sp} = 260\, E^{0.59}$$

where the specific impulse is in seconds, the energy in joules, respectively. In accordance with the latter relation, or the experimental results of Figure 5 of Reference 16 one finds:

Discharge Energy, joules	1	5	10	20	40
Specific Impulse, sec.	260	660	990	1475	2210

The weight of a thruster system comprised of a single capacitor powering a single thruster nozzle* (see Figure 1) can be estimated by the following considerations. A single nozzle thruster system encompasses:

a) a thruster capacitor
b) a thruster nozzle
c) a discharge initiating network
d) propellant, a guide and feed spring
e) a power conditioner
f) a driver

A weight of the thruster is essentially that of the capacitor. The capacitor weight for radiation cooled capacitors which have been life tested in a vacuum in conjunction with thruster tests has been shown to be 6 joules/lb or 16 watts/lb. Selecting a particular desired performance, i.e., impulse bit, thrust level and specific impulse, defines an energy level of operation. The corresponding capacitor weight will then also be known. The thruster nozzle and the discharge initiating circuitry introduce a fixed weight of about 0.6 lb.

For application up to roughly 3000 lb-sec in the thrust range from roughly 50 to 200 μ lb, the weight of the propellant system is essentially that of the propellant (see Figures 3, 4, 48, 49). The weight of a typical negator spring is roughly 15 grams. A typical track which guides and supports the propellant in the laboratory thruster** weighs about 35 grams. For purposes of calculation the propellant subsystem weight is essentially:

$$\text{Propellant subsystem weight} = 50 \text{ grams} + \text{propellant weight}$$

$$= 50 \text{ grams} + \frac{\text{total impulse}}{\text{specific impulse}}$$

---

* The saving in weight that can be had by connecting more than one thruster to a single capacitor will be treated in Section 5.2.

** In flight-type hardware this guide is incorporated as part of the structure which houses the thruster, propellant, and discharge initiating circuitry.

In Section 2.3.3c it was shown that the power conditioner weight is in accordance with Table 6, i.e., below 200 watts, the power conditioner weighs 500 grams plus 11 grams/watt, above 200 watts it weighs 500 grams plus 5 grams/watt, respectively. Other than the driver*, only connecting leads introduce additional weight.

The weight of a system can thus be calculated to within a reasonable degree of accuracy in accordance with the schedules outlined above. For a Teflon propelled single nozzle single capacitor solid propellant pulsed microthruster system with a thrust level of up to 800 μ lb we arrive at a weight schedule as:

$$\text{System weight in grams} = 825 \text{ grams} + 39.4 \text{ grams/watt} + (453.6)\ \frac{\text{lb-sec total impulse}}{\text{specific impulse}}$$

or with the thrust level expressed in μ lb:

$$\text{System weight in grams} = 825 \text{ grams} + 9.85\ \frac{\text{grams}}{\mu \text{ lb of thrust}} + (453.6)\ \frac{\text{lb-sec total impulse}}{\text{specific impulse}}$$

In order that a given pulsed microthruster deliver a certain total impulse (I), it must deliver (n) discrete impulse bits (i). The total number of discharges that the thruster has to survive is thus

$$n = I/i$$

At this point it should be noted that any desired thrust level may be achieved by any one of a number of possible designs. The power requirements remain essentially constant at 0.25 watts per micropound of thrust. However, a given thrust level can be arrived at by either a few number of discharges per second at high energy per discharge impulse bits, or more discharges per second at lower

---

* Any source which supplies a 6 volt pulse when an impulse bit is desired.

energy per discharge impulse bits. For example, a 100 μ lb thrust level thruster delivering 1000 lb-sec of total impulse may assume any one of the designs tabulated in Table 14.

TABLE 14. POSSIBLE DESIGNS OF A 100 μ lb THRUST LEVEL THRUSTER DELIVERING 1000 lb-sec TOTAL

Discharge energy, joules	1	5	10	20	40
Impulse/discharge, μ lb-sec	4	20	40	80	160
Pulse frequency, pulses/sec	25	5	2.5	1.25	0.625
Power at thruster, watts	25	25	25	25	25
Input power	31.2	31.2	31.2	31.2	31.2
Specific impulse, sec	260	660	990	1475	2210
Total number of discharges	2.5×10^8	5×10^7	2.5×10^7	1.25×10^7	6.25×10^6
Total system weight, grams	3555	2498	2268	2117	2015

The results presented in Table 17, show that at a given thrust and power level of operation, the most reliable (i.e., the system requiring the least number of discharges to attain a given total impulse) thruster system will also be the lightest one. However, this latter system will most likely be larger in size than the lower discharge energy systems.

Should the total number of discharges n be considerably beyond the number demonstrated by state-of-the-art capacitors, it will be necessary to either derate the capacitor to operate at a lower power density (lbs/watt) or to operate the thruster with a heat sink which maintains the capacitor temperature below that of a radiation cooled capacitor. In this latter case, the capacitor life is roughly doubled for each 10°C decrease in capacitor temperature achieved by heat sinking. It is also possible to achieve maximum reliability of delivering a certain total impulse by incorporating redundancy in system components (see Figures 49 and 57, respectively).

The above considerations applied to a thruster system when each thruster had its own capacitor, power conditioner, discharge initiating network and driver. Many applications require more than one thruster. The next section considers an approach

that may be adopted for such applications in order to obtain the lightest possible system weight, but yet retaining a high degree of reliability.

5.2 Thruster System Weight Reduction Scheme

In any practical application of our thruster system for attitude control, stationkeeping, or other space missions, anywhere from 8 to 12 thrusters may be required in a given satellite. The purpose of this calculation is to show that the weight of a multi-thruster system is minimized if more than one thruster nozzle is connected to a single derated capacitor. In the first set of calculations to follow such a propulsion system configuration is called "Scheme A".

Scheme A

The calculation is carried out by comparing the weight of a single capacitor which is derated with respect to voltage to give it the same life as the total life of n capacitors which the single capacitor is to replace. It is assumed that:

1) Only one thruster of the multi-thruster system would ever be operated at any instant.

2) The capacitance of the single capacitor is equal in magnitude to the capacitance of each one of the n units which it is to replace.

3) The energy/discharge delivered by the single capacitor is the same as that delivered by any one of the n units it replaces.

4) The joules-per-pound ratio of the single capacitor is equal to the joules-per-pound ratio of each of the n capacitors it replaces.

5) That the voltage acceleration factor α is constant over the voltage derating range of interest.

6) The weight of power leads are negligible.

The voltage power law (at constant temperature) states:

$$\frac{L_1}{L_2} = \left(\frac{V_2}{V_1}\right)^{\alpha} \quad (\text{with } L_1/L_2 > 1)$$

with L the life and V the applied potential. The exponent α varies with voltage stress level for any given dielectric and also with the type of dielectric. For the

present purposes the exponent α will be taken to be 5 (valid for paper-oil capacitors) and 6.4. The value 6.4 applies to Sprague metalized-paper capacitors.

In order that a single capacitor have the same life as the n capacitors it replaces, it is necessary that:

$$L_s = n L_m$$

with L_s and L_m the life of the single unit and the life of each of the multiple units being replaced, respectively. From the voltage power law it is evident that the design voltage (V_d) of the single capacitor is related to the voltage (V_s) at which the thruster is operated by:

$$\frac{L_s}{L_m} = \left(\frac{V_d}{V_s}\right)^{\alpha} > 1$$

with L_s and L_m as defined above. From the latter two relations, one finds,

$$n = \left(\frac{V_d}{V_s}\right)^{\alpha}$$

It is now possible to compare the weight (W_n) of the n capacitors for the cases where each thruster has its own capacitor, to the weight (W_s) of a single capacitor replacing the n units. Thus,

$$W_n = KE_n n = Kn \frac{1}{2} CV_s^2$$

$$W_s = KE_s = K \frac{1}{2} CV_d^2$$

with K the pounds-per-joule of a capacitor and C the capacitance. Thus,

$$\frac{W_s}{W_n} = \frac{1}{n} \left(\frac{V_d}{V_s}\right)^2 = \left(\frac{1}{n}\right)^{(\alpha-2)/\alpha}$$

Since $\alpha > 5$ and $n \geq 1$, it is seen that $W_s \leq W_n$. In all cases the weight of a single derated capacitor will be less than the weight of the n units it replaces! This latter result is presented in Figure 65 for $\alpha = 5$ (paper-oil capacitors) and for $\alpha = 6.4$ (Sprague metalized paper capacitors).

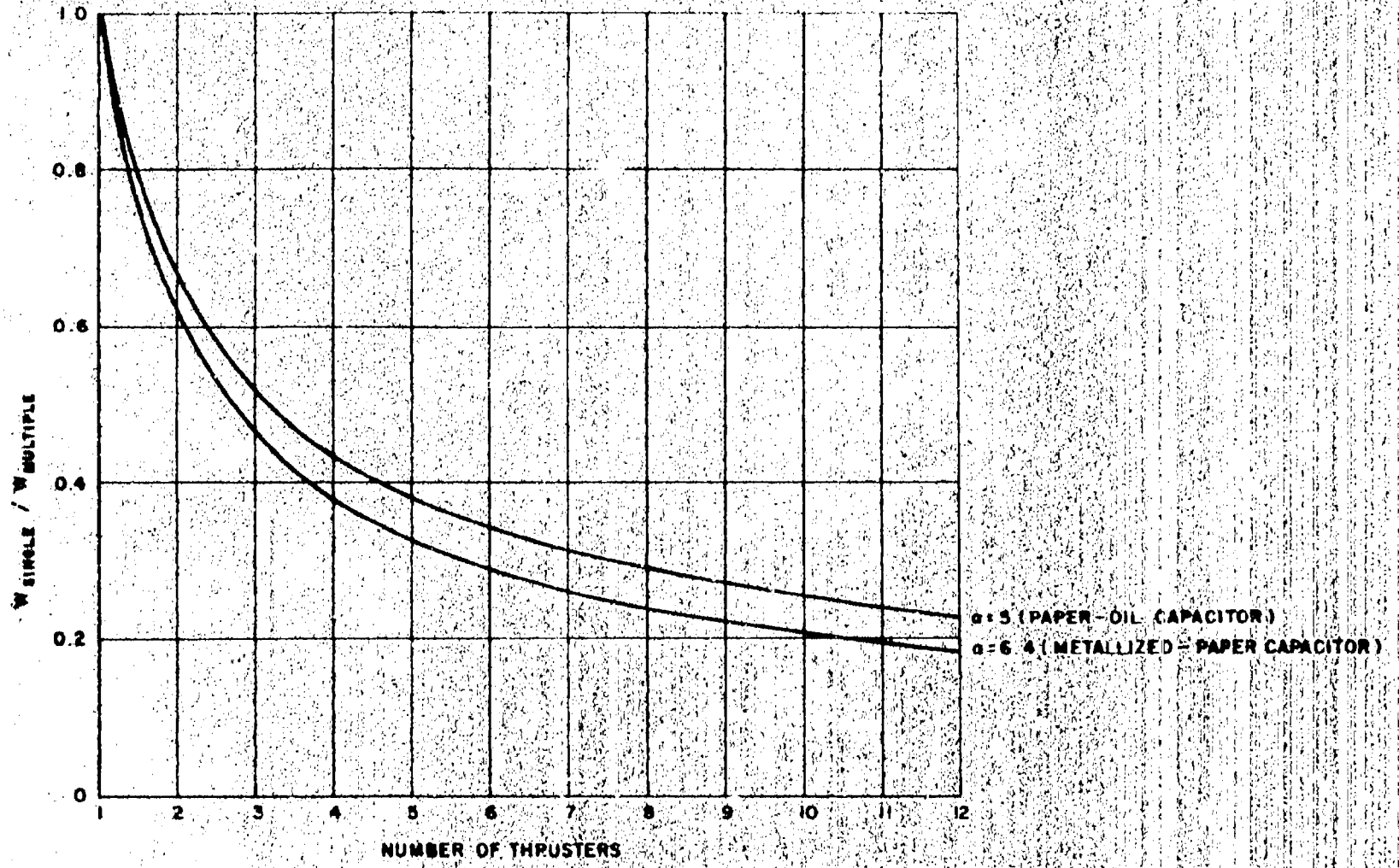

Figure 65. Weight Ratio as a Function of Number of Capacitors

Scheme B

For enhanced reliability of the overall propulsion system one may not want to connect all thrusters to one capacitor. One may want to use m capacitors and have n thruster nozzles connected to each of the m capacitors; i.e., Scheme B. It is possible to compare the weight of the m derated capacitors with the weight of the single capacitor scheme as calculated above. Figure 66 shows the comparison being made.

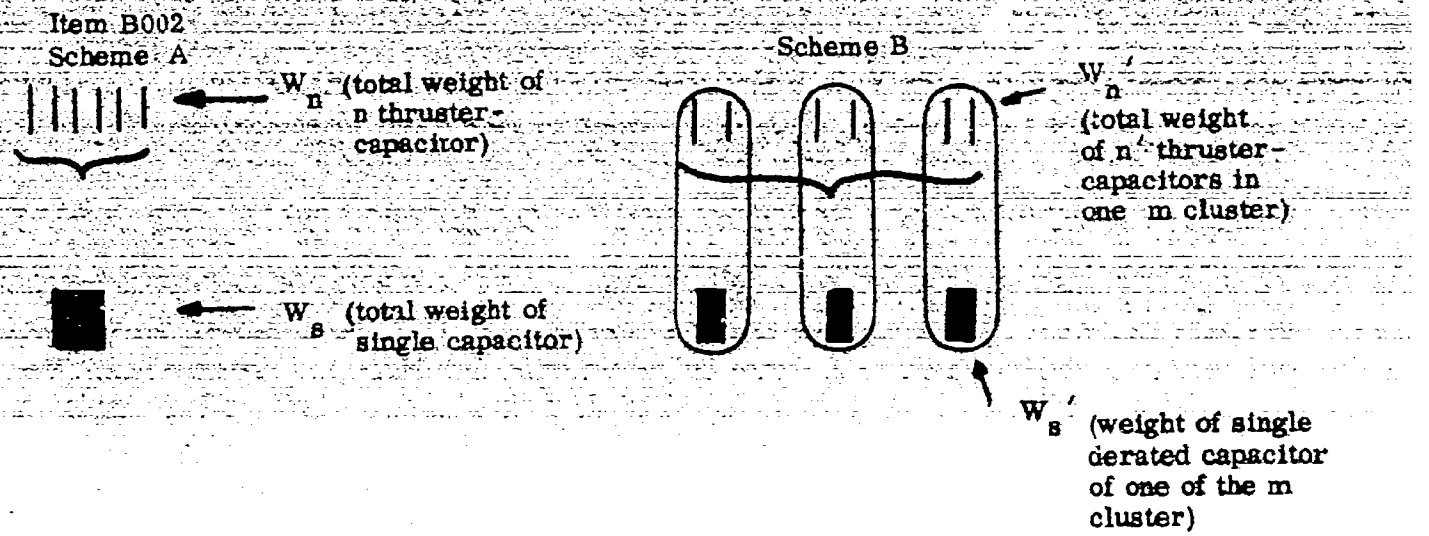

Figure 66. Comparison of Schemes

In a meaningful comparison of Scheme A with Scheme B it is necessary that the total number of individual capacitor-thrusters being replaced in each scheme be the same, hence,

$$mn' = n$$

Furthermore,

$$mW_n' = W_n$$

The problem is to evaluate the ratio:

$$\frac{mW_s'}{W_s}$$

From the relation derived for Scheme A, it follows that for each of the m clusters of Scheme B:

$$\frac{W_s'}{W_n'} = \left(\frac{1}{n'}\right)^{(\alpha-2)/\alpha} \quad \text{or} \quad W_s' = W_n' \left(\frac{1}{n'}\right)^{(\alpha-2)/\alpha}$$

Thus

$$\frac{mW_s'}{W_s} = \frac{mW_n' \left(\frac{1}{n'}\right)^{(\alpha-2)/\alpha}}{W_n \left(\frac{1}{n}\right)^{(\alpha-2)/\alpha}} = \frac{mW_n' \left(\frac{m}{n}\right)^{(\alpha-2)/\alpha}}{W_n \left(\frac{1}{n}\right)^{(\alpha-2)/\alpha}}$$

Since $mW_n' = W_n$, it follows that

$$\frac{mW_s'}{W_s} = m^{(\alpha-2)/\alpha}$$

Since $m > 1$ and $(\alpha-2)/\alpha > 0$, it follows that $W_s' > W_s$ as one might expect.

Figure 67 shows the weight ratio mW_s'/W_s as a function of the number of clusters m for $\alpha = 5$ (paper-oil capacitors) and for $\alpha = 6.4$ (metallized-paper capacitors).

Figure 67. Weight Ratio as a Function of Number of Clusters

With the relations presented above it is now possible to analyze the weight of the various capacitor-thruster combinations that we may want to consider in a propulsion system. The trade-off between reliability and system weight can be readily assessed.

In any practical application the saving in weight must be balanced against the extra shielding required for RFI control and any likely reduced thruster performance likely to arise because of the extra circuit inductance that is introduced.

SECTION VI

CAPACITOR DEVELOPMENT*

6.1 PROBLEM STATEMENT

Capacitors are required for use as an energy storage source in a family of pulsed plasma electric thrusters. These capacitors must operate in a hard vacuum environment at a maximum environmental temperature of approximately 150°F. Voltages will be in the range of 1 KV to 1.5 KV in an under-damped discharge circuit which will cause reversal to the extent of approximately 40%. The pulse repetition rate for design purposes will be approximately 4 pps.

The design life objective is 4×10^7 discharges with a goal of 10^8 discharges at 10 joules/lb. The former value reflects the total course correction required for a five-year mission time with suitable safety factors.

The optimum mechanical capacitor configuration must be studied and several configurations tested. The major objective of the program will be a minimum weight and size to meet the other program requirements.

6.2 TESTING AND TEST FACILITIES

Testing, with the exception of some preliminary evaluation, was accomplished at Fairchild Hiller, Republic Aviation's test facility. This was necessitated by the lack of high vacuum equipment and microthruster engines at Sprague Electric to simulate actual space flight conditions. Preliminary testing, accomplished to evaluate various metallized films, consisted of discharge life testing under high vacuum conditions through an ignitron discharge circuit. Advanced life testing consisted of actual engine firing. Individual unit histories are included in Tables 15 through 17.

---

* This section was written by Messrs: C.W.Chase, Program Director and F.W.Pinkall, Program Engineer, of the Sprague Electric Company. This work was performed under P.O. No. 3-6283-844529 of contract F33615-67-C-1395.

6.3 INITIAL DESIGN

In order to realize fully the best possible energy density available, it was decided to employ metallized dielectric systems. This realization is achieved by the replacement of metal foil conductors with a thin-metal deposition of from 250 to 350 angstroms thickness. The metallized dielectric systems afford considerable size savings as well as weight reduction. The self-healing property of the metallized system was also considered a valuable asset for this application. All systems, with the exception of the metallized paper with plain mylar, were designed as 6.0 μf - 1300 volt, un-impregnated, single section capacitors. The sections were round in configuration stressed at 1300 volts/mil and assembled into round steel cans.

These capacitors were built for evaluation in order to select final dielectric systems for Phase II of this program. Dielectric systems employed were:

- Metallized paper with plain mylar
- Metallized mylar with plain mylar
- Metallized polycarbonate with plain polycarbonate
- Metallized tedlar with plain tedlar
- Metallized kapton with plain kapton

a) Metallized Paper with Plain Mylar

This system was selected as being representative of the present state-of-the-art in the manufacture of energy storage capacitors. Capacitors of two ratings were designed and built for life test controls against the metallized film systems. The two ratings were 9.0 μf at 1.9 KV peak-to-peak and 20.0 μf at 1.95 KV peak-to-peak. The units were designed as two pressed sections wired in parallel and stressed at 2200 volts/mil. The capacitors were impregnated with mineral oil and assembled in rectangular stainless steel containers. The positive termination consisted of a ceramic terminal with the negative side connected to the case. This is done in order to obtain current cancellation; thereby lowering the inductance. Inductance of these capacitors, measured by the insertion loss method, was in the range of 20×10^{-9} henry.

b) Metallized Mylar with Plain Mylar: (Polyester Film)

This system was selected because of the excellent dielectric strength properties of the film and its good temperature characteristics. The system displayed the best discharge life results of those tested. However, this was far below program requirements.

c) Metallized Polycarbonate with Plain Polycarbonate

This system was selected because of its low dissipation factor and capacitance stability with temperature change. The system test results proved negative due to relatively low dielectric strength (approximately 50% that of mylar) and extremely short life under charge-discharge conditions.

d) Metallized Tedlar with Plain Tedlar: (PVF Film)

This system was selected because of its high dielectric constant. System test results proved negative due to comparative low dielectric strength, the evolution of hydrogen fluoride gas during clearing and short charge-discharge life. This film also exhibited mild parameter changes with temperature. Capacitance, for instance, changed 83% from room temperature to 85°C.

e) Metallized Kapton with Plain Kapton: (Polyamide Film)

This system was selected because of its excellent dissipation factor and temperature characteristics. It was impossible to roll sections of suitable quality to test because of severe static conditions within the rolls. The static charge increases the "cling" characteristics of the material, causing deep creases and wrinkles resulting in low voltage breakdown.

Life testing under charge-discharge conditions resulted in short time failures of all units tested. Failure analysis revealed a complete loss of end connection due to clearing of the metallized layer along the contact edge. The clearing is caused by high current density along the edge and the contact resistance between metallized layer and end spray. Clearing occurs which reduces the effective length of connection resulting in an increase in the amps per linear inch ratio which in turn causes more clearing. The process avalanches, with the degree of severity varying with the number of discharge cycles and the contact resistance.

6.4 SECOND GENERATION METALLIZED CAPACITORS

In an effort to improve the end connection difficulties, it was decided that the 20 uf - 1.95 KV peak-to-peak capacitor be redesigned with the following improvements over the initial design:

a) The section was redesigned into seven (7) round parallel sections. The round section geometry yields the best surface for end spray and the use of parallel sections reduces the inductance and resistance.

b) A current collector disc, brazed directly to the terminal stud was added. Wire leads were taken from the positive end of each section and individually soldered to the disc. This was done to increase the current carrying capability of the capacitor.

c) A wire lead from the negative end of each section was brought through and attached to the case bottom. This again was an effort to reduce lead resistance and increase the current carrying capability.

Test results showed an improvement over units of the initial design. Both units, however, failed after approximately 50,000 discharges. Subsequent test results would indicate that very probably a temperature problem existed. Recordings made on the case exterior indicate temperatures of 164°F with no indication of temperature stabilization. See temperature run in Figure 68. Thrust measurement results are approximately 50% lower than required for the application. This is interesting in view of the fact that a study of the discharge current waveshape indicates I peak and di/dt of acceptable degree for required thrust. Evidently, heat generated by the relatively high resistance is the cause of losses. It now appears that the program aim of increased joule per pound ratio is not as important or meaningful as the thrust per pound ratio. It also appears that a fair estimate of thrust level can be pre-determined by a study of the capacitor L, R, and Q.

6.5 L, R, AND Q CONSIDERATIONS

Studies, made by Republic Aviation Division of Fairchild Hiller, of test results indicate that inductance of approximately 20 nanohenry, resistance of from .033 to .005 ohms and Q of 7 to 9 are required to achieve thrust levels of acceptable degree. It also follows that as R decreases, thrust increases. Measurements made on metallized capacitors indicate that inductance is within acceptable proportion, resistance is high (approximately .01 ohms) and Q is low (approximately 3.0). It is felt that resistance of the thin metal deposition is the cause of the high R, low Q. Parameter measurements are made by a method developed by Republic. This method involves taking photographs of the resonant ringout of a shorted capacitor which has been excited by a fast pulse. L, R, and Q formulae are derived by taking a logarithmic decrement of the ringout. Comparison of the results of this method with the results of much more tedious methods have been made. The results of both methods follow one another very closely. The method will be used to measure all future units to facilitate further study of parameter value to thrust level. The results also serve as a fast indicator of the results of capacitor improvement attempts.

6.6 6.0 μf CAPACITOR OF METALLIZED MYLAR

6.0 μf - 1500 volt capacitors were designed of metallized mylar with plain mylar. The stress on the dielectric was designed at 2000 volts/mil. The capacitors were constructed with all of the improvements built in to the second generation 20 μf units. In an effort to further reduce the end connection resistance, copper was high vacuum RF sputtered onto the aluminum metallized material and over-sprayed with tin-lead. It was felt that by bombarding the oxides, built upon the foil surface, with minute particles of copper that end connections of superior quality would result. Parameter measurements indicate inductance in the order of 20 nanohenry, resistance of .01 ohms and Q of 4.65. The capacitors failed after a short time on test. The failure mode again was a loss of end connection due to clearing along the contact edge.

6.7 CHANGE OF SCOPE

A meeting was held at Republic Aviation to discuss the program as it stood in view of the failures encountered with metallized dielectric systems. It was decided that the inherent high resistance and low Q of the metallized capacitor as we know them today, make them unsuitable for pulsed plasma thrusters requiring high peak currents. A change to foil capacitors was recommended with mylar selected as the dielectric because of its good dielectric strength and temperature characteristics.

6.8 FIRST GENERATION MYLAR FOIL CAPACITORS: (10 JOULE)

Twenty joule capacitors, rated 20 uf - 1500 volts were designed of mylar with aluminum foil conductors in single, round sections stressed at 2300 volts/mil. The capacitors were impregnated with silicone oil. End connections were made by scrub soldering techniques using a composition of 75% tin and 25% zinc to tin the aluminum foils. Seven (7) number 18 wire leads soldered to the positive end of the unit were in turn soldered to a current collector disc. The negative connection was made by soldering seven (7) number 18 wire leads from section to case bottom. The case material was brass finished with a hot tin dip. The foil conductor was 6-1/4" wide. Preliminary test data showed Q ranging from 7.1 to 10.4, R ranging from .003 to .005 ohms; and L ranging from 24 to 27 nanohenry. Thrust measurements, made during engine firing, indicated that impulse/discharge was of satisfactory proportion. Energy densities of 10.55 joules/pound were realized.

During actual engine firing, one unit failed short and two units leaked impregnant at approximately 25,000 shots each. All units were returned to Sprague for failure analysis.

Temperature measurements made during engine operation, showed no thermal equilibration. The shorted capacitor proved to have failed due to a dielectric puncture, possibly set up by high stress at extreme temperature. The units which leaked impregnant proved to be electrically sound. A review of thermal transfer problems in high vacuum, prompted a decision to repair the leaks, re-impregnate the capacitors and paint the cases black in order to improve

emissivity, thereby increasing thermal transfer capability by radiation. The capacitors were returned to Republic and fired again on engines. The units now thermally equilibrated at 170°F. (See Figure 69).

One unit failed due to an impregnant leak following short time engine operation. The leak was found to be caused by mechanical damage, inflicted during engine assembly. The remaining unit failed short due to a random dielectric failure following 1.35×10^6 shots.

An additional capacitor was built unimpregnated for test purposes. Parameters of L, R, and Q were equivalent to the impregnated units. The capacitor failed short due to a dielectric puncture following 25,000 shots. This is the same time to failure as encountered on the original unpainted capacitors making thermal runaway a suspected contributor to failure. One theory, as to the reason for thermal runaway even though the case was painted black, is that the oil impregnation is required to improve the heat transfer from section to case.

6.9 SECOND GENERATION OF MYLAR FOIL CAPACITORS: (20 JOULE)

In an effort to improve the life of the mylar foil capacitor and to improve the overall quality, the following changes in design were made.

a) Voltage stress was reduced from 2300 to 2000 volts/mil to increase life and reliability.

b) Case material was changed from brass to aluminum in order to reduce weight, reduce resistance and improve heat transfer.

c) Foil width was reduced from 6-1/4" to 3-1/8" in order to decrease conductor losses and improve section geometry to increase Q.

d) Positive end termination was changed from seven (7) number 18 wire leads to twelve (12) 3/8" by .003" tinned copper tabs to reduce resistance.

e) Negative end termination was changed from seven (7) number 18 wire leads to twelve (12) 3/8" by .005" aluminum tabs welded into the case to cover seam. This also was done to reduce resistance.

In addition to these changes, special drain and seal techniques were established to minimize the threat of leaks. These techniques involve draining units as 90°C and sealing at 50°C in order to insure the inclusion of a compressible pocket of air within the capacitor case.

Two capacitors were built as unimpregnated units. The first unit failed short at 73,665 shots due to a random dielectric puncture. The unit case temperature at the time of failure was 154°F. It appears that the temperature had stabilized. (See Figure 20 for temperature run). It was assumed that the increased life of this unit over the unimpregnated first generation unit was the increased heat transfer capability supplied between section and case by the twelve aluminum tabs. The assumption was also made that the internal temperature of the section was probably much higher than the case temperature. Therefore, the capacitor should be impregnated for ultimate life. The second unimpregnated unit was not tested to date due to limited chamber and engine capability.

Four capacitors were manufactured as silicone oil impregnated units. Of the four, one unit was never tested, but was delivered to the firm responsible for the development of the engine power conditioner. Parameter values of the remaining three showed some improvement over first generation units with Q ranging from 8.53 to 9.37; R ranging from .0034 to .0038 ohms; and L ranging from 19.95 to 21.3 nanohenry. Energy density of 8.5 joules/pound was realized on the capacitors.

The first unit failed as an impregnant leak following 171,946 shots. The failure was found to be caused by a fault in a welded seam in the case. Temperature of the case at the time of failure was 185°F and had stabilized. The capacitor has been checked electrically and found to be sound.

The remaining two units failed short, one following 939,240 and the other at 4.9×10^6 shots. Analysis of the parts revealed random dielectric failures with no visible assignable causes found. Temperature of the units at time of failure was 160 to 170°F.

Additional experimentation utilizing narrower foil widths, in an effort to reduce losses and increase Q has been performed with negative results. It now appears that the 3-1/8" foil width of the 20 joule capacitor is optimum. That is, foil loss is negligible as compared with interface and end connection resistance. The present 20 joule design, therefore, is the basic capacitor design for 20 joule units which we will hold firm for the remainder of this program.

6.10 THIRD GENERATION OF MYLAR FOIL CAPACITORS: (20 JOULE)

The third generation of the 20 joule mylar foil capacitor were built of the same design as the second generation. Efforts toward extending life and reliability were expended through the setting-up and adhering-to of the following tightened quality control procedures:

a) Completely clean the rolling machine, polishing all spindles and idler rolls at the time of each set-up.

b) Remove from the immediate machine vicinity all sources of dust and dirt particles.

c) Set-up the machine to the proper design and roll one capacitor section.

d) Using a thickness figure of the total dielectric between foils minus one layer, flash the sections at 7000 volts/mil. If the unit fails, roll one additional section and flash at the same stress level. If the second section fails, strip the machine of material and repeat the clean-up procedure. Complete the machine set-up again, using a new batch of material.

e) Repeat step (d) until a suitable set-up of machine and material has been achieved.

f) Roll the number of sections required plus five (5) additional units.

g) Flash all sections to the stress of (d) above and discard all rejects.

h) The five extra units are to be broken down electrically to insure that material meets the provisions of incoming material specifications.

i) Flash the sections again at the stress level of (d) prior to cover welding and prior to shipping.

Once again parameter values showed some improvement over the previous generation. Q ranged from 7.3 to 12.5; R ranged from .0025 to .0045 ohms; and L ranged from 19.2 to 23.2 nanohenry. In addition to the above changes, Republic has attached cooling fins to the sides of the units. The fins are 2" x 3" and are positioned 90° apart. To date, one unit has completed testing. This unit failed short following 7.15×10^6 shots. Analysis of the failure revealed a random dielectric failure with no assignable cause found.

6.11 FOURTH GENERATION OF MYLAR FOIL CAPACITORS: (20 JOULE)

Two additional units were built to the same specification as the third generation capacitor. The sections were modified slightly by rolling thermocouples into their interior to study temperature gradients across the capacitor. This study was performed to determine whether or not internal section heat was of sufficient degree to cause short capacitor life. Both capacitors were engine fired for sufficient time to reach thermal stability and then thermally checked. Air was forced through a coil placed around the unit. The temperature of the air was monitored and considered to be ambient temperature. The temperature gradient from section core to capacitor case was only .5°F on each unit. This gradient is not considered excessive and should not degrade life of the unit. (See Figure 71 for temperature information).

6.12 FIRST GENERATION OF 40 JOULE MYLAR FOIL CAPACITORS

Forty-joule capacitors, rated 40 μf - 1500 volts, were designed and built for experiments with high energy engines. The designed stress was 2000 volts/mil; the conductor width was 3-1/8" and an energy density of 8.5 joules/pound was realized. The unit was designed as a single round section to be silicone oil impregnated. All quality control procedures, practiced in the construction of the 20 joule capacitors, were adhered to. Parameter values again fell within acceptable limits with inductance ranging from 16.8 to 21.4 nanohenry; R ranging from .0024 to .0039 ohms; and Q ranging from 7.3 to 9.35. The capacitors were engine fired at a repetition rate of 1 pulse/second. Two units leaked impregnant from the terminal assembly. This was found to be a combination of failure of soft solder seals and undue stress placed on the terminal stud during engine assembly. All future units will be braze-sealed to prevent re-occurrence of this failure mode. One unit failed short following 3.3×10^6 shots.

6.13 FIVE (5) JOULE CAPACITORS OF MYLAR FOIL CONSTRUCTION

Five-joule capacitors, rated 10 μf - 1000 volts, were designed and built. The capacitors were designed in three groups, each stressed to different levels. All groups were designed as single round sections with all of the construction improvements and quality control procedures developed during the program employed. Foil width was reduced to 1-7/8" to further determine whether or not losses could be decreased resulting in lower R and increased Q. Parameter values fell within acceptable limits with inductance ranging from 14.9 to 20.2 nanohenry; resistance ranging from .0036 to .00576 ohms; and Q ranging from 7.0 to 11.0. Of interest is the fact that the parameter levels have not improved with the decreased conductor width. This tends to confirm results of earlier tests along these lines. Findings at that time were that interface and end connection resistances are substantially greater than foil losses. The capacitors are to be engine fired at 4 pulses/second at 1000 volts.

a) Group I

This group was designed to stresses of 1430 volts/mil with an energy density of 3.45 joules/pound. The capacitors of this group have been delivered for testing.

b) Group II

This group was designed to stresses of 1335 volts/mil with an energy density of 3.05 joules/pound. Two capacitors of this group have been tested to date. One capacitor failed as an impregnant leak following 45,000 shots. The failure was caused by a soft solder seal defect around the terminal stud assembly. These units were constructed prior to the failure of the 40-joule capacitors which prompted our decision to change to brazed seals.

The second capacitor failed short following 1.7×10^6 shots. Case temperature at the time of failure was 171°F and had stabilized. (See Figure 72 for temperature information). Analysis revealed a random dielectric failure with no assignable cause found.

c) Group III

This group was designed to stresses of 950 volts/mil with an energy density of 1.81 joules/pound. The capacitors of this group have been delivered for testing.

6.14 CONCLUSIONS

A study of the results of this program led one to the following conclusions:

a) Metallized dielectric systems, as we know them today, are not suited to this application requiring large peak discharge currents. Current densities are too great for end connection survival and resistance of the metal deposition on the dielectric system is too high to yield thrust levels of acceptable degree.

b) Capacitor resistance becomes lower as foil width decreases to a point, and then remains fairly constant. Consequently, interface and end connection resistance becomes the dominant

factor where foil width is considered optimum. Foil losses from this point on become less and less significant.

c) Every effort to improve the emissivity of capacitor cases should be taken for applications involving space (hard vacuum). Heat is dissipated only through radiation in this application.

d) Thermal conductivity from capacitor to case is critical under hard vacuum ambients. Therefore, it becomes necessary to impregnate the capacitors using the impregnant as the heat transfer medium.

e) Special draining and sealing techniques are necessary to prevent leaks during operation in space atmosphere.

f) Capacitor life was substantially increased by the addition of quality control procedures. It will be necessary to manufacture units of this type under strict quality control procedures and controlled clean ambient conditions.

g) Radiation cooled energy storage capacitors driving thrusters at 7.7 joules/lb have been developed with a life of 7.1×10^6 discharges. The life can be extended significantly by derating the capacitor below the state-of-the-art energy density of 7.7 joules/lb.

TABLE 15. Record of

Rating	Part No. & Serial No.	Shape & No. Sections	Dielectric	Conductor	Conductor Width	Section Termination	Impregnant	C
6.0 μfd 1600 v	——	Round 1 Section	1X. 0003 M. Teflon 1X. 0005 P. Teflon	Metallized Aluminum	3 1/4"	Tin-Lead Spray	None	5
6.0 μfd 1500 v	——	Round 1 Section	1X. 0005 M. Poly 1X. 0005 P. Poly	Metallized Aluminum	3 1/4"	Tin-Lead Spray	None	5
6.0 μfd 1500 v	——	Round 1 Section	1X. 0005 M. Mylar 1X. 0005 P. Mylar	Metallized Aluminum	3 1/4"	Tin-Lead Spray	None	6
6.0 μfd 1500 v	——	Round 1 Section	1X. 0005 M. Teflon 1X. 0005 P. Teflon	Metallized Aluminum	3 1/4"	Tin-Lead Spray	None	5
6.0 μfd 1500 v	——	Round 1 Section	1X. 0005 M. Poly 1X. 0005 P. Poly	Metallized Aluminum	3 1/4"	Tin-Lead Spray	None	5
6.0 μfd 1500 v	——	Round 1 Section	1X. 0005 M. Mylar 1X. 0005 P. Mylar	Metallized Aluminum	3 1/4"	Tin-Lead Spray	None	6
6.0 μfd 1500 v	T-1	Round 1 Section	1X. 0005 M. Teflon 1X. 0005 P. Teflon	Metallized Aluminum	3 1/4"	Tin-Lead Spray	None	5
6.0 μfd 1500 v	T-2	Round 1 Section	1X. 0005 M. Teflon 1X. 0005 P. Teflon	Metallized Aluminum	3 1/4"	Tin-Lead Spray	None	5
6.0 μfd 1500 v	P-1	Round 1 Section	1X. 0005 M. Poly 1X. 0005 P. Poly	Metallized Aluminum	3 1/4"	Tin-Lead Spray	None	5
6.0 μfd 1500 v	P-2	Round 1 Section	1X. 0005 M. Poly 1X. 0005 P. Poly	Metallized Aluminum	3 1/4"	Tin-Lead Spray	None	5
6.0 μfd 1500 v	M-1	Round 1 Section	1X. 0005 M. Mylar 1X. 0005 P. Mylar	Metallized Aluminum	3 1/4"	Tin-Lead Spray	None	6
6.0 μfd 1500 v	M-2	Round 1 Section	1X. 0005 M. Mylar 1X. 0005 P. Mylar	Metallized Aluminum	3 1/4"	Tin-Lead Spray	None	6
6.0 μfd 1500 v	T-100	Round 1 Section	1X. 0005 M. Teflon 1X. 0005 P. Teflon	Metallized Aluminum	3 1/4"	Tin-Lead Spray	None	5
6.0 μfd 1500 v	T-101	Round 1 Section	1X. 0005 M. Teflon 1X. 0005 P. Teflon	Metallized Aluminum	3 1/4"	Tin-Lead Spray	None	5
6.0 μfd 1500 v	P-100	Round 1 Section	1X. 0005 M. Poly 1X. 0005 P. Poly	Metallized Aluminum	3 1/4"	Tin-Lead Spray	None	5
6.0 μfd 1500 v	P-101	Round 1 Section	1X. 0005 M. Poly 1X. 0005 P. Poly	Metallized Aluminum	3 1/4"	Tin-Lead Spray	None	5
6.0 μfd 1500 v	M-100	Round 1 Section	1X. 0005 M. Mylar 1X. 0005 P. Mylar	Metallized Aluminum	3 1/4"	Tin-Lead Spray	None	6
6.0 μfd 1500 v	M-101	Round 1 Section	1X. 0005 M. Mylar 1X. 0005 P. Mylar	Metallized Aluminum	3 1/4"	Tin-Lead Spray	None	6
6.0 μfd 1500 v	——	Round 1 Section	1X. 0005 M. Mylar 1X. 0005 P. Mylar	Metallized Aluminum	3 1/4"	Tin-Lead Spray	None	6
6.0 μfd 1500 v	——	Round 1 Section	1X. 0005 M. Mylar 1X. 0005 P. Mylar	Metallized Aluminum	3 1/4"	Tin-Lead Spray	None	5
6.0 μfd 1500 v	——	Round 1 Section	1X. 0005 M. Mylar 1X. 0005 P. Mylar	Metallized Aluminum	3 1/4"	Tin-Lead Spray	None	6
6.0 μfd 1500 v	——	Round 1 Section	1X. 0005 M. Mylar 1X. 0005 P. Mylar	Metallized Aluminum	3 1/4"	Tin-Lead Spray	None	6
6.0 μfd 1500 v	——	Round 1 Section	1X. 0005 M. Poly 1X. 0005 P. Poly	Metallized Aluminum	3 1/4"	Tin-Lead Spray	None	5
6.0 μfd 1500 v	——	Round 1 Section	1X. 0005 M. Poly 1X. 0005 P. Poly	Metallized Aluminum	3 1/4"	Tin-Lead Spray	None	5
6.0 μfd 1500 v	——	Round 1 Section	1X. 0005 M. Poly 1X. 0005 P. Poly	Metallized Aluminum	3 1/4"	Tin-Lead Spray	None	5

A

Record of Capacitor Tests

gnal	Cap	L	R	Q	Test Conditions	Test Results	Failure Mode	Analysis	Remarks
e	5.45	—	—	—	T.C.	+63% ΔC 25°C to 85°C	—	—	Avg of 6 units
e	5.60	—	—	—	T.C.	0% ΔC 25°C to 85°C	—	—	Avg of 6 units
e	6.8	—	—	—	T.C.	+7% ΔC 25°C to 85°C	—	—	Avg of 6 units
e	5.95	—	—	—	Voltage Breakdown	3750 V/m	Short	Random Failures	Avg of 4 units
e	5.60	—	—	—	Voltage Breakdown	3750 V/m	Short	Random Failures	Avg of 4 units
e	6.0	—	—	—	Voltage Breakdown	7125 V/m	Short	Random Failures	Avg of 4 units
e	5.45	—	—	—	1 Hz in Vac. 1300 V	Failed at ≈ 700 shots	Open	Loss of Connection Heat Damage	Possible Heat Damage During Welding
e	5.45	—	—	—	1 Hz in Vac. 1300 V	Failed at ≈ 700 shots	Open	Loss of Connection Heat Damage	Possible Heat Damage During Welding
e	5.60	—	—	—	1 Hz in Vac. 1300 V	Failed at ≈ 700 shots	Open	Loss of Connection Heat Damage	Possible Heat Damage During Welding
e	5.60	—	—	—	1 Hz in Vac. 1300 V	Failed at ≈ 700 shots	Open	Loss of Connection Heat Damage	Possible Heat Damage During Welding
e	6.0	—	—	—	1 Hz in Vac. 1300 V.	Failed at ≈ 700 shots	Open	Loss of Connection Heat Damage	Possible Heat Damage During Welding
e	6.0	—	—	—	1 Hz in Vac. 1300 V.	Failed at ≈ 700 shots	Open	Loss of Connection Heat Damage	Possible Heat Damage During Welding
	5.7	—	—	—	1 Hz in Vac. 1300 V	Failed at 1500 shots	Open	Loss of Connection	Clearing along edge
	5.7	—	—	—	1 Hz in Vac. 1300 V.	Failed at 1531 shots	Open	Loss of Connection	Clearing along edge
e	5.0	—	—	—	1 Hz in Vac. 1300 V.	Failed at 360 shots	Open	Loss of Connection	Clearing along edge
e	5.0	—	—	—	1 Hz in Vac. 1300 V.	Failed at 0 shots	Low Cap. Hi D.F.	Loss of Connection	Clearing along edge
e	6.1	—	—	—	1 Hz in Vac. 1300 V.	Engine fired erratically	—	—	Stopped Testing due to erratic firing
e	6.2	—	—	—	1 Hz in Vac. 1300 V.	Engine fired erratically	—	—	Stopped Testing due to erratic firing
e	6.0	—	—	—	1 Hz at 5 kv 8Ω Load	Failed after 741 shots	Open	Loss of Connection	Clearing along edge Tested at Sprague
e	5.95	—	—	—	1 Hz at 4.5 kv 8Ω Load	Failed after 3324 shots	Open	Loss of Connection	Clearing along edge Tested at Sprague
e	6.0	—	—	—	1 Hz at 4 kv 8Ω Load	Failed after 16,495 shots	Open	Loss of Connection	Clearing along edge Tested at Sprague
e	6.0	—	—	—	1 Hz at 3.5 kv 8Ω Load	Failed after 19,529 shots	Open	Loss of Connection	Clearing along edge Tested at Sprague
e	5.56	—	—	—	1 Hz at 3 kv 2Ω Load	Failed after 11,268 shots	Open	Loss of Connection	Clearing along edge Tested at Sprague
e	5.65	—	—	—	1 Hz at 3.5 kv 2Ω Load	Failed after 21,906 shots	Open	Loss of Connection	Clearing along edge Tested at Sprague
e	5.60	—	—	—	1 Hz at 4 kv. 2Ω Load	Failed after 53,690 shots	Open	Loss of Connection	Clearing along edge Tested at Sprague

TABLE 16. Record of Capacit

Rating	Part No. & Serial No.	Shape & No. Sections	Dielectric	Conductors	Conductor Width	Section Termination	Impregnant	Cap
6.0 μfd 1500v	P-102	Round 1 Section	1X. 0005 M. Poly 1X. 0005 P. Poly	Metallized Aluminum	3 1/4"	Tin-Lead Spray	None	5.6
6.0 μfd 1500v	P-103	Round 1 Section	1X. 0005 M. Poly 1X. 0005 P. Poly	Metallized Aluminum	3 1/4"	Tin-Lead Spray	None	5.9
6.0 μfd 1500v	M-102	Round 1 Section	1X. 0003 P. Mylar 1X. 0003 M. Mylar	Metallized Aluminum	3 1/4"	Tin-Lead Spray	None	6.0
6.0 μfd 1500v	M-103	Round 1 Section	1X. 0005 P. Mylar 1X. 0005 M. Mylar	Metallized Aluminum	3 1/4"	Tin-Lead Spray	None	6.0
6.0 μfd 1500v	T-102	Round 1 Section	1X. 0005 P. Tedlar 1X. 0005 M. Tedlar	Metallized Aluminum	3 1/4"	Tin-Lead Spray	None	5.55
6.0 μfd 1500v	T-103	Round 1 Section	1X. 0005 P. Tedlar 1X. 0005 M. Tedlar	Metallized Aluminum	3 1/4"	Tin-Lead Spray	None	5.40
20 μfd 1500v	H-1754 A W-1493	Pressed Flat 2 Sections	1X. 00035 M. Paper 1X. 0003 P. Kraft 1X. 00025 Mylar	Metallized Aluminum	4 1/8"	Tin-Lead Spray	Mineral oil	20.9
20 μfd 1500v	H-1754 A W-1494	Pressed Flat 2 Sections	1X. 00035 M. Paper 1X. 0003 P. Kraft 1X. 00025 Mylar	Metallized Aluminum	4 1/8"	Tin-Lead Spray	Mineral Oil	21.0
20 μfd 1.95kv	H-1754 B W-1571	Round 7 Sections	1X. 00035 M. Paper 1X. 0003 Kraft 1X. 00025 Mylar	Metallized Aluminum	4 1/8	Tin-Lead Spray w/ Disc	Mineral Oil	18.0
20 μfd 1.95kv	H-1754 B W-1572	Round 7 Sections	1X. 00035 M. Paper 1X. 0003 Kraft 1X. 00025 Mylar	Metallized Aluminum	4 1/8	Tin-Lead Spray w/ Disc	Mineral oil	18.0
6.0 μfd 1500v	H-1950 A W-1600	Round 7 Sections	1X. 00025 M. Mylar 2X. 00025 P. Mylar	Metallized Aluminum	1 3/4"	Copper Spatter Tin Lead Spray Disc - Stud	Mineral oil	6.73
6.0 μfd 1500v	H-1950 A W-1601	Round 7 Sections	1X. 00025 M. Mylar 2X. 00025 P. Mylar	Metallized Aluminum	1 3/4"	Copper Spatter Tin Lead spray Disc - Stud	Mineral oil	6.85
9.0 μfd 1.9kv	H-1803 A	Pressed Flat 2 Sections	1X. 00035 M Paper 1X. 00025 Kraft 1X. 00025 Mylar	Metallized Aluminum	2 3/4"	Tin-Lead Spray	Mineral Oil	—
20 μfd 1.5kv	H-1856 A W-1623	Round 1 Section	2X. 00025 Mylar 1X. 00015 Mylar	Aluminum Foil	6 1/4"	Scrub Solder Disc & Stud Wire Leads	Silicone Oil	23.81
20 μfd 1.5kv	H-1856 A W-1624	Round 1 Section	2X. 00025 Mylar 1X. 00015 Mylar	Aluminum Foil	6 1/4"	Scrub Solder Disc & Stud Wire Leads	Silicone Oil	23.57
20 μfd 1.5kv	H-1856 A W-1625	Round 1 Section	2X. 00025 Mylar 1X. 00015 Mylar	Aluminum Foil	6 1/4"	Scrub Solder Disc & stud Wire Leads	Silicone Oil	23.66
20 μfd 1.5kv	H-1856 A W-1626	Round 1 Section	2X. 00025 Mylar 1X. 00015 Mylar	Aluminum Foil	6 1/4"	Scrub Solder Disc & Stud Wire Leads	None	23.36
20 μfd 1.5kv	H-1869 A W-1967	Round 1 Section	3X. 00025 Mylar Solid Mandrel	Aluminum Foil	3 1/8"	Scrub Solder Disc & Stud Wire Tabs	Silicone Oil	21.44
20 μfd 1.5kv	H-1869 A W-1965	Round 1 Section	3X. 00025 Mylar Solid Mandrel	Aluminum Foil	3 1/8"	Scrub Solder Disc & Stud Tabs	None	16.51
20 μfd 1.5kv	H-1869 A W-1966	Round 1 Section	3X. 00025 Mylar Solid Mandrel	Aluminum Foil	3 1/8"	Scrub Solder Disc & Stud Tabs	None	16.46
20 μfd 1.5kv	H-1869 A W-1968	Round 1 Section	3X. 00025 Mylar Solid mandrel	Aluminum Foil	3 1/8"	Scrub Solder Disc & stud Tabs	Silicone Oil	19.71
20 μfd 1.5kv	H-1869 A W-1969	Round 1 Section	3X. 00025 Mylar Solid mandrel	Aluminum Foil	3 1/8"	Scrub Solder Disc & Stud Tabs	Silicone Oil	21.93
20 μfd 1.5kv	H-1869 A W-1970	Round 1 Section	3X. 00025 Mylar Solid mandrel	Aluminum Foil	3 1/8"	Scrub Solder Disc & Stud Tabs	Silicone Oil	20.0

A

Cap	L	R	Q	Test Conditions	Test Results	Failure Mode	Analysis	Remarks
5.6	—	—	—	1 Hz in Vac 1300 v	Not Recorded	Open	Loss of Connection	Clearing along edge Short time to failure
5.7	—	—	—	1 Hz in Vac 1300 v	Not Recorded	Open	Loss of Connection	Clearing along edge Short time to failure
6.0	—	—	—	1 Hz in Vac 1300 v	Not Recorded	Open	Loss of Connection	Clearing along edge Short time to failure
6.0	—	—	—	1 Hz in Vac 1300 v	Not Recorded	Open	Loss of Connection	Clearing along edge Short time to failure
5.55	—	—	—	1 Hz in Vac 1300 v	Not Recorded	Open	Loss of Connection	Clearing along edge Short time to failure
5.40	—	—	—	1 Hz in Vac 1300 v	Not Recorded	Open	Loss of Connection	Clearing along edge Short time to failure
20.9	—	—	—	1 Hz in Vac 1500 v	1781 shots	Low Cap. Hi D.F.	Loss of Connection	Clearing along edge
21.0	27×10^{-9} flaring	—	—	Not tested because of short time failure of W-1493				
18.0	23.23×10^{-9}	.043	2.84	1 Hz in Vac 1300 v	40,379 shots	Low Cap. Hi D.F.	Loss of Connection	No Temp. stabilization Clearing along edge
18.0	15.65×10^{-9}	—	—	1 Hz in Vac 1300 v	57,800 shots	Short	1 shorted section	Short in center section possible heat problem
6.73	26×10^{-9}	.0135	4.65	Not tested because of short time failure of W-1601				
6.85	26×10^{-9}	.0135	4.65	4 Hz in Vac 1220 v	8800 shots	Decreased Thrust - Lo Cap.	Loss of Connection	Clearing along edge 3 sections open
—	—	—	—	5 units delivered but not tested due to short time failures on previous units of similar design.				
23.91	26.8×10^{-9}	.00435	7.75	2 Hz in Vac 1500 v	25,988 shots	Short	Random Puncture	Later results indicate Temperature problem
23.57	29.3×10^{-9}	.00416	7.7	2 Hz in Vac 1500 v	29,360 shots	Leaked	Heat problem	Leak repaired - unit painted black & returned
				2 Hz in Vac 1500 v	2,038 shots	Lead Short	Caused by #8 threading on Stud	Not shorted - Carbon path across Terminal
23.66	29.2×10^{-9}	.0047	7.3	2 Hz in Vac 1500 v	21,340 shots	Leaked	Heat problem	Lead repaired - unit painted black & returned
	28.9×10^{-9}	.003	10.4	2 Hz in Vac 1500 v	1,351,553 shots	Short	Puncture in Mandrel area	possible burr on mandrel
19.36	25.2×10^{-9}	.0051	7.1	2 Hz in Vac 1500 v	25,500 shots	Short	Heat Problem	No impregnant to carry heat to case
21.49	21.3×10^{-9}	.00338	9.35	Unit Sent to Supplier of the power Conditioner				
16.57	23.2×10^{-9}	.00346	10.9	2 Hz in Vac 1500 v	73,665 shots	Short	Random Puncture	Temp. Problem. No impregnant to transfer heat to case
16.46	22.1×10^{-9}	.00515	7.1	Not tested because of short time failure history on unimpregnated capacitors. Unit remains at Republic				
19.71	20.75×10^{-9}	.00397	7.37	2 Hz in Vac 1500 v	4,879,737 shots	Short	Random Puncture	
21.43	19.95×10^{-9}	.00362	8.59	2 Hz in Vac 1500 v	171,946 shots	Leak	Faulty weld on seam	Unit electrically good Case Temp. 185°F
20.0	19.4×10^{-9}	.00483	7.42	2 Hz in Vac 1500 v	859,240 shots	Short	Random Puncture	Case Temp. 166°F

TABLE 17. Record of Capacitor

Rating	Part No. & Serial No.	Shape & No. Sections	Dielectric	Conductors	Conductor Width	Section Termination	Impregnant	Cap	
10 μfd 1kV	H-1880A W-2058	Round 1 Section	3x.00035 Mylar Solid Mandrel	Aluminum Foil	1 3/4"	Scrub Solder Disc & Stud Tabs	Silicone Oil	11.5	
10 μfd 1kV	H-1880A W-2059	Round 1 Section	3x.00035 Mylar Solid Mandrel	Aluminum Foil	1 3/4"	Scrub Solder Disc & Stud Tabs	Silicone Oil	11.3	
10 μfd 1kV	H-1880A W-2060	Round 1 Section	3x.00035 Mylar Solid mandrel	Aluminum Foil	1 3/4"	Scrub Solder Disc & stud Tabs	Silicone Oil	11.6	
10 μfd 1kV	H-1880A W-2061	Round 1 Section	3x.00035 Mylar Solid mandrel	Aluminum Foil	1 3/4"	Scrub Solder Disc & Stud Tabs	Silicone Oil	11.3	
10 μfd 1kV	H-1882B W-2065	Round 1 Section	3x.00025 Mylar Solid mandrel	Aluminum Foil	1 7/8"	Scrub Solder Disc & Stud Tabs	Silicone Oil	9.0	
10 μfd 1kV	H-1882B W-2066	Round 1 Section	3x.00025 Mylar Solid mandrel	Aluminum Foil	1 7/8"	Scrub Solder Disc & Stud Tabs	Silicone Oil	9.4	
10 μfd 1kV	H-1882B W-2067	Round 1 Section	3x.00025 Mylar Solid mandrel	Aluminum Foil	1 7/8"	Scrub Solder Disc & Stud Tabs	Silicone Oil	9.4	
10 μfd 1kV	H-1882A W-2063	Round 1 Section	2x.00035 Mylar Solid mandrel	Aluminum Foil	1 13/16	Scrub Solder Disc & Stud Tabs	Silicone Oil	10.2	
10 μfd 1kV	H-1882A W-2063	Round 1 Section	2x.00035 Mylar Solid Mandrel	Aluminum Foil	1 13/16	Scrub Solder Disc & Stud Tabs	Silicone Oil	10.4	
10 μfd 1kV	H-1882A W-2064	Round 1 Section	2x.00035 Mylar Solid Mandrel	Aluminum Foil	1 13/16	Scrub Solder Disc & Stud Tabs	Silicone Oil	10.3	
20 μfd 1.5kV	H-1869A W-2091	Round 1 Section	3x.00025 Mylar Solid mandrel	Aluminum Foil	3 1/8	Scrub Solder Disc & Stud Tabs	Silicone Oil	21.0	
20 μfd 1.5kV	H-1869A W-2092	Round 1 Section	3x.00025 Mylar Solid mandrel	Aluminum Foil	3 1/8	Scrub Solder Disc & Stud Tabs	Silicone Oil	21.0	
20 μfd 1.5kV	H-1869A W-2093	Round 1 Section	3x.00025 Mylar Solid mandrel	Aluminum Foil	3 1/8	Scrub Solder Disc & Stud Tabs	Silicone Oil	21.0	
20 μfd 1.5kV	H-1869A W-2099	Round 1 Section	3x.00025 Mylar Solid mandrel	Aluminum Foil	3 1/8	Scrub Solder Disc & Stud Tabs	Silicone Oil	20.8	
20 μfd 1.5kV	H-1869A W-2101	Round 1 Section	3x.00025 Mylar Solid mandrel	Aluminum Foil	3 1/8	Scrub Solder Disc & Stud Tabs	Silicone Oil	20.8	
20 μfd 1.5kV	H-1869A W-2102	Round 1 Section	3x.00025 Mylar Solid mandrel	Aluminum Foil	3 1/8	Scrub Solder Disc & Stud Tabs	Silicone Oil	21.2	
20 μfd 1.5kV	H-1869A W-2103	Round 1 Section	3x.00025 Mylar Solid mandrel	Aluminum Foil	3 1/8	Scrub Solder Disc & Stud Tabs	Silicone Oil	21.0	
40 μfd 1.5kV	H-1907A W-2104	Round 1 Section	3x.00025 Mylar Solid mandrel	Aluminum Foil	3 1/8	Scrub Solder Disc & Stud Tabs	Silicone Oil	40.6	
40 μfd 1.5kV	H-1907A W-2105	Round 1 Section	3x.00025 Mylar Solid mandrel	Aluminum Foil	3 1/8	Scrub Solder Disc & Stud Tabs	Silicone Oil	40.8	
40 μfd 1.5kV	H-1907A W-2106	Round 1 Section	3x.00025 Mylar Solid mandrel	Aluminum Foil	3 1/8	Scrub Solder Disc & Stud Tabs	Silicone Oil	41.0	
40 μfd 1.5kV	H-1907A W-2107	Round 1 Section	3x.00025 Mylar Solid mandrel	Aluminum Foil	3 1/8	Scrub Solder Disc & Stud Tabs	Silicone Oil	40.6	
40 μfd 1.5kV	H-1907A W-2108	Round 1 Section	3x.00025 Mylar Solid mandrel	Aluminum Foil	3 1/8	Scrub Solder Disc & Stud Tabs	Silicone Oil	40.9	
20 μfd 1.5kV	H-1869A W-2150	Round 1 Section	3x.00025 Mylar Solid mandrel	Aluminum Foil	3 1/8	Scrub Solder Disc & Stud Tabs	Silicone Oil	20.2	
20 μfd 1.5kV	H-1869A W-2151	Round 1 Section	3x.00025 Mylar Solid mandrel	Aluminum Foil	3 1/8	Scrub Solder Disc & Stud Tabs	Silicone Oil	20.2	

of Capacitor Tests

Unit	Cap	L	R	Q	Test Conditions	Test Results	Failure Mode	Analysis	Remarks
	11.5	19.2 $\times 10^{-9}$	.00365	11	Units Not tested		—	—	—
	11.3	19.5 $\times 10^{-9}$	.0044	9.55	Unit Not Tested		—	—	—
	11.6	19.7 $\times 10^{-9}$	.0041	10.1	Unit Not tested		—	—	—
	11.3	20.3 $\times 10^{-9}$	.0042	10.1	Unit Not tested		—	—	—
	9.8	16.3 $\times 10^{-9}$	.0046	9.8	1 He in Vac 1 KV	15,000 shots	Leak	Failure of Solder seal	Possibly Temp problem No Temp data taken
	9.9	16.9 $\times 10^{-9}$	.0055	7.75	1 He in Vac 1 KV	1,685,434 Shots	Short	Random Puncture	Case temp 141°F
	9.4	16.9 $\times 10^{-9}$	.00576	9.8	1 He in Vac 1 KV	573,819 Shots	Test Halted Unit good	— Limited chamber facilities mechanically & electrically	
	10.2	14.9 $\times 10^{-9}$	.00397	9.64	Unit Not tested		—	—	—
	10.4	16.5 $\times 10^{-9}$	.0047	8.4	Unit Not tested		—	—	—
	10.3	16.7 $\times 10^{-9}$	.00575	7.0	Unit Not tested		—	—	—
	21.0	03.2 $\times 10^{-9}$	.0045	7.3	2 He in Vac 1400 V	7,151,140 Shots	Short	Random puncture	
	21.0	19.35 $\times 10^{-9}$	.00352	8.65	2 He in Vac. 1900 V	2,081,398 Shots	Unit sent unit.	to Dayton as demonstration	
	21.0	19.35 $\times 10^{-9}$	.0039	7.75	2 He in Vac. 1900 V	538,687	Test Halted — Unit good mechanically and electrically		
	20.8	20 $\times 10^{-9}$	.0025	12.5	Unit Not tested		—	—	—
	20.8	19.6 $\times 10^{-9}$	.0033	9.35	Unit Not tested		—	—	—
	21.2	19.2 $\times 10^{-9}$	.00248	12.2	Unit Not tested		—	—	—
	21.0	19.4 $\times 10^{-9}$	.00374	8.15	Unit Not tested		—	—	—
	40.6	19.6 $\times 10^{-9}$	.00283	7.75	Unit leaked prior to shoulder.	Test due to excessive			grinding of stud
	40.8	20.9 $\times 10^{-9}$	.00242	9.35	1 He in Vac. 1900 V	12,303 Shots	Leak	Solder seal Failure	Future units to be braze sealed. Unit electrically good.
	41.0	16.8 $\times 10^{-9}$	.00244	8.3	1 He in Vac. 1900 V	In excess of 1,970,000 shots	Testing	continues	
	40.6	21.4 $\times 10^{-9}$	.00314	7.4	Unit Not Tested				
	40.9	20.8 $\times 10^{-9}$	.00394	7.3	1 He in Vac. 1900 V	3,311,861 Shots	Leak	Solder seal Failure	Future units to be braze sealed.
	20.2	15 $\times 10^{-9}$	.00294	8.96	.85 He in Vac. 1700 V	7.5°C Temp gradient	Unit equipped with internal thermocouple. Run to thermal stability. gradient from Unit center to can.		
	20.2	15 $\times 10^{-9}$	.00292	9.0	.85 He in Vac. 1900 V	7.5°C Temp gradient	Same as above		

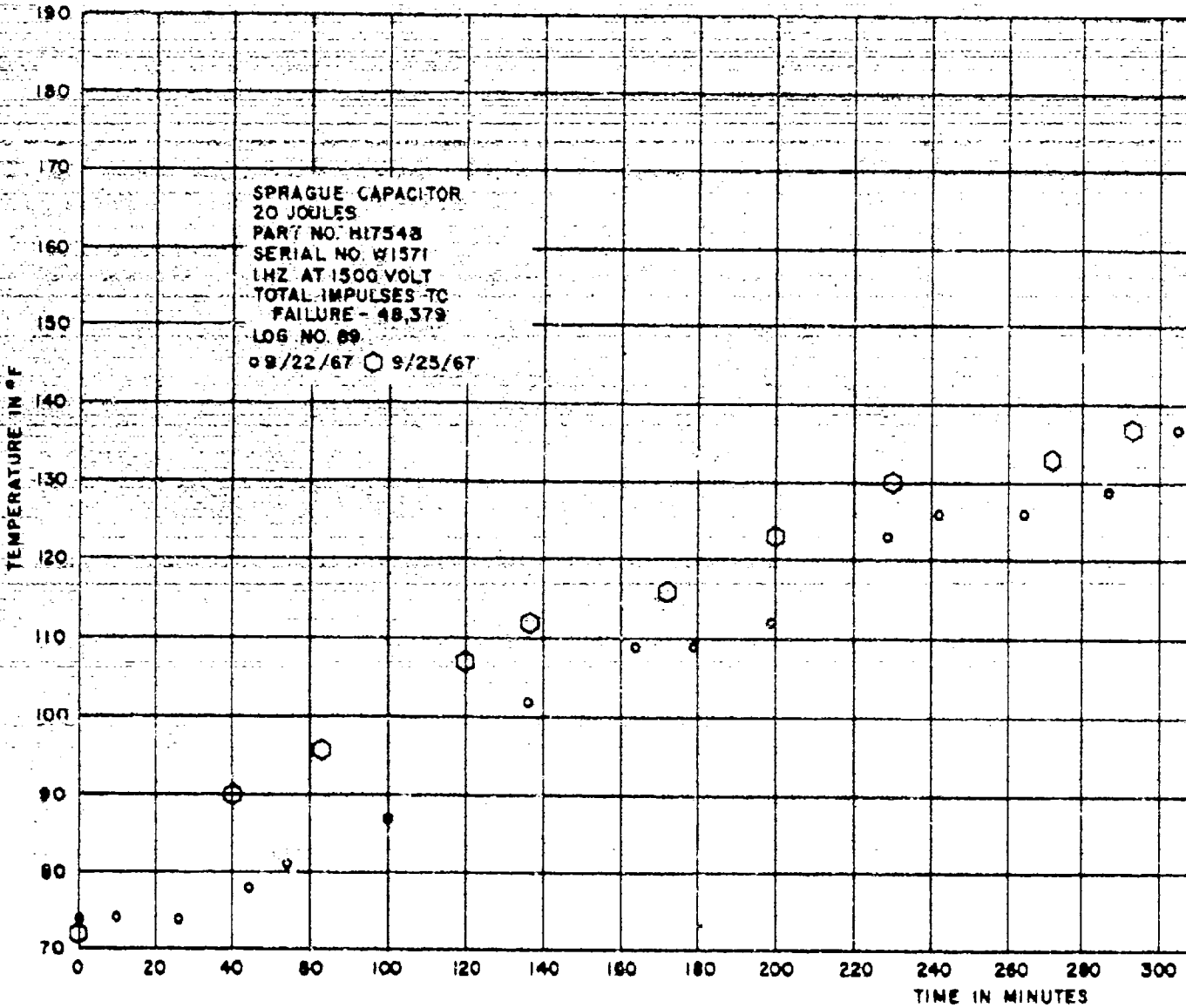
SPRAGUE CAPACITOR
20 JOULES
PART NO. HI7548
SERIAL NO. W1571
1 HZ AT 1500 VOLT
TOTAL IMPULSES TO FAILURE - 48,379
LOG NO. 89
9/22/67
9/25/67
TEMPERATURE IN °F
TIME IN MINUTES
190
180
170
160
150
140
130
120
110
100
90
80
70
0
20
40
60
100
120
140
160
180
200
220
240
260
280
300

A

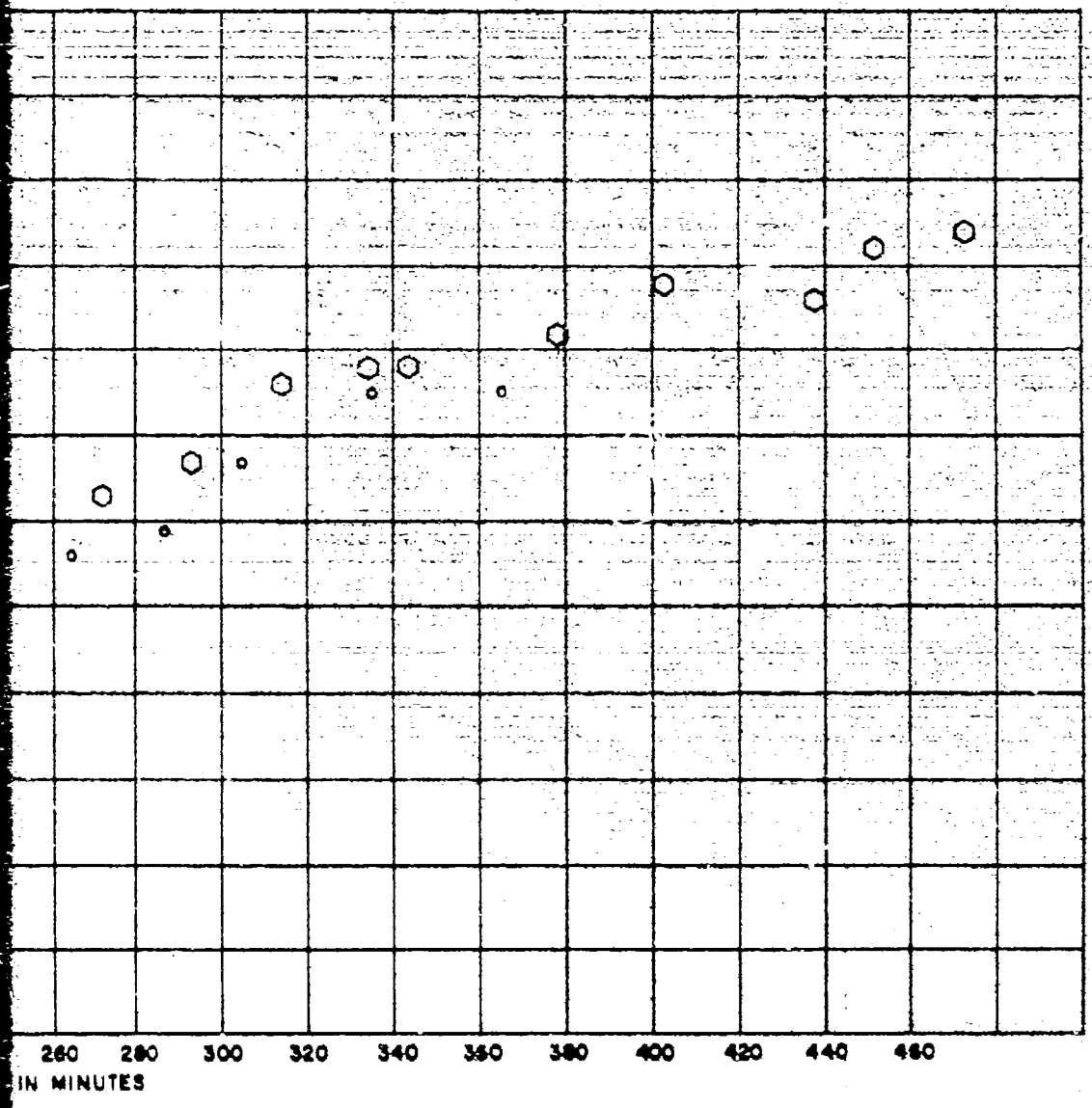

Figure 68. Temperature - Time History

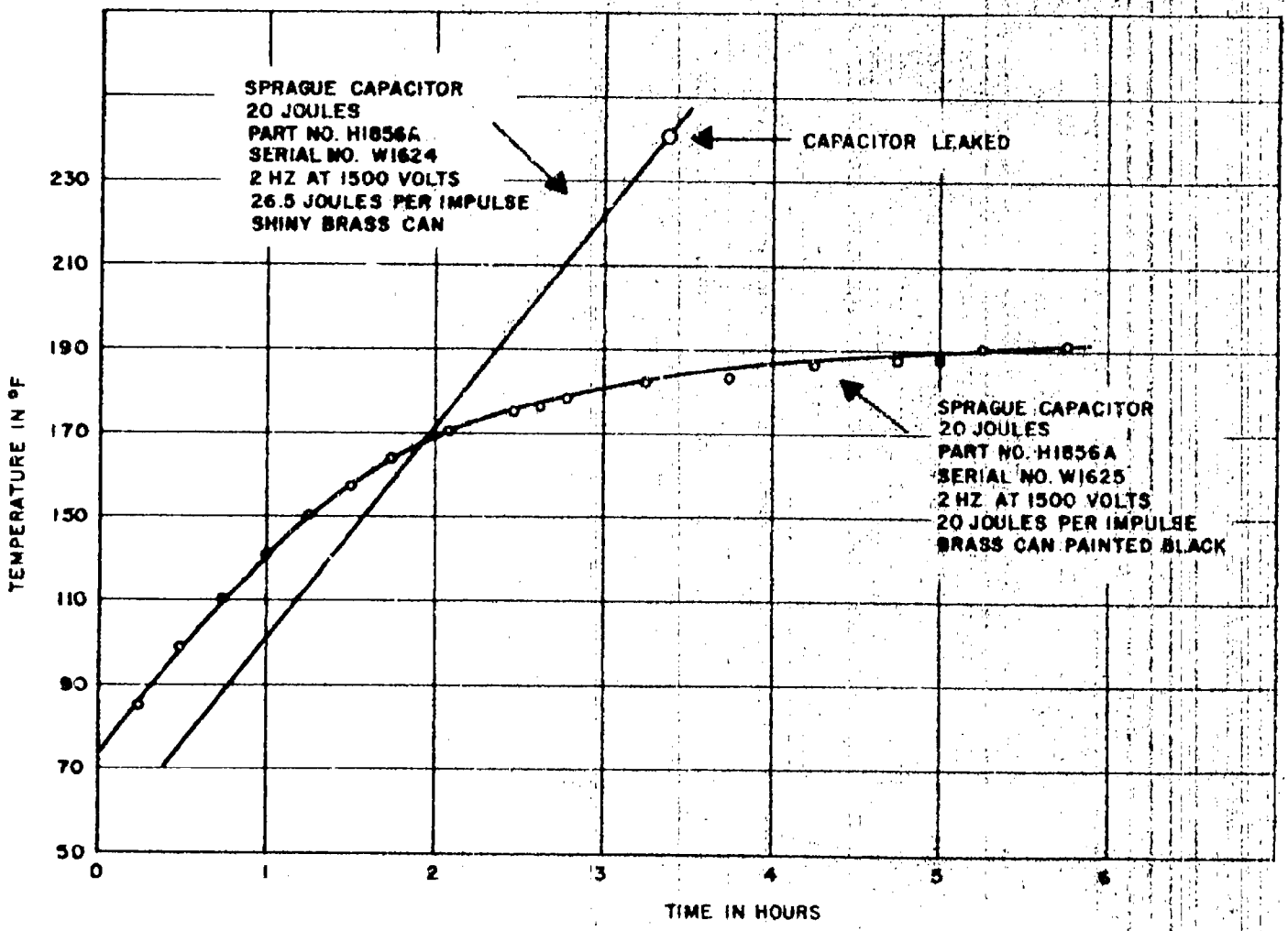

Figure 69. Temperature – Time History

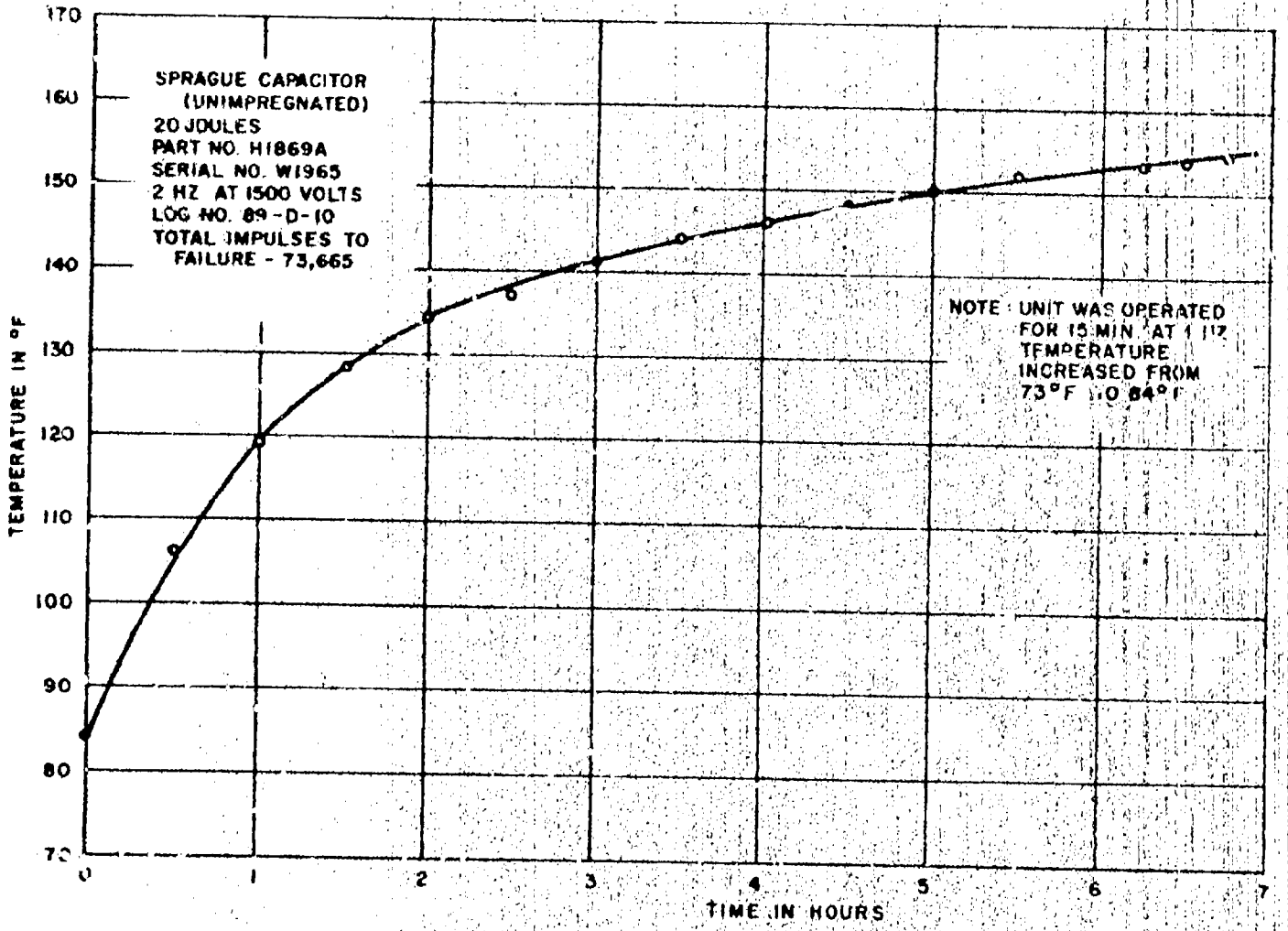

Figure 70. Temperature - Time History

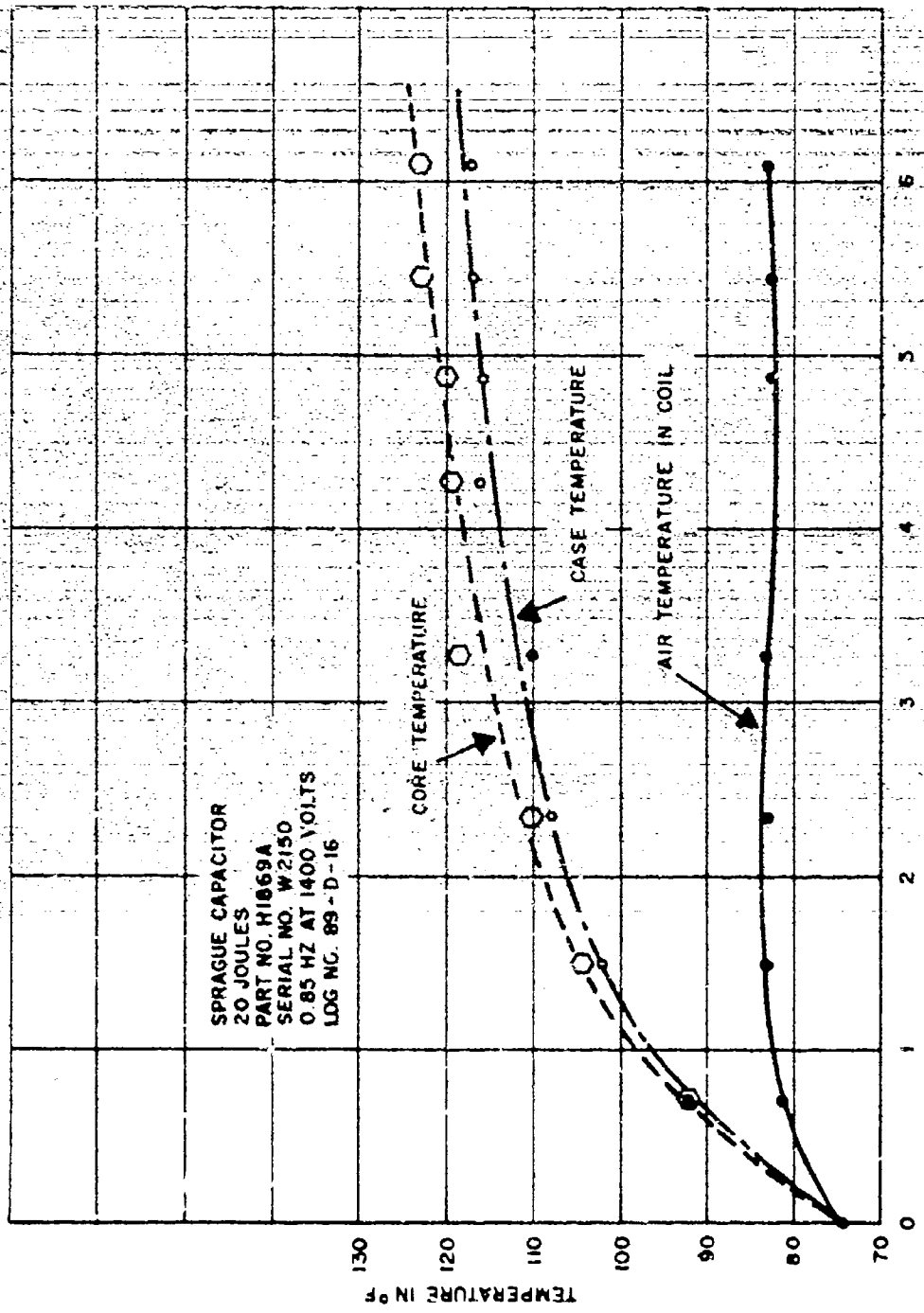

Figure 71. Temperature – Time History

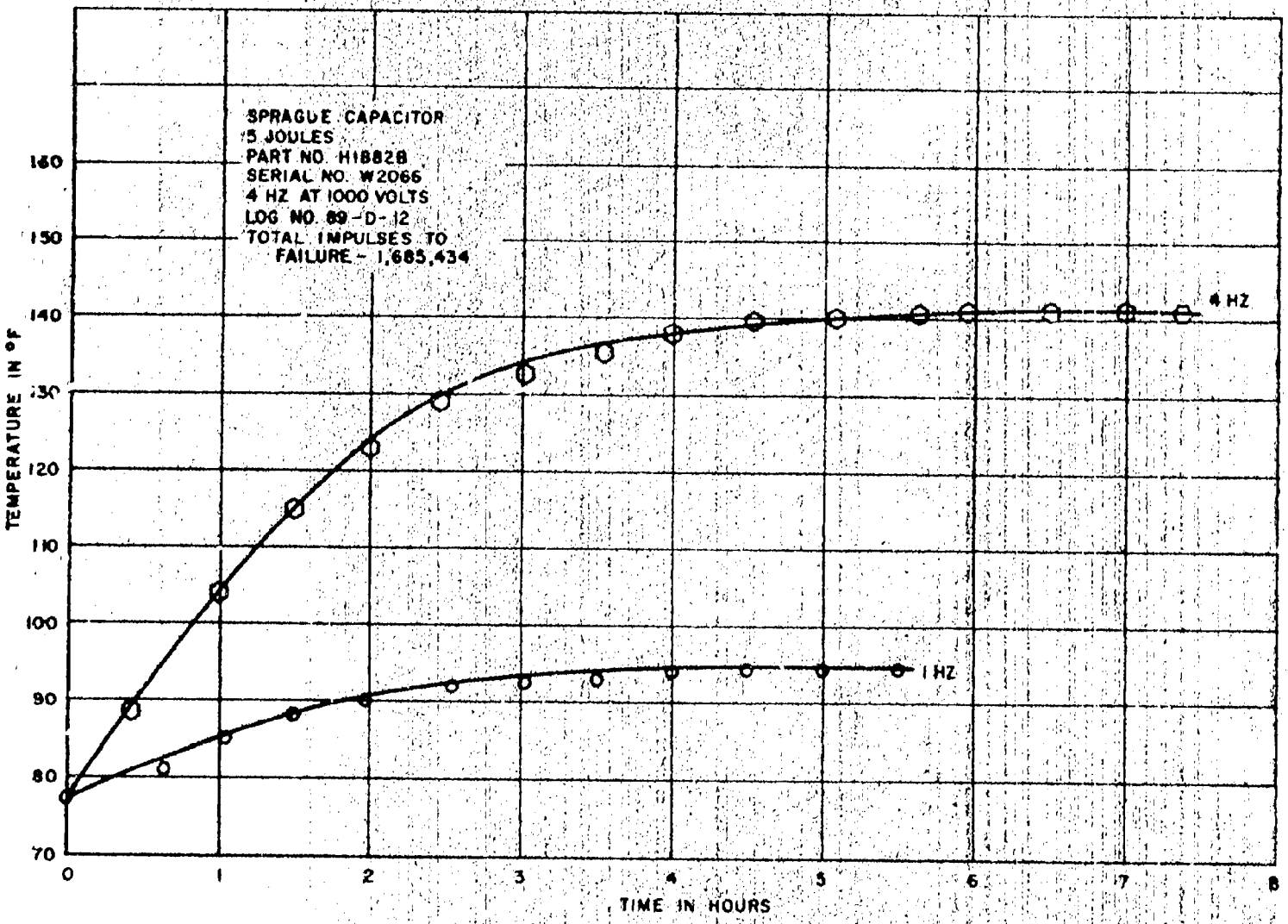

Figure 72. Temperature - Time History

SECTION VII

REFERENCES

1. Naval Research Laboratory/Republic Aviation Plasma Jet Satellite Description, PCD-TN-65-15, October 28, 1965, Fairchild Hiller Corp./ Republic Aviation Division, Farmingdale, New York.

2. Guman, W.: "Calorimetric Measurements of a Pulsed Plasma Accelerator," J. Appl. Phys., Vol. 36, No. 6, pp. 2092-2093, June 1965.

3. Temps, A.J.: "Life of a Capacitor When Subjected to a Time Varying Voltage," Interoffice Communication dated December 4, 1967, Fairchild Hiller/Republic Aviation Divis on, Farmingdale, New York.

4. Granet, I., "Thermal Testing of Capacitor," Interoffice Communication dated May 8, 1967, Fairchild Hiller/Republic Aviation Division, Farmingdale, New York.

5. Granet, I.: "A Proposed Method of Evaluating the Performance of a Capacitor," Interoffice Correspondence dated February 21, 1967, Fairchild Hiller/Republic Aviation Division, Farmingdale, New York.

6. Kern, D.Q.: Process Heat Transfer, McGraw-Hill Book Company, 1950.

7. Hsu, S.T.: Engineering Heat Transfer, D. VanNostrand Company, 1963.

8. Moore, E.T., Wilson, T.G. and McIntire, J.N.: "Lightweight Power Conditioning System for Ion Engines Using Energy Storage Transformers for Conversion, Nondissipative Regulation and Protection," IEEE Transactions on Aerospace and Electronic Systems, Vol. AES-2, No. 4, pp. 151-159, July 1966.

9. Cox, D.M., McIntire, N.J., Bemis, A.R., and Moore, E.T.: "Power Conditioning for Pulsed Load Applications Requiring Repetitive Capacitor Charging," Suppl. to IEEE Transactions on Aerospace and Electronic Systems, Vol. AES-3, No. 6, November 1967.

10. Temps, A.J.: "Power Conditioning Efficiency Analysis-Constant Energy Per Cycle Capacitor Charging," Interoffice Communication dated July 13, 1967, Fairchild Hiller/Republic Aviation Division, Farmingdale, New York.

11. Temps, A.J.: "Pulsed Plasma Discharge Simulator," Rev. Sci. Instruments, Vol. 39, pp. 918-919, June 1968.

12. Germain, C. and Rohrbach, F.: "High Voltage Breakdown," Vacuum, Vol. 18, No. 7, pp. 371-377, July 1968.

13. Hawley, R.: "Artificial Initiation of Vacuum Breakdown," Vacuum, Vol. 18, No. 1, pp. 21, January 1968.

14. Gruenberg, R.: Gesetzmaessigkeiten von Funkenentladungen im Nanosekundenbereich, Z. f. Naturforschung, Band 20a, Heft 2, February 1965.

15. Beynon, J.: "Initiation of Vacuum Breakdown," Vacuum, Vol. 18, No. 6, p. 335, June 1968.

16. Guman, W.J. and Peko, P.E.: "Solid Propellant Pulsed Plasma Microthruster Studies," AIAA Paper 68-85 (Figure 5), January 1968.

SECTION VIII

PROJECT PUBLICATIONS

1. Guman, W.J. and Peko, P.E.: "Solid Propellant Pulsed Plasma Microthruster Studies," AIAA Paper 68-85, AIAA 6th Aerospace Sciences Meeting, New York, N.Y., January 22-24, 1968.

2. Temps, A.J.: "Pulsed Plasma Discharge Simulator," Rev. Sci. Instr., Vol. 39, pp. 918-919, June 1968.

3. Guman, W.J. and Peko, P.E., "Solid Propellant Pulsed Plasma Microthruster Studies," J. of Spacecraft and Rockets, Vol. 5, No. 6, pp. 732-733, June 1968.

Unclassified

Security Classification

DOCUMENT CONTROL DATA - R & D

(Security classification of title, body of abstract and indexing annotation must be entered when the overall report is classified)

1. ORIGINATING ACTIVITY (Corporate author) Fairchild Hiller Corporation/Republic Aviation Division Farmingdale, New York 11735	2a. REPORT SECURITY CLASSIFICATION Unclassified 2b. GROUP

3. REPORT TITLE

PULSED PLASMA TECHNOLOGY IN MICROTHRUSTERS

4. DESCRIPTIVE NOTES (Type of report and inclusive dates)

Final Report for period: February, 1967 through September, 1968

5. AUTHOR(S) (First name, middle initial, last name)

Dr. William J. Guman

6. REPORT DATE	7a. TOTAL NO. OF PAGES	7b. NO. OF REFS
NOVEMBER, 1968	185	16

8a. CONTRACT OR GRANT NO.	9a. ORIGINATOR'S REPORT NUMBER(S)
F33615-67-C-1395 b. PROJECT NO.	PCD-TR-68-14 9b. OTHER REPORT NO(S) (Any other numbers that may be assigned this report) AFAPL-TR-68-132

10. DISTRIBUTION STATEMENT

This document is subject to special export controls and each transmittal to foreign governments or foreign nationals may be made only with prior approval of AFAPL (APIE-1)

11. SUPPLEMENTARY NOTES	12. SPONSORING MILITARY ACTIVITY
	Air Force Aero Propulsion Laboratory Wright-Patterson AFB, Ohio

13. ABSTRACT

~~This Final~~ Report describes the pertinent results of the studies carried out in advancing solid propellant pulsed plasma microthruster system technology in the thrust range from below 1 micropund up to roughly 200 micropounds and encompassing the (system) specific impulse range up to 2400 seconds. Thruster nozzles have been operated up to 3800 hours at the 50 micropound thrust level. Radiation cooled energy storage capacitors driving thrusters at 7.7 joules/lb have been developed with a life of 7.1×10^6 discharges (476lb-sec of total impulse). Discharge initiating circuitry has been operated for 1.54×10^8 discharges and 80% efficient power conditioners have been developed and tested beyond 4.5×10^7 discharges. Complete thruster systems have been operated up to 630 hours at the 140 micropound thrust level (317 lb-sec of total impulse). A thrust stand capable of accurately and rapidly measuring thrust of a microthruster was delivered ~~to the Air Force Aero Propulsion Laboratory~~.

Since an ion pumped vacuum chamber having sorption roughing was not available, it was not possible to reliably determine maximum thruster system life capability.

The results of this program have made it possible to design, test, and deliver flight qualified thrusters and power conditioners to another laboratory under a separate program within roughly 30 weeks for installation in a synchronous orbit satellite.

Guidelines for including a solid propellant pulsed plasma microthruster system in application studies are included.

DD FORM 1 NOV 68 1473

Unclassified

Security Classification

14. KEY WORDS	LINK A		LINK B		LINK C	
	ROLE	WT	ROLE	WT	ROLE	WT
Electric Propulsion						
Energy Storage Capacitors						
Microthruster						
Plasma						
Plasma Propulsion						
Power Conditioning						
Pulsed-Plasma-Propulsion						
Solid Propellant Electric Rocket						
Space Propulsion						
Teflon						
Thruster						
Vacuum Arc						